LEVEL II

12

Final Report

on

CONTRACT F 44620-76-C-0060

CALCULATION OF CERAMIC PHASE DIAGRAMS

1 December 1975 to 30 September 1979

Submitted to

Air Force Office of Scientific Research (AFSC)
Bolling Air Force Base, D.C. 20332

30 November 1979

by

Larry Kaufman
ManLabs, Inc.
21 Erie Street
Cambridge, Massachusetts 02139

Unclassified

SECURITY CLASSIFICATION OF THIS PAGE (When Data Entered)

(19) REPORT DOCUMENTATION PAGE

READ INSTRUCTIONS BEFORE COMPLETING FORM

(18) AFOSR TR-80-0041

2. GOVT ACCESSION NO.

3. RECIPIENT'S CATALOG NUMBER

(6) 4. TITLE (and Subtitle)

Calculation of Ceramic Phase Diagrams.

5. TYPE OF REPORT & PERIOD COVERED

Final Report, December 1975 to SEPT 79

6. PERFORMING ORG. REPORT NUMBER

7. AUTHOR(s)

(10) Larry Kaufman

8. CONTRACT OR GRANT NUMBER(s)

(15) F 44620-76-C-0060

9. PERFORMING ORGANIZATION NAME AND ADDRESS

ManLabs, Inc.
21 Erie St.
Cambridge, Massachusetts 02139

(12) 100

10. PROGRAM ELEMENT, PROJECT, TASK AREA & WORK UNIT NUMBERS

2306/A2
61102F

11. CONTROLLING OFFICE NAME AND ADDRESS

Air Force Office of Scientific Research/NE
Bolling Air Force Base BLDG 410
Washington, D.C. 20332

(11) 12. REPORT DATE

30 November 1979

13. NUMBER OF PAGES

99

14. MONITORING AGENCY NAME & ADDRESS(if different from Controlling Office)

(9) Final rept. 1 Dec 75-30 Sep 79,

15. SECURITY CLASS. (of this report)

Unclassified

15a. DECLASSIFICATION/DOWNGRADING SCHEDULE

16. DISTRIBUTION STATEMENT (of this Report)

(16) 2306 1
(17) A9 1

Approved for public release;
distribution unlimited.

17. DISTRIBUTION STATEMENT (of the abstract entered in Block 20, if different from Report)

18. SUPPLEMENTARY NOTES

19. KEY WORDS (Continue on reverse side if necessary and identify by block number)

Data Base	Quasibinary	Hydrogen storage
Phase Diagrams	Quasiternary	Electroptical semiconductors
Ceramic Systems	Superalloys	HEM silicon solar cells
Sialons	Molten Salts	metatectic reactions in hafnium alloys
Thermochemistry	Battery Electrodes	Doped Germanium Borosilicate Glasses

20. ABSTRACT (Continue on reverse side if necessary and identify by block number)

A data base is being developed for calculation of quasibinary and quasiternary phase diagrams of oxide and oxynitride ceramic systems. The current base covers combinations of Cr_2O_3, MgO, Al_2O_3, Fe_2O_3, Fe_3O_4, FeO, CaO, SiO_2, Si_3N_4 and AlN. Lattice Stability, Solution and Compound Phase Parameters were derived covering the liquid, spinel, periclase, corundum alpha and beta

over

DD FORM 1 JAN 73 1473 EDITION OF 1 NOV 65 IS OBSOLETE

215 770

UNCLASSIFIED JOB

SECURITY CLASSIFICATION OF THIS PAGE (When Data Entered)

quartz, crystobalite, tridymite and beta Si_3N_4 structures in all of the quasibinary systems composed of the data base compounds. Evaluation of these parameters permit calculation of the thermochemical properties of these systems in good agreement with limited thermochemical data. In addition, isothermal quasiternary systems of selected oxide and oxynitride systems composed of data base compounds have also been calculated over a wide range of temperature. The free energy of formation of beta sialons in the Si_3N_4-Al_2O_3-AlN system and the X phase in the SiO_2-Al_2O_3-Si_3N_4 system have been calculated. Recent examples of the use of data bases and computer techniques in solving problems associated with: in-situ formation of columbium, nickel and cobalt based superalloys, sigma phase formation, multicomponent electroptical semiconductors, sialon ceramics, molten salt, sulfide and oxide slags, high temperature battery electrodes, hardenability, synthesis of hydrogen storage compounds, grain refinement in aluminum alloys, metatectic reactions in hafnium alloys and the growth of HEM silicon solar cell materials. The initial results obtained by applying these techniques to CVD synthesis of doped germanium-borosilicate glasses for C^3I applications are reported.

DISTRIBUTION LIST

AFOSR/NE
Attn: Maj. W.C. Simmons
Bldg #410
Bolling AFB
Washington, D.C. 20332 (16 copies)

AFML/LLM
Attn: Branch Chief
W-P AFB, Ohio 45433

AFML/LLS
Attn: Branch Chief
W-P AFB, Ohio 45433

AFML/LLN
Attn: Branch Chief
W-P AFB, Ohio 45433

U.S. Army Research Office
Metallurgy & Materials Sciences
P.O. Box 12211
Research Triangle Park, NC 27709

AFML/MBM
Attn: W.L. Baun
W-P AFB, Ohio 45433

Office of Naval Research
Attn: Dr. A.M. Diness
800 N. Quincy Street
ARlington, VA 22203

N.S.F. (Materials Res.)
Attn: R.J. Reynik
1800 G Street, N.W.
Washington, DC 20550

Materials Research Lab (AMMRC)
Attn: Dr. R.N. Katz
Watertown, MA 02172

U.S. Naval Research Laboratory
Attn: Dr. R.W. Rice, Chem. Div.
Washington, DC 20375

Prof. A.H. Heuer
Prof. T.E. Mitchell
Dept. of Materials Science
Case Western Reserve University
Cleveland, Ohio 44106

Professor T.Y. Tien
University of Michigan
Materials Engineering
Ann Arbor, Michigan 48105

Prof. D.L. Johnson
Department of Materials Science
Northwestern University
Evanston, Illinois 60201

Dr. F.F. Lange
Dr. A.G. Evans
Rockwell International
Science Center
Thousand Oaks, California 91360

Dr. D.D. Cubicciotti
Stanford Research Institute
Materials Research Center
Menlo Park, California 94025

Dr. Fred S. Pettit
Pratt & Whitney Aircraft
East Hartford, Conn. 06108

Dr. Harold Posen
RADC-ESMC
Building 1126 Rm. 102
Hanscom AFB
Bedford, Mass. 01731 (5 copies)

AIR FORCE OFFICE OF SCIENTIFIC RESEARCH (AFSC)
NOTICE OF TRANSMITTAL TO DDC
This technical report has been reviewed and is
approved for public release IAW AFR 190-12 (7b).
Distribution is unlimited.
A. D. BLOSE
Technical Information Officer

ABSTRACT

A data base is being developed for calculation of quasibinary and quasiternary phase diagrams of oxide and oxynitride ceramic systems. The current base covers combinations of A_2O_3, MgO, Al_2O_3, Fe_2O_3, Fe_3O_4, FeO, CaO, SiO_2, Si_3N_4 and AlN. Lattice Stability, Solution and Compound Phase Parameters were derived covering the liquid, spinel, periclase, corundum alpha and beta quartz, crystobalite, tridymite and beta Si_3N_4 structures in all of the quasibinary systems composed of the data base compounds. Evaluation of these parameters permit calculation of the thermochemical properties of these systems in good agreement with limited thermochemical data. In addition, isothermal quasiternary systems of selected oxide and oxynitride systems composed of data base compounds have also been calculated over a wide range of temperature. The free energy of formation of beta sialons in the Si_3N_4-Al_2O_3-AlN system and the X phase in the SiO_2-Al_2O_3-Si_3N_4 system have been calculated. Recent examples of the use of data bases and computer techniques in solving problems associated with: in-situ formation of columbium, nickel and cobalt based superalloys, sigma phase formation, multicomponent electroptical semiconductors, sialon ceramics, molten salt, sulfide and oxide slags, high temperature battery electrodes, hardenability, synthesis of hydrogen storage compounds, grain refinement in aluminum alloys, metatectic reactions in hafnium alloys and the growth of HEM silicon solar cell materials. The initial results obtained by applying these techniques to CVD synthesis of doped germanium-borosilicate glasses for C^3I applications are reported.

TABLE OF CONTENTS

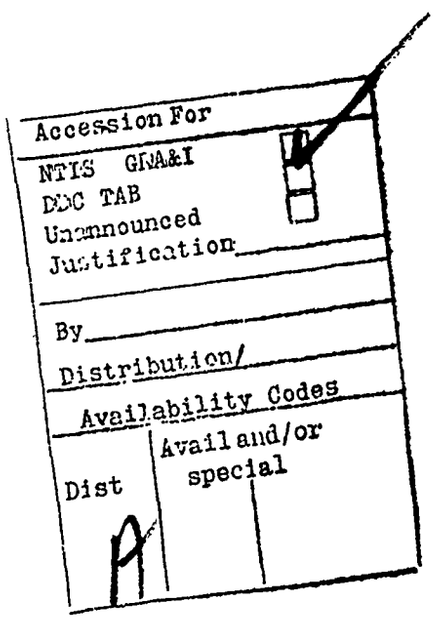

Section I. Introduction and Summary

The utility of computer based methods for developing and utilizing coupled phase diagram and thermochemical data on metallic systems has been well documented. Sections II and V of the current report contain suitable references and examples. Not withstanding the development and applications of metallic data bases the growth of similar facilities for ceramic and oxide systems has proceeded at a much slower pace. This was certainly the case in 1975 when the present program was initiated (see page 6). Accordingly, the current work was initiated in order begin the development of a data base for oxide and oxynitride ceramic systems which could be applied to computation of phase equilibria and stability over a wide range of temperature, pressure and composition. One of the objectives of this study was to develop the capability of dealing with SIALON systems which are based on combinations of Si_3N_4, AlN, Al_2O_3 and SiO_2. Reference to Sections III and VI shows that this objective has been achieved through our own efforts and those which were carried on by other workers in the "CALPHAD group" (i.e. references 2,3 page 42 and references 3 and 4 page 61). Section 4 provides a number of examples of computed ternary sections through systems composed of oxynitride ceramics. The data base which has been developed for the purpose of performing the calculations displayed in Section 4 can be employed to explore stable and metastable equilibrium in multi component oxynitride systems.

The three technical papers contained in Sections II-IV trace the development of the present data base which currently covers Cr_2O_3, Al_2O_3, MgO, FeO, Fe_2O_3, Fe_3O_4, SiO_2, CaO, Si_3N_4 and AlN. Section II discusses the initial segment dealing with combinations of Cr_2O_3, MgO, Al_2O_3, Fe_2O_3, FeO and Fe_3O_4. The twelve quasibinary systems and three quasiternary

systems were calculated and compared with limited experimental data. The development of lattice stability, solution and compound phase parameters for the liquid, spinel, corundum and periclase phases can be employed to calculate phase equilibria activity, vapor pressure and free energy of formation of solution phases and compounds in quasibinary and quasiternary systems composed of the above listed compounds. The ternary isothermal sections which were calculated in this work include the Fe_3O_4-Cr_2O_3-Al_2O_3 system between 1600 and 2400K, the MgO-Fe_3O_4-Al_2O_3 system between 1600K and 2850°K and the MgO-Cr_2O_3-Al_2O_3 between 1300°K and 2800K. In the last case the computed results were found to compare favorably with experimental results.

The second phase of the development covered in Section III deals with inclusion of CaO and SiO_2. Each of the quasibinary systems between their compounds and the forgoing group (i.e. Cr_2O_3, Al_2O_3, MgO, FeO, Fe_2O_3 and Fe_3O_4) was analysed permitting calculation of phase diagram and thermochemical free energy of formation of quasibinary compounds. This description covered the liquid, spinel, periclase, corundum, crystobalite, tridymite and the alpha and beta quartz structures which occur in these quasibinary systems. In addition, ternary isothermal sections were computed between 1600 and 2800K for the MgO-Fe_3O_4-Cr_2O_3 system.

The extension to oxynitride ceramic systems described in Section IV was carried out by developing lattice stability, solution and compound phase parameters for each of the quasibinary systems between Si_3N_4 and AlN and MgO, Al_2O_3 and SiO_2. The beta Si_3N_4 and hexagonal AlN structures were included along with the liquid and previously listed solid phase structures. The melting point and decomposition temperatures of Si_3N_4 and AlN at one atmosphere pressure were calculated in the course of tis analysis. Isothermal sections in the SiO_2-Al_2O_3-Si_3N_4 and Si_3N_4-Al_2O_3-AlN systems were computed which are in good agreement with experimental findings. Moreover, the free energy of formation of the ternary compound phase X which forms in the

SiO_2-Al_2O_3-Si_3N_4 and the beta sialon phase of the Si_3N_4-Al_2O_3-AlN system were calculated. Comparison of the latter results with independent findings obtained by the Stuttgart group yields good results which can be further improved by iteration.

Section V provides a listing of recent cased in which thermochemical data have been employed successfully in dealing with practical problems. Such documentation is difficult to obtain because the secrecy and confidentiality restrictions which surround economically viable processes necessarily limit publication of such information. Nevertheless, such examples come to light over a period of years. The discussion in Section V covers processing of in-situ eutectic composite formation in columbium, nickel and cobalt base superalloys, sigma phase formation in high temperature alloys, multicomponent semiconductors for electroptical devices, SIALON ceramics, molten salt, sulfide and oxide slags for ore reduction and refining, high temperature battery electrodes, hardenability calculations in alloy steels, synthesis of hydrogen storage alloy compounds, grain refinement in aluminum alloys, metatectic reactions in hafnium alloys and the growth of HEM silicon solar cell materials.

The final section of this report discusses application of the present computational methods to the CVD processing of doped germanium-borosilicate glasses. Section VI illustrates the utilization of Data Bank information in computing the temperature/pressure range over which the halides of potential dopents can be employed effectively in the CVD processing of preforms. As the first step in an analysis of these glasses, Section VI contains an analysis of the SiO_2-GeO_2, SiO_2-B_2O_3 and B_2O_3-GeO_2 quasibinary systems as well as the SiO_2-GeO_2-B_2O_3 quasiternary system over the temperature range from 1000K to 1600K. Future activities will include consideration of the addition of Sb_2O_5, P_2O_5 and CeO_2 to this system.

Section Ia. Program Personnel

Technical activities on this program have been performed by L. Kaufman, H. Nesor, E.P. Warekois, D. Pendse, J. Smith, G. Zilberstein, C. Thielen, K. Taylor, A.P. Miodownik, and J. Nell during the course of this study.

Section Ib. Interaction with Other Technical Activities

During the course of this study technical presentations covering this work were given at the ASM/AIME Materials Congresses in Chicago, Illinois (October 1978) and Milwaukee, Wisconsin (September 1979), CALPHAD VI-Harwell, Oxford England April 1977, CALPHAD VII-Stuttgart, West Germany (April 1978), Technion-Haifa Israel (May 1978), CALPHAD VIII-Stockholm Sweden (May 1979) and National Physical Laboratory/Chemical Society of London Symposium on Industrial Use of Thermochemical Data, University of Surrey Guildford Surrey England (September 1979). Specific interactions with scientific personnel at the Max Plank Institute-Stuttgart, West Germany, University of Surrey, Guildford Surrey, England and at the Israel Institute of Technology-Technion City Haifa Israel were most helpful.

Section II. Calculation of QuasiBinary and QuasiTernary Systems - I, CALPHAD (1978) 2 pp 35-53

CALPHAD Vol. 2, No. 1, pp. 35-53. Pergamon Press, 1978. Printed in Great Britain.

CALCULATION OF QUASIBINARY AND QUASITERNARY OXIDE SYSTEMS - I*

Larry Kaufman and Harvey Nesor
ManLabs, Inc., 21 Erie Street
Cambridge, Massachusetts 02139, USA

ABSTRACT. A data base is being developed for calculation of quasi-binary and quasi-ternary phase diagrams of ceramic systems. The initial segment of this base covers combinations of Cr_2O_3, MgO, Al_2O_3, Fe_2O_3, Fe_3O_4 and "FeO". Lattice Stability, Solution and Compound Phase Parameters are presented covering the liquid, spinel, periclase and corundum phases in systems composed of these oxides. These parameters permit calculation of the thermochemical properties and phase diagrams of combinations of these oxides in good agreement with limited experimental data. Twelve calculated quasi-binary phase diagrams and three calculated quasi-ternary phase diagrams are presented illustrating the applicability of the data base.

1. Introduction

The utility of computer based methods for coupling phase diagrams and thermochemical data for metallic systems has been demonstrated in many papers published in this journal. A considerable effort is being applied toward development of a suitable data base for metallic systems (1). Numerous examples have been published showing how such data on metallic systems can be synthesized to successfully predict the thermochemical properties and phase relations in ternary metallic systems (1-12). Such predictions can be applied practically to explore conditions for in-situ eutectic growth, metallic glass formation, spinodal decomposition, metastable equilibrium, and diffusionless transformations. In a recent workshop on "Applications of Phase Diagrams in Metallurgy and Ceramics" held in January, 1977 at the National Bureau of Standards in Gaithersburg, Maryland (13), many informational gaps in ceramic phase diagram data were noted and the need to develop computational techniques to bridge these gaps became evident. Such efforts have been proceeding individually for some time (14,15). However, in view of the success achieved in developing a tractable data base for metallic systems, it seemed to be an auspicious time for launching the development of a similar data base for ceramic systems. This is particularly true, since the need for such information is apparent (i.e., metastable reactions are quite common in ceramic systems, pressure is an important variable, etc.) and experimental data is limited and difficult to obtain. Accordingly, the present work should be considered as a beginning, much like the initial attempt at estimating the lattice stability of metals (16,17). The only difference is the experience gained with development of a data base for metals over the past ten years and the availability of suitable computational programs.

*This work has been sponsored by the Air Force Office of Scientific Research, Bolling AFB, Washington, D.C., under Contract F44620-76-C-0060.

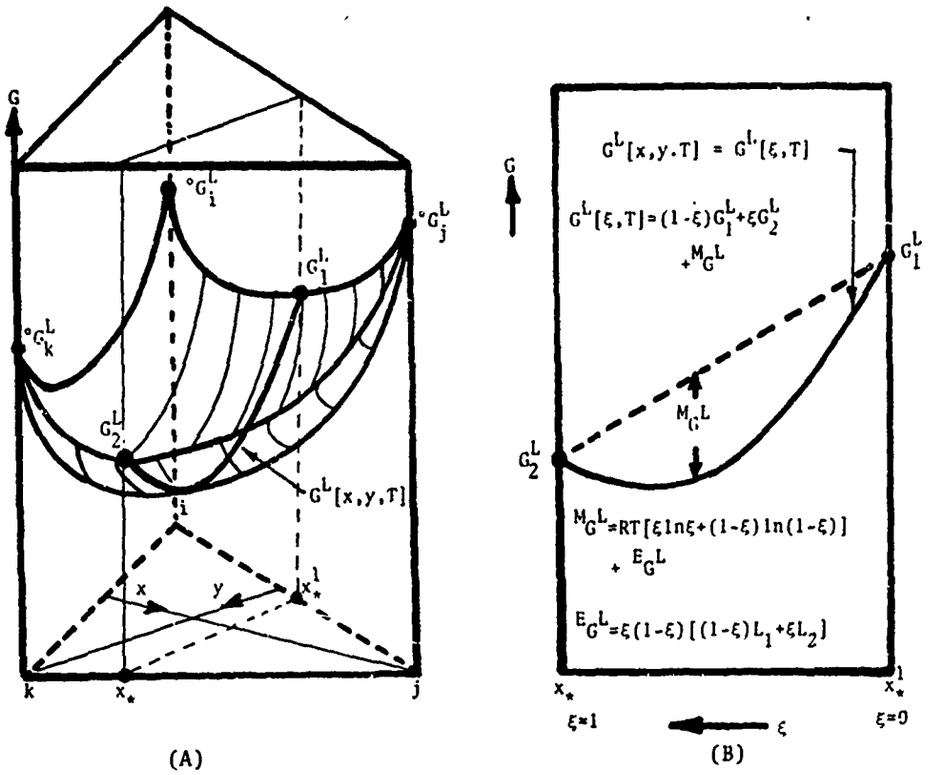

Figure 1. Illustration of Quasi-Binary Approximation of the Excess Free Energy of Mixing of Solution Phases, E_G^L in Terms of the Ternary Approximation to the Free Energy $G^L(x,y,T)$ [Mass Basis Equal to One Gram Atom or One Mole of Atoms].

2. Description Of The Thermochemical System Employed To Describe Solution And Compound Phases

The method utilized for describing solution and compound phases is essentially the same as that employed earlier (1,3), except that some symbolic usage has evolved which facilitates data handling as indicated below. The free energy, G^L, of a liquid (solution) phase, L, in the binary system I-J is given by Equation (1) where T is in Kelvins, x is the atomic fraction of J and the mass basis is a mole of atoms (i.e., a gram atom).

$$G^L = (1-x)^{\circ}G_i^L + {}^{\circ}G_j^L + RT(x\ell nx + (1-x)\ell n(1-x)) + x(1-x)[LIJ(1-x) + xLJI] \qquad (1)$$

In this expression, $^{\circ}G_i^L$ and $^{\circ}G_j^L$ are the free energies of a gram atom of pure liquid I and J, R = 8.314 J/g.at.°K, and LIJ and LJI are functions of temperature (but not of compostion). Similar equations can be written

TABLE 1

Lattice Stability, Solution Phase and Compound Parameters Employed for Calculation of Several Metal - Oxygen Systems

(All units in Joules per gram atom (mole of atoms), T in Kelvins)

Lattice Stability Parameters

FEFEVL = 371200 - 118.4T, ALALVL = 301250 - 107.9T
CRCRVL = 367360 - 120.5T, OOOOVL = 3410 - 37.9T
MGMGVL = 133890 - 98.3T, OOOOLB = 230. - 4.2T

Solution Phase Parameters

	0 to 50 a/o Oxygen	50 to 100 a/o Oxygen
LFEOO	0	423420 - 456.1T
LOOFE	-1000810 + 125.5T	-1424230 - 581.6T
LCROO	0	-882820 + 117.2T
LOOCR	-1765650 + 234.3T	-882820 + 117.2T
LMGOO	-90790 - 411.3T	-90790 - 411.3T
LOOMG	-1940120 + 626.3T	-1940120 + 626.3T
LALOO	-1287830 + 147.7T	-1287830 + 147.7T
LOOAL	-1287830 + 147.7T	-1287830 + 147.7T

Compound Phase Parameters

(Base Phase is BCC)

Compound	Structure	Compound Parameter
$Fe_{0.5}O_{0.5}$	Periclase (P)	28030 + 12.55T
$Fe_{0.429}O_{0.571}$	Spinel (S)	40170 + 11.63T
$Fe_{0.4}O_{0.6}$	Corundum (C)	51040 + 11.71T
$Cr_{0.4}O_{0.6}$	Corundum (C)	112130 - 8.37T
$Mg_{0.5}O_{0.5}$	Periclase (P)	182004 - 16.74T
$Al_{0.4}O_{0.6}$	Corundum (C)	96650 - 2.51T

for each solution phase with ${}^{\circ}G_i^L$ replaced by ${}^{\circ}G_i^B$, ${}^{\circ}G_i^E$ etc., for the B=bcc, E=hcp phases etc., and with LIJ replaced by BIJ and EIJ etc. In the present symbolism, one uses the symbol FEFELB to designate the free energy of pure liquid iron minus the free energy of pure bcc form of iron. Thus FEFELB= -FEFEBL. Similarly, the free energy of pure liquid chromium minus the free energy of pure bcc chromium is designated by CRCRLB. If I=iron and J=nickel in Equation (1), then Table 10 of Reference 1 shows that LFENI= -8368 + 2.72T (J/g.at.) and LNIFE= -32217 + 9.205T (J/g.at.). Figure 1 and Appendix I shows how the free energy of a solution phase can be described along a specific quasi-binary join in a given ternary system. This approximation is used here to reduce the ternary description to a quasi-binary description in order to employ the information stored in the data bank to deal with high order systems. The free energy, G^{ψ}, of a compound phase $i_{(1-x_*)}{}^{j}x_*$ is defined by Equation (2), (see Equation 14 page 60 of (1)) as

$$G^{\psi} = (1-x_*)\ {}^{\circ}G_i^{\theta} + x_*{}^{\circ}G_j^{\theta} + x_*(1-x_*)\ [(1-x_*)LIJ + x_*LJI\text{-}C[T]] \qquad (2)$$

where θ refers to the base phase selected for the compound and C[T] (which is a temperature dependent function) is the compound parameters. Tables 1-4 define the iron-oxygen, chromium-oxygen, aluminum-oxygen, magnesium-oxygen, iron-magnesium, chromium-magnesium, iron-aluminum, iron-chromium, aluminum-chromium,

TABLE 2

Comparison of Calculated and Observed (18,20) Free Energy of Formation of Binary Oxide Compounds

(All units in Joules per mole, T in Kelvins)
(P=Periclase, S=Spinel, C=Corundum)

Compound	Free Energy of Formation	
	Calculated	Observed
FeO (P)	-267860 + 67.15T	-271120 + 66.94T
Fe_3O_4 (S)	-1166600 + 382.21T	-1086580 + 292.88T
Fe_2O_3 (C)	-894330 + 322.59T	-803328 + 251.04T

$0.5FeO \rightarrow 0.125Fe + 0.125\ Fe_3O_4$; ΔG = -11900 + 14.18T; T_o = 839K

$0.133Fe_3O_4 \rightarrow 0.033 4O_2 \rightarrow 0.2Fe_2O_3$; ΔG = -23700 + 13.71T; T_o = 1726K

	Calculated	Observed
Cr_2O_3 (C)	-1204990 + 276.77T	-1129680 + 251.04T
T=1000	-874460	-928220
1500	-747260	-789830
2000	-618810	-651450
	Calculated	Observed
$A\ell_2O_3$ (C)		
T=1000	-1359800	-1359800
1500	-1202900	-1196620
2000	-1046000	-1035540
	Calculated	Observed
MgO (P)		
T= 500	-552960	-547520
1000	-499360	-492460
1500	-426810	-423840
2000	-322210	-319240
2500	-217610	-215060
3000	-113010	-110460

TABLE 3

Solution Phase Parameters for Several Binary Metal Systems

(All units in Joules per gram atom (mole of atoms), T in Kelvins)

LFEMG = 64850	LFECR = 87000 - 10.46T
LMGFE = 64850	LCRFE = 87000 - 10.46T
LCRMG = 51050	LALCR = -46440
LMGCR = 51050	LCRAL = -46440
LFEAL = -62760 - 4.60T	LALMG = -10040 + 3.35T
LALFE = -96230 + 33.05T	LMGAL = -10040 + 3.35T

TABLE 4

Ternary Liquid Solution Phase Parameters
(For Several Metal-Metal-Oxygen Systems)

(All units in Joules per gram atom (mole of atoms, T in Kelvins)

System	TRNL	System	TRNL
Aℓ-O-Cr	0	Fe-O-Aℓ	1757280 - 1125.5T
Fe-O-Cr	1439300 - 912.1T	Aℓ-O-Mg	1882800 - 1121.3T
Cr-O-Mg	2217520 - 1255.0T		

TABLE 5

Lattice Stability Parameters for Oxides

(All units in Joules per gram atom (mole of atoms), T in Kelvins)

Symbol	Name	Type	Example
C	Corundum	HR 10	$A\ell_2O_3$
S	Spinel	CF 56	Fe_3O_4 (Co_3O_4)
P	Periclase	CF 10	MgO (NaCℓ)

Abbreviations WO = $Fe_{0.5}O_{0.5}$, FO = $Fe_{0.4}O_{0.6}$, HO = $Fe_{0.429}O_{0.571}$

AO = $A\ell_{0.4}O_{0.6}$, CO = $Cr_{0.4}O_{0.6}$, MO = $Mg_{0.5}O_{0.5}$

WOWOLC = 7280 - 7.28T	AOAOLC = 23640 - 10.21T
WOWOLS = 9017 - 6.44T	AOAOLS = 19205 - 9.08T
WOWOLP = 14016 - 8.54T	AOAOLP = 4477 - 12.84T
FOFOLC = 18117 - 8.37T	COCOLC = 34350 - 13.47T
FOFOLS = 15355 - 7.29T	COCOLS = 22594 - 12.55T
FOFOLP = 9414 - 6.28T	COCOLP = 34058 - 15.48T
HOHOLC = 9707 - 9.71T	MOMOLC = 22594 - 12.55T
HOHOLS = 15816 - 8.45T	MOMOLS = 19560 - 10.46T
HOHOLP = 12217 - 7.20T	MOMOLP = 47698 - 15.40T

and aluminum-magnesium systems in order to apply the description shown in Figure 1 and Appendix I. In these Tables, L refers to the liquid phase while B and V refer to the bcc and vapor phase respectively. The symbol MG is used for magnesium, AL for aluminum and OO for $1/2O_2$. Thus, the basis in all cases is one mole of atoms or one gram atom. The numerical values chosen for the lattice stability, solution and compound phase parameters were derived from relevant thermochemical and phase diagram data for oxygen-containing systems (18-24) supplemented by previous assessments of lattice stability (1,17) and solution phase parameters (i.e., iron-chromium (1,2), iron-aluminum and aluminum-chromium (2), aluminum-magnesium (9)). The selection of the ternary liquid interaction parameters for the aluminum-oxygen-chromium, iron-oxygen-chromium, chromium-oxygen-magnesium, iron-oxygen-aluminum and aluminum-oxygen-magnesium systems shown in Table 4 was made on the basis of the data contained in Reference (20). The description of Tables 1-4 permits calculation of the thermochemical properties of the above noted oxide systems and calculation of their phase diagrams under standard (one atom phase pressure) conditions. In addition, it permits calculation of the excess free energy of the liquid phase in the quasi-binary join of a ternary metal-oxygen-metal system as shown in Figure 1 and Appendix I. This facility will be employed subsequently. The calculated iron-oxygen and chromium-oxygen phase diagrams resulting from this

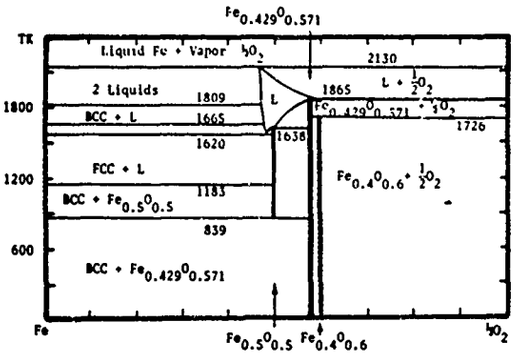

Figure 2. Calculated Iron-Oxygen Phase Diagrams.

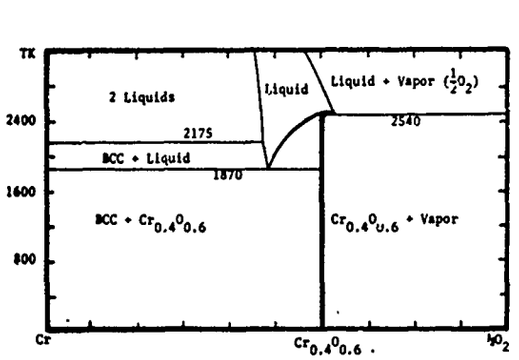

Figure 3. Calculated Chromium-Oxygen Phase Diagram.

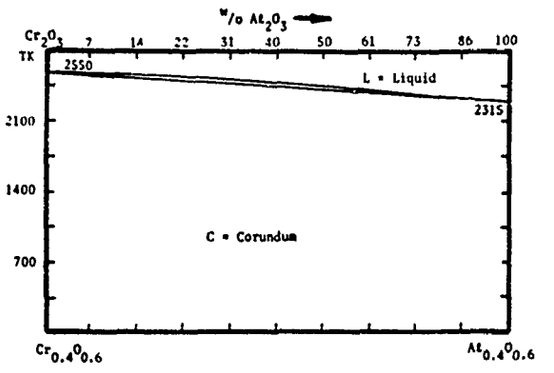

Figure 4. Calculated $Cr_{0.4}O_{0.6}$ - $Al_{0.4}O_{0.6}$ Phase Diagram.

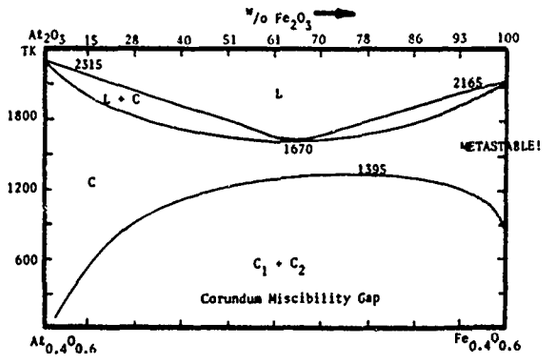

Figure 5. Calculated $Al_{0.4}O_{0.6}$-$Fe_{0.4}O_{0.6}$ Phase Diagram. (Note: Figure 2 shows that $Fe_{0.4}O_{0.6}$ Decomposes into $Fe_{0.429}O_{0.571}$ and $\frac{1}{2}O_2$ above 1726K).

description are shown in Figures 2 and 3. These diagrams are in reasonably good agreement with the observed diagrams if one allows for the idealizations inherent in treating iron oxide (wustite) as a line compound at 50/50 stoichiometry.

3. The Lattice Stability, Solution and Compound Phase Parameters for the Spinel, Periclase and Corundum Structures

Table 5 shows the values derived for the lattice stability of the liquid, L, spinel, S, periclase, P, and corundum, C, structures of the oxides Al_2O_3, Cr_2O_3, MgO, Fe_3O_4, Fe_2O_3 and "FeO". These lattice stability values were employed to compute the quasi-binary phase diagrams shown in Figures 4-15. It should be noted that the lattice stability values are given for a gram atom (one mole of atoms) of each of the oxides! Moreover, examination of Table 5 shows that a gram atom of each of the oxides (i.e., $Cr_{0.4}O_{0.6}$) has been assigned a specific abbreviation (i.e.) CO = $Cr_{0.4}O_{0.6}$. The g-atom free energy of the liquid minus the corundum form of $Cr_{0.4}O_{0.6}$ is designated by the symbol COCOLC and equals 34350 - 13.47T Joules as shown in Table 5. In direct analogy to the discussion of solution phase parameters in Section 2 above, the solution phase

TABLE 6

Quasibinary Solution Parameters for Oxide Systems

(All units in Joules per gram atom (mole of atoms), T in Kelvins)

LAOCO = -7422 + 13.05T		LAOFO = -14297 + 5.65T	
SAOCO = -7422 + 13.05T		SAOFO = -14297 + 5.65T	
PAOCO = -7422 + 13.05T		PAOFO = 6623 + 5.65T	
CAOCO = -7422 + 13.05T		CAOFO = 6623 + 5.65T	
LAOHO = -20350 + 11.25T		LAOMO = -33530 + 22.93T	
SAOHO = -20350 + 11.25T		SAOMO = -33530 + 22.93T	
PAOHO = 570 + 11.25T		PAOMO = 29230 - 4.69T	
CAOHO = 570 + 11.25T		CAOMO = -12610 + 22.93T	
LAOWO = -39330 + 25.73T		LCOAO = -7422 + 13.05T	
SAOWO = -39330 + 25.73T		SCOAO = -7422 + 13.05T	
PAOWO = -18410 + 25.73T		PCOAO = -7422 + 13.05T	
CAOWO = -18410 + 25.73T		CCOAO = -7422 + 13.05T	
LCOFO = -26080 + 19.16T		LCOHO = -37780 + 26.19T	
SCOFO = -26080 + 19.16T		SCOHO = -37780 + 26.19T	
PCOFO = -26080 + 19.16T		PCOHO = -4310 + 15.73T	
CCOFO = 7390 + 8.70T		CCOHO = -4310 + 15.73T	
LCOMO = 780 + 7.45		LCOWO = -70760 + 44.22T	
SCOMO = 780 + 7.45		SCOWO = -70760 + 44.22T	
PCOMO = 21700 + 3.26		PCOWO = -49840 + 44.22T	
CCOMO = 21700 + 7.45		CCOMO = -37290 + 33.76T	
LFOAO = 58150 - 30.03T		LFOCO = 41000 - 18.49T	
SFOAO = 58150 - 30.03T		SFOCO = 41000 - 18.49T	
PFOAO = 79070 - 30.03T		PFOCO = 41000 - 18.49T	
CFOAO = 79070 - 30.03T		CFOCO = 41000 - 18.49T	
LFOMO = -51350 + 26.82T		LHOAO = 59390 - 35.77T	
SFOMO = -51350 + 26.82T		SHOAO = 59390 - 35.77T	
PFOMO = -9510 + 14.27T		PHOAO = 80310 - 35.77T	
CFOMO = -30430 + 26.82T		CHOAO = 80310 - 35.77T	
LHOCO = 37810 - 15.44T		LHOMO = -30040 + 19.75T	
SHOCO = 37810 - 15.44T		SHOMO = -34220 + 19.75T	
PHOCO = 37810 - 15.44T		PHOMO = 6360 + 11.38T	
CHOCO = 37810 - 15.44T		CHOMO = -9120 + 19.75T	
LMOAO = 59910 - 27.11T		LMOCO = 87520 - 39.96T	
SMOAO = 59910 - 27.11T		SMOCO = 87520 - 39.96T	
PMOAO = 122670 - 54.73T		PMOCO = 108440 - 44.14T	
CMOAO = 80830 - 27.11T		CMOCO = 87520 - 39.96T	
LMOFO = -22340 + 13.56T		LMOHO = -10370 + 10.54T	
SMOFO = -22340 + 13.56T		SMOHO = -14556 + 10.54T	
PMOFO = 18500 + 1.00T		PMOHO = 26030 + 2.18T	
CMOFO = -2420 + 13.56T		CMOHO = 10550 + 10.54T	
LMOWO = 16890 - 4.06T		LWOAO = 63180 - 31.71T	
SMOWO = 16890 - 4.06T		SWOAO = 63180 - 31.71T	
PMOWO = 8520 - 4.06T		PWOAO = 84100 - 31.71T	
CMOWO = 8520 - 4.06T		CWOAO = 84100 - 31.71T	

TABLE 6 (continued)

LWOCO = 31440 - 10.00T	LWOMO = 16800 + 3.93T
SWOCO = 31440 - 10.00T	SWOMO = 16800 + 3.93T
PWOCO = 50840 - 10.00T	PWOMO = 8430 + 3.93T
CWOCO = 31440 - 10.00T	CWOMO = 8430 + 3.93T

TABLE 7

Quasibinary Compound Parameters for Oxide Systems

(All units in Joules per gram atom (mole of atoms) T in Kelvins)

Compound	Structure	Base	Compound Parameters
$(Al_{0.286}O_{0.428})\cdot(Mg_{0.143}O_{0.143})$	(SP)	(S)	74050
$(Al_{0.286}O_{0.428})\cdot(Fe_{0.146}O_{0.143})$	(SP)	(S)	40580 + 7.11T
$(Cr_{0.286}O_{0.428})\cdot(Mg_{0.143}O_{0.143})$	(SP)	(S)	134720 - 7.11T
$(Cr_{0.286}O_{0.428})\cdot(Mg_{0.143}O_{0.143})$	(SP)	(S)	38910 + 16.74T
$(Fe_{0.286}O_{0.428})\cdot(Mg_{0.143}O_{0.143})$	(SP)	(S)	18410 + 13.72T
$(Fe_{0.306}O_{0.408})\cdot(Mg_{0.143}O_{0.143})$	(SP)	(S)	0

TABLE 8

Comparison of Calculated and Observed (20) Free Energies of Formation of Complex Spinel Oxides

(P=Periclase, C=Corundum, SP=Spinel)

Reaction	Free Energy of Formation, Joules, T in Kelvins	
$FeO(P) + Al_2O_3(C) \rightarrow FeO\cdot Al_2O_3(SP)$	-40070 - 6.74T	(CALC)
	-39740 - 7.12T	(OBS)
$MgO(P) + Cr_2O_3(C) \rightarrow MgO\cdot Cr_2O_3(SP)$	-40770 - 13.03T	(CALC)
	-41120 - 14.00T	(OBS)
$MgO(P) + Al_2O_3(C) \rightarrow MgO\cdot Al_2O_3(SP)$	-36961 - 3.22T	(CALC)
	-35560 - 2.05T	(OBS)
$FeO(P) + Cr_2O_3(C) \rightarrow FeO\cdot Cr_2O_3(SP)$	-46100 + 8.32T	(CALC)
	-45190 + 8.38T	(OBS)
$MgO(P) + Fe_2O_3(C) \rightarrow MgO\cdot Fe_2O_3(C)$	-20940 - 2.20T	(CALC)
	-19330 - 2.05T	(OBS)

parameters for one gram atom of the liquid on the Al_2O_3-MgO join of the Al-O-Mg system are designated by LAOMO and LMOAO. These parameters have been computed from Tables 1-4 and the procedure outlined in Appendix I, and are also displayed in Table 6. Reference to Table 6 shows that LAOMO = -33530 + 22.93T and LMOAO = 59910 - 27.11T respectively.

Tables 6-8 summarize the solution phase parameters for the remaining phases (i.e., C, corundum, S, spinel, P, periclase). Thus the solution parameters for one gram atom of the corundum solution in the $Al_{0.4}O_{0.6}$-$Cr_{0.4}O_{0.6}$ join of the Al-O-Cr system, can be read as CAOCO = -7422 + 13.05T and CCOAO = -7422 + 13.05T Joules respectively. Tables 7 and 8 display the compound parameters employed in calculating the quasi-binary phase diagrams shown in Figures 4-15. Table 8 shows that these same parameters can be employed to generate the free energy of formation of complex spinel oxides in agreement with observation (20).

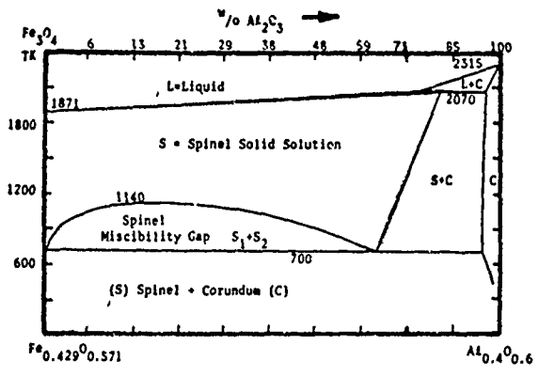

Figure 6. Calculated $Fe_{0.429}O_{0.571}$-$Al_{0.4}O_{0.6}$ Phase Diagram.

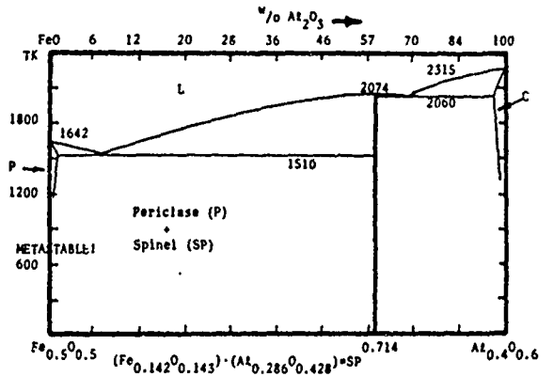

Figure 8. Calculated $Fe_{0.5}O_{0.5}$-$Al_{0.4}O_{0.6}$ Phase Diagram. (Note: Figure 2 shows that $Fe_{0.5}O_{0.5}$ Decomposes into Fe and $Fe_{0.429}O_{0.571}$ below 839).

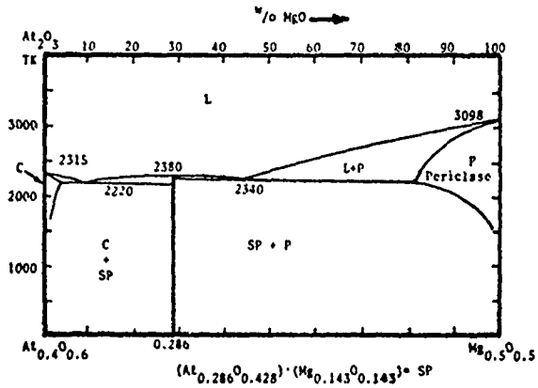

Figure 7. Calculated $Al_{0.4}O_{0.6}$-$Mg_{0.5}O_{0.5}$ Phase Diagram.

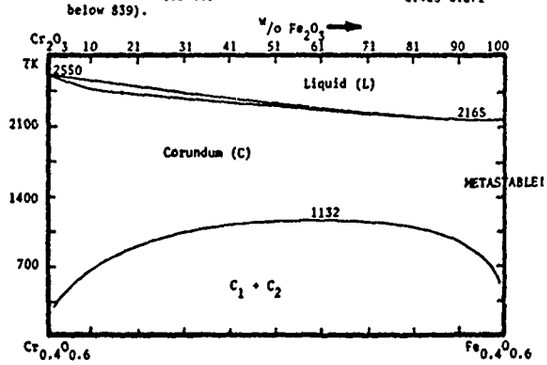

Figure 9. Calculated $Cr_{0.4}O_{0.6}$-$Fe_{0.4}O_{0.6}$ Phase Diagram (Note: Figure 2 shows that $Fe_{0.4}O_{0.6}$ Decomposes into $Fe_{0.429}O_{0.571}$ and $\frac{1}{2}O_2$ above 1729K.

Thus the definitions of Equations (1) and (2) coupled with the quasi-binary approximation shown in Appendix I and parameters shown in Tables 1-8 generate the one atmosphere, thermochemical properties and phase diagrams for the quasi-binary joins displayed in Figures 4-15.

4. Discussion Of The Results Of The Quasi-Binary Approximation

Table 5 provides the "liquid-solid" free energy differences (and the lattice stability parameters) for the six oxides of current interest. Thus, AOAOLC is equal to the free energy of liquid $Al_{0.4}O_{0.6}$ (i.e., $1/5Al_2O_3$) minus the free energy of the corundum form of $Al_{0.4}O_{0.6}$. Information on the heat of fusion for the stable forms of each oxide was taken from review publications and recent experimental studies (18,20,25). As indicated earlier, AOAOLS and AOAOLP represent the corresponding free energy differences between the liquid and spinel and the liquid and periclase forms. This description permits calculation of the free energy differences between the C, S and P forms since

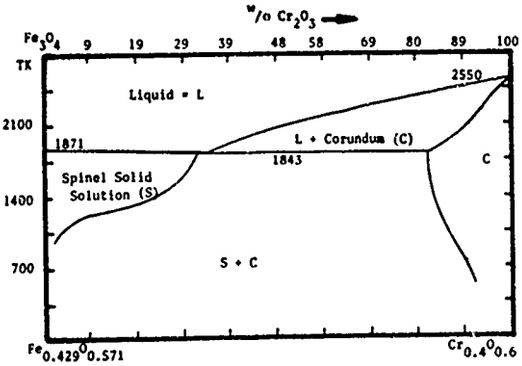

Figure 10. Calculated $Fe_{0.429}O_{0.571}$-$Cr_{0.4}O_{0.6}$ Phase Diagram.

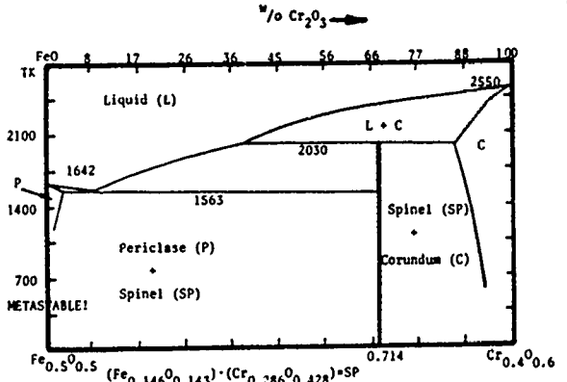

Figure 12. Calculated $Fe_{0.5}O_{0.5}$-$Cr_{0.4}O_{0.6}$ Phase Diagram. (Note: Figure 2 shows that $Fe_{0.5}O_{0.5}$ decomposes into Fe and $Fe_{0.429}O_{0.571}$ below 839).

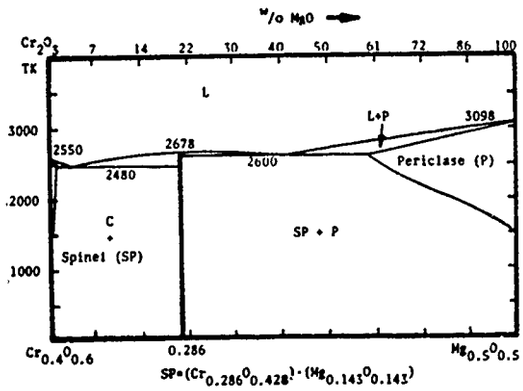

Figure 11. Calculated $Cr_{0.4}O_{0.6}$-$Mg_{0.5}O_{0.5}$ Phase Diagram.

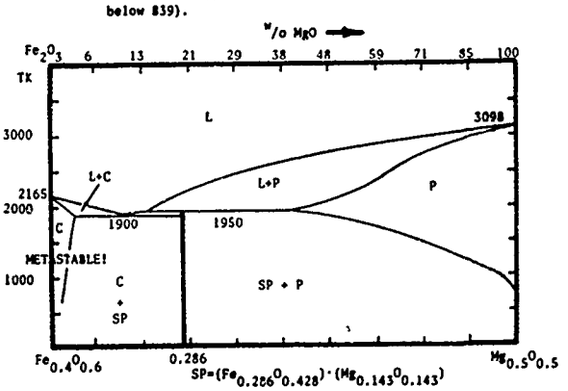

Figure 13. Calculated $Fe_{0.4}O_{0.6}$-$Mg_{0.5}O_{0.5}$ Phase Diagram. (Note: Figure 2 shows that $Fe_{0.4}O_{0.6}$ decomposes into $Fe_{0.429}O_{0.571}$ and $\frac{1}{2}O_2$ above 1726).

the free energy of the spinel form minus the free energy of the corundum form of $Al_{0.4}O_{0.6}$, AOAOSC, is equal to AOAOLC - AOAOLS = 4435 - 1.13T J/g.at. The enthalpy difference of 4435 J/g.at. is in keeping with experimentally observed results (26,28). A similar conclusion can be drawn for the enthalpy difference of 2762 J/g.at. between the spinel and corundum forms of $Fe_{0.4}O_{0.6}$ derived from the difference FOFOLC - FOFOLS given in Table 5 (26,28). The lattice stability parameters shown in Table 5 were derived by using experimental values as a base and "filling in" the missing components by performing an "ideal solution" iteration on Figures 4-15 as in the case of metals (16,17). The solution phase parameters for the liquid shown in Table 6 are fixed by the procedure outlined in Appendix I and the results for the metal-oxygen, metal-metal and metal-oxygen-metal systems shown in Tables 1-4. Reference to Table 6 discloses that the corresponding values for the S, P and C solid solutions are usually equal to, or more positive than the L parameters. The S, spinel solution parameters are usually equal to the liquid parameters while the periclase, P, and corundum, C, parameters are usually more positive than

L and S (and equal). These small differences were obtained by iterative calculation of Figures 4-15 starting with equal values of L, S, P and C.

Finally, the quasi-binary compound parameters shown in Table 7 were fixed to yield conformity with the phase diagram and the observed thermochemical data shown in Table 8.

5. Calculation of the Activity of Quasibinary and Ternary Components of Solution Phases

Defining the activity of quasi-binary components across a given join is quite straightforward (2) based on the definitions of Equation (1). Thus, the activity of CO and AO in the C phase of the CO-AO system (Fig. 4) where x is the fraction of AO and the reference states are pure corundum CO and pure corundum AO is given by Equation (3) and (4) as

$$RT\ell na^{C}_{CO} = RT\ell n(1-x) + x^2[CCOAO+(2x-1)(CAOCO-CCOAO)] \quad (3)$$

and

$$RT\ell na^{C}_{AO} = RT\ell nx + (1-x)^2\,[CCOAO+2x(CAOCO-CCOAO)] \quad (4)$$

Similar expressions can be generated for each of the phases. Derivation of equations for the activity of the ternary components (i.e., Cr, O and Aℓ) can only be carried out for the liquid phase where the free energy has been explicitly stated in terms of ternary components (and not in terms of end members on a given binary join). To illustrate this procedure, consider the liquid Aℓ-O-Mg case where it is desired to compute $RT\ell na^{L}_{A\ell}$, $RT\ell na^{L}_{Mg}$ and $RT\ell na^{L}_{O}$. In the case of the first two components, $a^{L}_{A\ell} = p^{L}_{A\ell}/{}^{\circ}p^{L}_{A\ell}$ and $a^{L}_{Mg} = p^{L}_{Mg}/{}^{\circ}p^{L}_{Mg}$ where p^{L}_{AL} and p^{L}_{Mg} are the vapor pressures of Al and Mg over the liquid oxide and ${}^{\circ}p^{L}_{A\ell}$ and ${}^{\circ}p^{L}_{Mg}$ are the vapor pressures of the pure metals at the temperature in question. A similar result holds for the oxygen with a slight complication due to the use of $(1/2)O_2$ as a component! Thus $a^{L}_{O}=(p^{L}_{O_2}/{}^{\circ}p^{L}_{O_2})^{1/2}$ and since $0.5RT\ell n{}^{\circ}p^{L}_{O_2} = 0000LV = -3410 + 37.9T$ at one atmosphere, then $RT\ell np^{L}_{O_2} = -6820 + 75.8T + 2RT\ell na^{L}_{O}$, where $p^{L}_{O_2}$ is the pressure in atmospheres. The equations for component activities and vapor pressures can now be written explicitly as Equations (5)-(7) for the Aℓ-O-Mg case where x is the fraction of O and y is the fraction of Mg. Note that along the $A_{0.4}O_{0.6}$-$Mg_{0.5}O_{0.5}$ join the

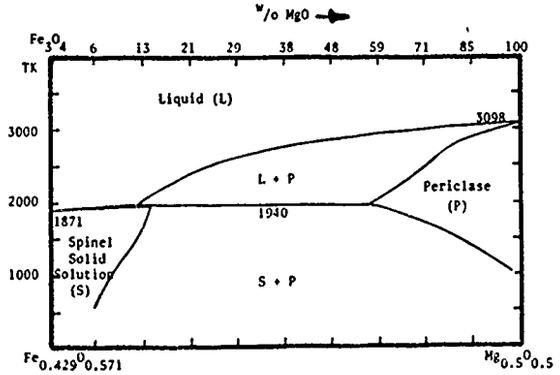

Figure 14. Calculated $Fe_{0.429}O_{0.571}$-$Mg_{0.5}O_{0.5}$ Phase Diagram.

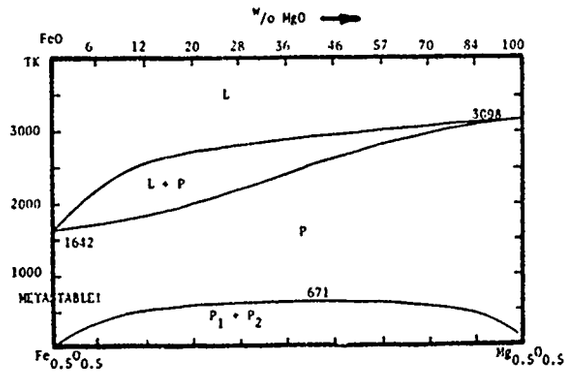

Figure 15. Calculated $Fe_{0.5}O_{0.5}$-$Mg_{0.5}O_{0.5}$ Phase Diagram. (Note: Figure 2 shows that $Fe_{0.5}O_{0.5}$ Decomposes into Fe and $Fe_{0.429}O_{0.571}$ Below 839K).

fraction of O varies from x = 0.6 when y = 0 to x = 0.6-0.2y. Nevertheless, Equations (5)-(7) apply to all values of x and y (17).

$$RT\ell n a^{L}_{A\ell} = RT\ell n(1-x-y) + x^2 LALOO + y^2 LALMG + xy[LALOO + LALMG - LOOMG] + x^2\left[\frac{x(2-y)}{(1-y)^2} - 1\right](LOOAL-LALOO) + y^2\left[\frac{y(2-x)}{(1-x)^2} - 1\right](LMGAL-LALMG) \frac{-xy^2}{(x+y)}(LMGOO-LOOMG) - xy[1-2(x+y)]TRNL(A\ell-O-Mg) \quad (5)$$

$$RT\ell n a^{L}_{O} = RT\ell n x + (1-x)^2 LALOO + y^2 LALMG - y(1-x)[LALOO + LALMG - LOOMG] + x^2\left[\frac{x(2-y)}{(1-y)^2} + \frac{(2-3x-2y)}{x(1-y)} - 1\right](LOOAL-LALOO) + y^2\left[\frac{y}{1-x} - 1\right](LMGAL-LALMG) \frac{+y^2}{(x+y)^2}[y(1-x)-x^2](LMGOO-LOOMG) + [y(1-y)-xy(3-2(x+y))]TRNL(A\ell-O-Mg) \quad (6)$$

$$RT\ell n a^{L}_{Mg} = RT\ell n y + x^2 LALOO + (1-y)^2 LALMG - x(1-y)[LALOO + LALMG - LOOMG] + x^2\left[\frac{x}{1-y} - 1\right](LOOAL-LALOO) + y^2\left[\frac{y(2-x)}{(1-x)^2} + \frac{(2-3y-2x)}{y(1-x)} - 1\right](LMGAL-LALMG) \frac{+xy}{(x+y)^2}[2x+y-xy-y^2](LMGOO-LOOMG) + [x(1-x)-xy(3-2(x+y))]TRNL(A\ell-O-Mg) \quad (7)$$

These equations can be employed to calculate the activity and vapor pressure of each elemental component in the liquid phase at any composition. Conversely they can be used to calculate the composition at a given oxygen pressure!

6. Calculation of Quasi-Ternary Phase Diagrams

The extension to quasi-ternary systems can be readily accomplished by letting each of the components i.e., CO, AO, FO etc., play the role of the elements in Appendix I and References (1) and (2). Figures 16-21 show the resulting isothermal sections computed for the Fe_3O_4-Cr_2O_3-$A\ell_2O_3$, MgO-Fe_3O_4-$A\ell_2O_3$ and MgO-Cr_2O_3-$A\ell_2O_3$ at selected temperatures. In line with previous practice,

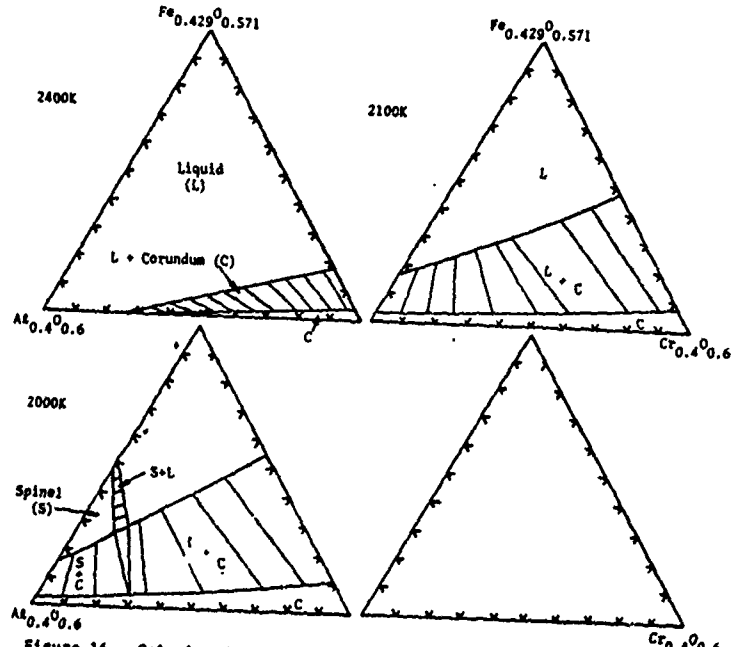

Figure 16. Calculated Isothermal Sections in the $Fe_{0.429}O_{0.571}$-$Cr_{0.4}O_{0.6}$-$A\ell_{0.4}O_{0.6}$ System.

the free energy of ternary solution phases are synthesized from their binary edge components by using Kohler's Equation (Appendix I) with a zero ternary interaction parameter. The free energy of ternary compound phases is defined along specific joins (see Reference 2, p 2117, Eqs. (1,8). As an example, we consider the spinel compound phase in the system AO-MO-CO (see Figure 21). This compound runs between the $Al_2O_3 \cdot MgO$ and $Cr_2O_3 \cdot MgO$ compositions designated (Table 7) as $(Al_{0.286}O_{0.428}) \cdot (Mg_{0.143}O_{0.143})$ and $(Cr_{0.286}O_{0.428}) \cdot (Mg_{0.143}O_{0.143})$. If x is the fraction MO and y is the fraction CO then the free energy of the spinel (SP) compound $AO_{(1-x_*^1)}MO_{x_*^1} - CO_{(1-x_*)}MO_{x_*}$ is given by Equation (8) as

$$G^{SP} = (1-x-y)G^S_{AO} + xG^S_{MO} + yG^S_{CO} + RT[y\ell ny+(1-x-y)\ell n(1-x-y)+(1-x)\ell n(1-x)] + [1 - \frac{y}{1-x}]\Delta G_A + (\frac{y}{1-x})\Delta G_B + \Delta G_E \quad (8)$$

where

$$\Delta G_E = 0,\ \Delta G_A = (1-x_*^1)x_*^1\ [(1-x_*^1)\ LAOMO + x_*^1 LMOAO - C_A]$$
$$\Delta G_B = (1-x_*)x_*\ [(1-x_*)\ LCOMO + x_*\ LMOCO - C_B] \quad (9)$$

and

$$x = x_*^1 + yp\ ;\ p = (x_* - x_*^1)/(1-x_*),\ x_*^1 = 0.286,\ x_* = 0.286,\ p = 0$$
$$C_A = 74050 \text{ and } C_B = 38910 + 16.74T \quad \text{(From Table 8)} \quad (10)$$

7. Discussion of Results

The present description of the iron-oxygen system summarized in Tables 1 and 2 which generate Figure 1, lead to the calculated expressions for the free energy of formation of "FeO", Fe_3O_4 and Fe_2O_3 shown in Table 2. These calculated free energies of formation can be employed to examine the decomposition of "FeO" into iron and Fe_3O_4 on cooling or the decomposition of Fe_2O_3 into Fe_3O_4 and oxygen gas on heating. Table 2 shows these calculations which are the basis upon which the reaction isotherms shown in Figure 2 were constructed. Any self consistent system of thermochemical data for this system would be required to generate the appropriate values of T_o for these decomposition reactions (i.e., 839K and 1726K respectively). Nevertheless in many instances, this test is not made!

Figure 2 shows that "FeO" is not stable below 839K. Consequently the quasi-binary joins which

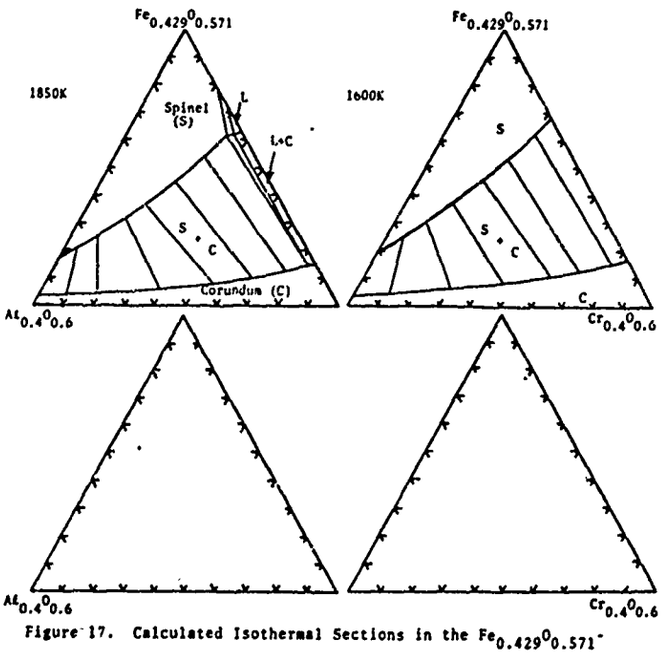

Figure 17. Calculated Isothermal Sections in the $Fe_{0.429}O_{0.571}$-$Cr_{0.4}O_{0.6}$-$Al_{0.4}O_{0.6}$ System.

include the $Fe_{0.5}O_{0.5}$ (i.e., WO) component (e.g., Figs 8, 12 15) are metastable with respect to the decomposition of WO below 839K. In a similar fashion, Figure 2 shows that $Fe_{0.4}O_{0.6}$ decomposes above 1726K. Thus each of the joins containing the component (FO) is metastable above 1726K. As a consequence, Figures 5, 9 and 13 illustrate this metastability. Thus the lattice stability, solution and compound phase parameters for the elemental components, and their binary combinations, shown in Tables 1-3, were employed to characterize the thermochemical properties and the phase diagrams of the iron-oxygen, aluminum-oxygen, magnesium-oxygen, chromium-oxygen, iron-magnesium, chromium- magnesium, iron-aluminum, iron-chromium, aluminum-chromium and aluminum-magnesium systems. These binary systems form the edges of the Aℓ-O-Cr, Fe-O-Cr, Cr-O-Mg, Fe-O-Aℓ and Aℓ-O-Mg ternary systems in which the quasi-binary "joins" of interest lie. Therefore, the development of the present base is built on defining the three edge binary systems (i.e., generating a small number of lattice stability, solution and compound parameters capable of being used to compute the binary phase diagrams and thermochemical properties) and then using the quasi-binary approximation shown in Appendix I to develop a description of the liquid free energy on a specific quasi-binary "join" in the ternary! The results of this procedure is shown in Table 6. These results are then combined with the lattice stability values for the quasi-binary components shown in Table 5 and the remaining solution phase parameters shown in Table 6 to compute the "quasi-binary" phase diagrams shown in Figures 4-15. Stable compound phases (mainly spinels (SP) are added by defining a base-phase (S) and a compound parameter as shown in Table 7. The resulting free energy of the compound must be consistent with the observed free energy of formation of the complex compound from it's "quasi-binary" components and the quasi-binary phase diagram. The means employed to define the free energy of the quasi-binary compound is identical to that employed for binary compounds (1-5, 17) and can be seen explicitly by considering the case of the spinel $AO_{0.714}MO_{0.286}$, which can be described as (1/7) ($Aℓ_2O_3 \cdot MgO$) or $(Aℓ_{0.286}O_{0.428}) \cdot (Mg_{0.143}O_{0.143})$. Reference to Tables 6 and 7; Figure 7 and Equations 8 and 9 illustrate how the present definitions fix the free energy of this compound. For example, the discussion of Equations 8-10 deals with the $AO_{0.714}MO_{0.286}$ - $CO_{0.714}MO_{0.286}$ join in which the fraction of CO is equal to y. When y = 0, Equation (8) provides a description of the free energy of the $AO_{0.714}MO_{0.286}$ (SP) spinel which is equal to:

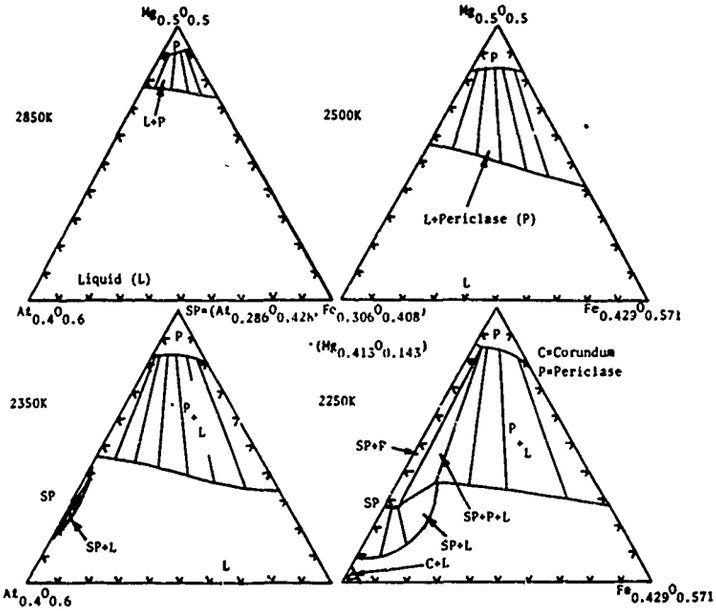

Figure 18. Calculated Isothermal Sections in the $Mg_{0.5}O_{0.5}$-$Fe_{0.429}O_{0.571}$-$At_{0.4}O_{0.6}$ System.

$$G^{SP} = 0.714G^{S}_{AO} + 0.286G^{S}_{MO} + (0.714)(0.286)[0.714LAOMO + 0.286LMOAO - C] \quad (11)$$

Reference to Tables 6 and 7 show that LAOMO = -33530 + 22.93T, LMOAO = 59910 - 27.11T and C = 74050 Joules respectively! These numerical parameters provide a means of defining the free energy of the compound (1/7) ($Al_2O_3 \cdot MgO$) (SP). The free energy of formation of this compound from the stable forms of alumina and magnesia (e.g., (1/5) Al_2O_3(C) and (1/2)MgO(P) is readily obtained by adding the quantities 0.714AOAOSC and 0.286 MOMOSP to the expression for G^{SP} in Equation (11). The result, -5280 - 0.460T Joule/g.at. is then multiplied by seven and displayed in Table 8 as the calculated free energy change in Joules for the formation of $MgO \cdot Al_2O_3$(SP) from Al_2O_3(C) and MgO(P) i.e., -36961 - 3.22T Joules. It is also compared with the observed value (20) of -35560 - 2.05T Joules.

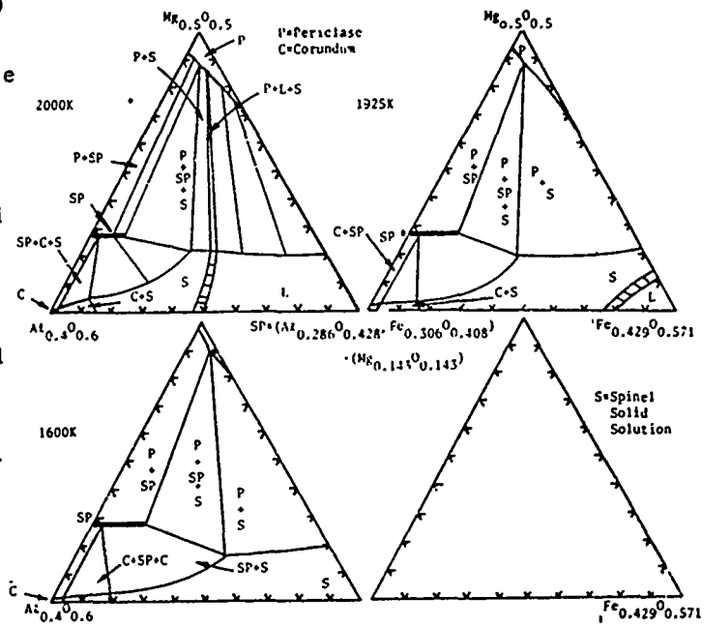

Figure 19. Calculated Isothermal Sections in the $Mg_{0.5}O_{0.5}$-$Fe_{0.429}O_{0.571}$-$Al_{0.4}O_{0.6}$ System.

In summary, Tables 5-8 and Figures 4-15 illustrate how the descriptions of the elemental edge binary systems are employed to synthesize the quasi-binary joins of interest within ternary systems which are composed of the elemental edge binaries.

The stability of the computed "quasi-binary joins" must be considered within the framework of the approximations noted in the earlier discussions of "FeO" (WO) and Fe_2O_3(FO). In particular, each of the computed "joins" shown in Figures 4-15 can be undercut by more stable interactions along intersecting joins in the same ternary. Such interactions are not likely across the joins between CO, AO, MO and HO. However joins in which FO and WO are partners may be susceptible to such intersections by competing pairs of compounds or solution phases within the elemental ternary system which lie on intersecting joins! Such interactions must be considered in computing the most stable configuration.

The extension of the computations into quasi-ternary systems is illustrated in Figures 16-21 for selected isothermal sections of the HO-CO-AO, MO-HO-AO and MO-CO-AO systems over a range of temperatures. These computations are carried out in a straightforward manner employing the methods and definitions detailed earlier. Development of such sections as a means for guiding experimental establishment of isothermal sections in such systems is probably the most useful application of the present framework. Indeed very little experimental data exist with which to compare the predicted results. Only the isothermal section of Greshkovich and Subican (30) in the MO-CO-AO system at 1973K which is shown in Figure 21 could be found for comparison with the computed results. The current framework can also be employed to predict interesting compositions for eutectic solidification or precipitation reactions on aging after high temperature solution treatment. The periclase solid solution in the MO-HO-AO and MO-CO-AL systems displayed in Figures 18-21 exhibits an extensive range of stability at high temperature which is sharply restricted

at lower temperatures. In both systems the complex spinel phase limits the range of stability of the periclase structure. Under such conditions, solution treatment at high temperatures (i.e., 2500K) followed by low temperature aging (i.e., below 1300K) could be employed to strengthen the periclase matrix.

8. Summary

A data base has been presented for describing the thermochemical properties and the phase diagrams for a group of six oxides. Treatment of these oxides as components of quasi-binary joins in true ternary systems has been employed to develop a quasi-binary approximation which can then be used to compute higher order systems for purposes of phase diagram computation and prediction of thermochemical properties.

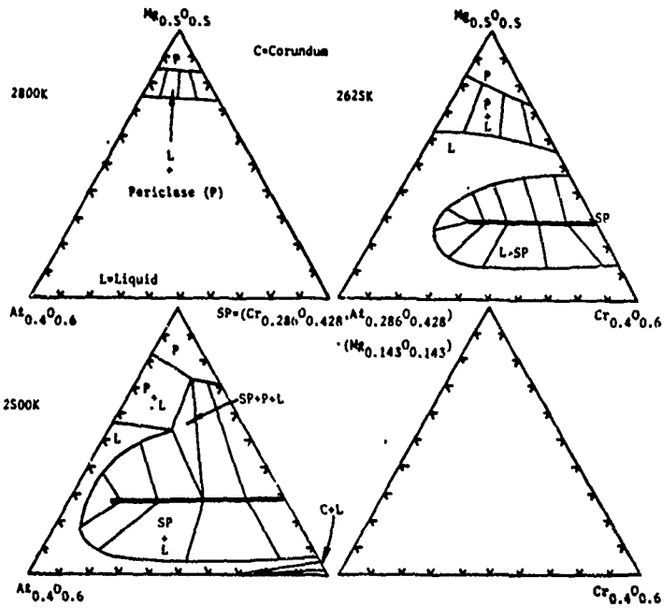

Figure 20. Calculated Isothermal Sections in the $Mg_{0.5}O_{0.5}$-$Cr_{0.4}O_{0.6}$-$Al_{0.4}O_{0.6}$ System.

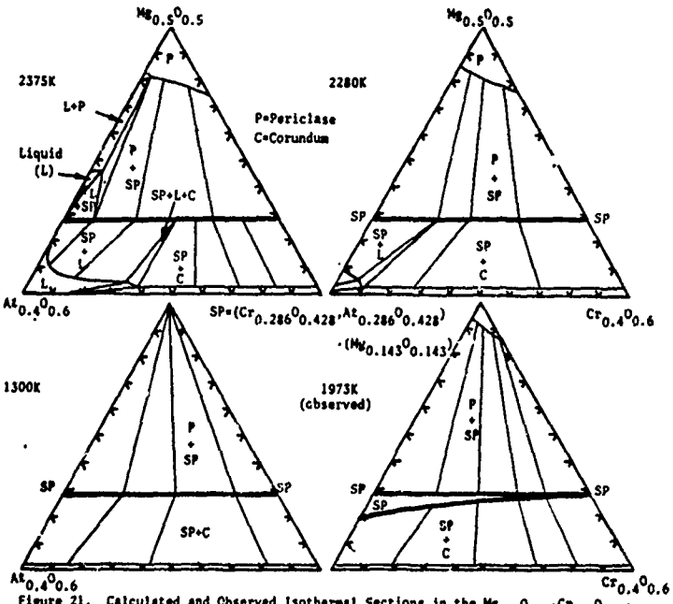

Figure 21. Calculated and Observed Isothermal Sections in the $Mg_{0.5}O_{0.5}$-$Cr_{0.4}O_{0.6}$-$Al_{0.4}O_{0.6}$ System. Observed Section at 1973K after Greshkovich and Stubican (50).

References

1. L. Kaufman CALPHAD 1, 7 (1977).
2. L. Kaufman and H. Nesor, Metallurigcal Transactions 5, 1617, 1623 (1975), 6A 2115, 2123 (1976).
3. L. Kaufman and H. Nesor, Canadian Metallurgical Quarterly 14, 221 (1975).
4. L. Kaufman and H. Nesor, Proceedings of the Second Conference on In-Situ Composites p 11, M. R. Jackson, J. L. Walter, F. D. Lemkey and R. W. Hertzberg Eds., Xerox Individualized Publishers, Lexington, Massachusetts (1976).
5. L. Kaufman and H. Nesor, Proceedings of International Symposium on Computer Simulation for Materials Applications p 63. Nuclear Metallurgy 20 (Part 1) R. J. Arsenault, J. R. Beeler and J. A. Simmons Eds., AIME, New York, N.Y., (1976).
6. M. Hillert and M. Waldenstrom, CALPHAD 1 97 (1977).
7. R. Lundberg, M. Waldenstrom and B. Uhrenius, CALPHAD 1 159 (1977).
8. C. Chatfield and M. Hillert, CALPHAD 1 201 (1977).
9. M. L. Saboungi and C. C. Hsu, CALPHAD 1 237 (1977).
10. A. D. Pelton and C. W. Bale, CALPHAD 1 253 (1977).
11. T. G. Chart, J. F. Counsell, G. P. Jones, W. Slough and P. J. Spencer, International Metallurgical Reviews 20 57 (1975).
12. T. Margaria, C. Alibert, I. Ansara and J. Driole, High Temperatures-High Pressures 8 451 (1976).
13. Proceedings of a Workshop on "Applications of Phase Diagrams in Metallurgy and Ceramics" National Bureau of Standards, Gaithersburg, Maryland, C. G. Carter and L. H. Bennett, Eds., (1977).
14. A. D. Pelton and H. Schmalried, Met. Trans. 4 1395 (1973).
15. G. Kaestle and K. Koch, "Zur Berechenung Von Phasendiagramen oxidischer Mehrstoff system mit Hilf Von mathematisch thermodynamischen Modellen" (to be published) CALPHAD 2 (1978).
16. L. Kaufman, Phase Stability in Metals and Alloys, P. S. Rudman, J. Stringer and R. Jaffee Eds, p 125 McGraw Hill, New York (1967).
17. L. Kaufman and H. Beinstein, Computer Calculation of Phase Diagrams, Academic Press, New York (1970).
18. M. Gleiser and J. F. Elliott, Thermochemistry for Steelmaking, Addison-Wesley, Reading, Massachusetts.
19. R. Hultgren, P. D. Desai, D. T. Hawkins, M. Gleiser and K. K. Kelly, Selected Values of the Thermodynamic Properties of Metals (and of Binary Alloys) (2 Volumes) ASM, Metals Park, Ohio (1973).
20. O. Kubaschewski, High Temperatures-High Pressures 4 1 (1972).
21. M. Hansen and K. Anderko, Constitution of Binary Alloys, McGraw Hill, New York (1958).
22. R. P. Elliott and F. Shunk, First Supplement (Ibid) (1965).
23. F. Shunk, Second Supplement (Ibid) (1969).
24. E. M. Levin, C. R. Robbins and H. F. McMurdie, Phase Diagrams for Ceramists, American Ceramics Sociey Columbus, Ohio (1964), First Supplement (Ibid) (1969), Second Supplement Ibid (1975).
25. E. N. Fomichev, V. P. Bondorenko and V. V. Kandyba, High Temperatures-High Pressures 5 1 (1973).

26. J. P. Sharples and A. Navrotsky, J. Solid State Chem. 12 126 (1975).

27. T. Yokokawa and O. J. Kleppa, J. Phys. Chem. 68 3246 (1964).

28. A. Ferrier, Comptes Rend. Academy Sci., Paris C246 919 (1967).

29. W. B. Pearson, Lattice Spacing and Structure of Metals 2 3 (1967), Pergamon Press, Oxford.

30. C. Greshkovich and V. S. Stubican J. American Ceramics Soc., 51 43 (1968).

APPENDIX I

Quasibinary Approximation to the Free Energy of Solution Phases (Mass Basis, One Gram Atom or One Mole of Atoms) (See Figure 1)

$$G^L=(1-x-y)\circ G_i^L+x\circ G_j^L+y\circ G_k^L+RT[(1-x-y)\ell n(1-x-y)+x\ell nx+y\ell ny]+{}^EG^L[x,y,T] \quad (A-1)$$

$${}^EG^L[x,y,T]=x(1-x-y)(1-y)^{-1}[(1-x-y)LIJ+xLJI]+y(1-x-y)(1-x)^{-1}[(1-x-y)LIK+yLKI]$$
$$+xy(x+y)^{-1}[xLJK+yLKJ]+xy(1-x-y)TRNL \quad (A-2)$$

where LIJ, LJI, LIK, LKI, LJK, LKJ and TRNL are all temperature dependent functions. If one considers the vertical plane which cuts G^L and contains the compositions $x=x_*^1$, $y=0$ and $x=x_*$, $y=1-x_*$, with a quasi binary definition of the excess free energy as

$${}^EG^L=\xi(1-\xi)[(1-\xi)L_1+\xi L_2] \quad (A-3)$$

where $\xi=(x-x_*^1)(x_*-x_*^1)^{-1}$, $y=\xi(1-x_*)$ and $(1-x-y)=(1-x_*^1)(1-\xi)$

The explicit relationship between L_1 and L_2 and the terms LIJ, LJI, LIK, LKI, LJK, LKJ and TRNL shown in Equation (A-2) can be obtained by equating the ternary and quasi binary descriptions shown in Figure 1 at $\xi=0$, 1/3, 2/3 and 1. The result is given by the following equations:

$$L_1=2M-N,\ L_2=2N-M,\ P=(x_*-x_*^1),\ Q=(1-x_*^1),\ S=(1-x_*) \quad (A-4)$$

$$M_1=0.667\ (1-0.333S)^{-1}(x_*^1+0.333P)Q[Q0.667LIJ+(x_*^1+P0.333LJI)] \quad (A-5)$$

$$N_1=0.333(1-0.667S)^{-1}(x_*^1+0.667P)Q[Q0.333LIJ+(x_*^1+P0.667LJI)] \quad (A-6)$$

$$M_2=0.222(Q-0.333P)^{-1}QS[Q0.667LIK+S0.333LKI] \quad (A-7)$$

$$N_2=0.222(Q-0.667)^{-1}QS[Q0.333LIK+S0.667LKI] \quad (A-8)$$

$$M_3=0.333(x_*^1+0.333Q)^{-1}S(x_*^1+0.333P)[(x_*^1+0.333P)LJK+S0.333LKJ] \quad (A-9)$$

$$N_3=0.667(x_*^1+0.667Q)^{-1}S(x_*^1+0.667P)[(x_*^1+0.667P)LJK+S0.667LKJ] \quad (A-10)$$

$$M_4=0.222TRNL\ QS(x_*^1+0.333P) \quad (A-11)$$

$$N_4=0.222TRNL\ QS(x_*^1+0.667P) \quad (A-12)$$

$$M_5=RT[0.667Q\ell n0.667Q+(x_*^1+0.333P)\ell n(x_*^1+0.333P)+0.33S\ell n0.333S] \quad (A-13)$$

$$N_5=RT[0.333Q\ell n0.333Q+(x_*^1+0.667P)\ell n(x_*^1+0.667P)+0.667S\ell n0.667S] \quad (A-14)$$

$$M_6=0.667Qx_*^1(QLIJ+x_*^1LJI) \quad (A-15)$$

$$N_6 = 0.333Qx_*^1(QLIJ + x_*^1 LJI) \quad \text{(A-16)}$$

$$M_7 = 0.333Sx_*(SLKJ + x_* LJK) \quad \text{(A-17)}$$

$$N_7 = 0.667Sx_*(SLKJ + x_* LJK) \quad \text{(A-18)}$$

$$M_8 = 0.667RT(x_*^1 \ell n x_*^1 + Q\ell nQ) + 0.333RT(x_* \ell n x_* + S\ell nS - 1.910) \quad \text{(A-19)}$$

$$N_8 = 0.333RT(x_*^1 \ell n x_*^1 + Q\ell nQ - 1.910) + 0.667RT(x_* \ell n x_* + S\ell nS) \quad \text{(A-20)}$$

$$M = 4.5(M_1 + M_2 + M_3 + M_4 + M_5 - M_6 - M_7 - M_8) \quad \text{(A-21)}$$

$$N = 4.5(N_1 + N_2 + N_3 + N_4 + N_5 - N_6 - N_7 - N_8) \quad \text{(A-22)}$$

Section III. Calculation of QuasiBinary and QuasiTernary Systems - II, CALPHAD (1979) 3 pp 27-44

CALPHAD Vol.3, No.1, pp.27-44.
Pergamon Press Ltd. 1979. Printed in Great Britain.

CALCULATION OF QUASIBINARY AND QUASITERNARY OXIDE SYSTEMS - II*

Larry Kaufman
ManLabs, Inc., 21 Erie Street
Cambridge, Massachusetts 02139, USA

ABSTRACT. A data base is being developed for calculation of quasi-binary and quasi-ternary phase diagrams of ceramic systems. The initial segment of this base covers combinations of Cr_2O_3, MgO, Al_2O_3, Fe_2O_3 Fe_3O_4 and "FeO". Lattice Stability, Solution and Compound Phase Parameters were derived covering the liquid, spinel, periclase and corundum phases in systems composed of these oxides. These parameters permit calculation of the thermochemical properties and phase diagrams of combinations of these oxides in good agreement with limited experimental data. This base has been extended to include SiO_2 and CaO by carrying out an analysis of the thirteen binary systems composed of the above mentioned systems with silica and calcium oxide. The current base of eight oxides can thus be employed to compute fifty six ternary systems. Isothermal sections in the $MgO-Fe_3O_4-Cr_2O_3$ are presented between 2800K and 1600K illustrating the usefulness of the data base.

1. Introduction

The utility of computer based methods for coupling phase diagrams and thermochemical data for metallic systems has been demonstrated in many papers published in this journal. A considerable effort is being applied toward development of a suitable data base for metallic systems. Numerous examples have been published showing how such data on metallic systems can be synthesized to successfully predict the thermochemical properties and phase relations in ternary metallic systems. Such predictions can be applied practically to explore conditions for in-situ eutectic growth, metallic glass formation, spinodal decomposition, metastable equilibrium, and diffusionless transformations. In addition, recent development of SIALON composites, combining silicon and aluminum nitrides with oxides of silicon, aluminum, magnesium and other metals, has provided additional motivation for developing methods for predicting multicomponent phase diagrams of ceramic systems. Accordingly present plans include further expansion of the current data base to cover Si_3N_4 and AlN. In addition to the present work (1) other efforts described in CALPHAD are currently in progress in order to develop predictive methods which can be used to compute multicomponent phase diagrams for ceramic systems (2,3).

*This work has been sponsored by the Air Force Office of Scientific Research, Bolling AFB, Washington, D.C., under Contract F44620-76-C-0060.

2. Description Of The Thermochemical System Employed To Describe Solution And Compound Phases

The method utilized for describing solution and compound phases is essentially the same as that employed earlier (1) except that some symbolic usage has evolved which facilitates data handling as indicated below. The free energy, G^L, of a liquid (solution) phase, L, in the binary system I-J is given by Equation (1) where T is in Kelvins, x is the atomic fraction of J and the mass basis is a mole of atoms (i.e., a gram-atom).

$$G^L = (1-x)\,{}^\circ G_i^L + x\,{}^\circ G_j^L + RT(x\ell nx + (1-x)\ell n(1-x)) + x(1-x)[LIJ(1-x) + xLJI] \quad (1)$$

In this expression, ${}^\circ G_i^L$ and ${}^\circ G_j^L$ are the free energies of a gram atom of pure liquid I and J, R = 8.314 J/g. at .°K, and LIJ and LJI are functions of temperature (but not of composition). The composition, x, is the atom fraction of J. Similar equations can be written for each solution phase with ${}^\circ G_i^L$ replaced by ${}^\circ G_i^P$, ${}^\circ G_i^C$, etc., for the P=Periclase, C=Corundum phases, etc., and with LIJ replaced by PIJ and CIJ etc. In the present symbolism, one uses the symbol DODOLP to designate the free energy of pure liquid CaO minus the free energy of pure Periclase form of CaO. Reference to Tables 1 and 2 show that DODOLP=39748-13.723T Joules, and that the liquid phase of the CaO-MgO system (i.e. DO-MO with i=DO, j=MO and x=atom fraction of MO) is described by LDOMO=-20920 and LMODO=-20920. The thermochemical data for stable phases listed in Table 1 was taken from the ManLabs-NPL Data Bank (4). The free energy, G^Ψ, of a compound phase $i_{(1-x_*)}j_{x_*}$ is defined by Equation (2) as,

$$G^\Psi = (1-x_*)\,{}^\circ G_i^\theta + x_*\,{}^\circ G_j^\theta + x_*(1-x_*)[(1-x_*)LIJ + x_*\,LJI\text{-}C[T]] \quad (2)$$

where θ refers to the base phase selected for the compound and C[T] (which is a temperature dependent function) is the compound parameter . Table 3 lists the compound parameters and base phases assigned to compounds in the systems of interest. Thus the free energy of one gram atom of the compound $CaO{\cdot}Cr_2O_3$ which is defined as $(1/7)(CaO{\cdot}Cr_2O_3)$ or $DO_{0.286}CO_{0.714}$ is defined as

$$G^\Psi = 0.286\,{}^\circ G_{DO}^S + 0.714\,{}^\circ G_{CO}^S + (0.286)(0.714)[(0.286)LDOCO + 0.714LCODO\text{-}C] \quad (3)$$

Reference to Table 2 and 3 shows that LDOCO=LCODO=0 and the compound parameter C in this case is equal to 101671. Thus the free energy of formation of $DO_{0.286}CO_{0.714}$ from the spinel forms of DO and CO is equal to -20741 Joules. In order to compute the free energy of formation of $DO_{0.286}CO_{0.714}$ from the stable P(Periclase) form of DO (i.e. CaO) and the stable C(Corundum)form of CO (i.e. Cr_2O_3) it is necessary to include the lattice stability terms DODOSP and COCOSC. The former is contained in Table 1 (DODOSP=DODOLP-DODOLS=28137-4.93T) while the latter was presented earlier (1) (i.e. COCOSC=11756-0.92T). With this additional information the free energy of formation of $DO_{0.286}CO_{0.714}$ from the P form of DO and the C form of CO can be computed as is shown in Table 4. Here the free energy of formation of $(1/7)(CaO{\cdot}Cr_2O_3)$ from (1/7)CaO (i.e. 0.286DO) and $(1/7)(Cr_2O_3)$ (i.e. 0.714 CO) with DO in the Periclase form and CO in the Corundum form. Reference to Tables 4 and 5 discloses that there are differences between the calculated values and the assessed "Data Bank Values" which are largely based on direct thermochemical measurements. However, it should be pointed out that there are several instances of "internal inconsistencies" in the "Data Bank Values". Thus for example the "assessed values" in Table 4 suggest that $CaO{\cdot}Fe_2O_3$ decomposes into Fe_2O_3 and $2CaO{\cdot}Fe_2O_3$ and that $3CaO{\cdot}A\ell_2O_3$ decomposes into CaO and $CaO{\cdot}A\ell_2O_3$ at 300K. Moreover the "assessed values" in Table 5 suggest decomposition of mullite $(3A\ell_2O_3{\cdot}2SiO_2)$ into SiO_2 and $A\ell_2O_3$ at low temperatures. Since none of the above reactions are actually observed it must be assumed that these

TABLE 1

SUMMARY OF LATTICE STABILITY PARAMETERS
(All units in Joules per gram atom (mole of atoms), T in Kelvins)

P = Periclase, C = Corundum, S = Spinel, X = Crystobalite,
T = Tridymite, H = hexagonal (α quartz), R = trigonal (β quartz)

AO = (1/5)Al_2O_3, CO = (1/5)Cr_2O_3, MO = (1/2)MgO, WO = (1/2)FeO
FO = (1/5)Fe_2O_3, HO = (1/7)Fe_3O_4,

SOSOLX* = (1/3)SiO_2(Liquid) - (1/3)SiO_2 (Crystobalite)
SOSOLT = (1/3)SiO_2(Liquid) - (1/3)SiO_2 (Tridymite)
SOSOTX = (1/3)SiO_2(Tridymite) - (1/3)SiO_2 (Crystobalite)
SOSOLX = SOSOLT + SOSOTX

SOSOLX = 3347 - 1.674T
SOSOLT = 3933 - 2.008T
SOSOTH = 858 - 0.795T
SOSOHR = 251 - 0.293T
SOSOLC = SOSOLP = SOSOLS = -2.092T

DODOLP = 39748 - 13.723T
DODOLC = 14644 - 10.878T
DODOLS = 11611 - 8.786T
DODOLX = - 1.674T
DODOLT = - 2.008T

AOAOLX = COCOLX = MOMOLX = WOWOLX = HOHOLX = FOFOLX = -1.674T
AOAOLT = COCOLT = MOMOLT = WOWOLT = HOHOLT = FOFOLT = -2.008T

* These differences specify the free energy of one phase (i.e. liquid) minus the free energy of the second phase (i.e. Crystobalite) of a given compound.

TABLE 2

Quasibinary Solution Parameters for Oxide Systems

(All units in Joules per gram atom (mole of atoms), T in Kelvins)

DO-AO ($1/2CaO-1/5Al_2O_3$)

LDOAO = -22595
CDOAO = 102926
PDOAO = 102926
LAODO = -22595
CAODO = 102926
PAODO = 102926

DO-CO ($1/2CaO-1/5Cr_2O_3$)

LDOCO = 0
CDOCO = 83680
PDOCO = 83680
LCODO = 0
CCODO = 83680
PCODO = 83680

DO-MO ($1/2CaO-1/2MgO$)

LDOMO = 23012
PDOMO = 41840
LMODO = 29288
PMOPO = 68199

DO-FO ($1/2CaO-1/2Fe_2O_3$)

LDOFO = -20920
CDOFO = 104600
PDOFO = 104600
LFODO = -20920
CFODO = 104600
PFODO = 104600

DO-HO ($1/2CaO-1/7Fe_3O_4$)

LDOHO = 0
SDOHO = 117152
POOHO = 117152
LHODO = 0
SHODO = 117152
PHODO = 117152

DO-WO ($1/2CaO-1/2FeO$)

LDOWO = -7113
PDOWO = 30962
LWODO = -20501
PWODO = 17573

SO-DO ($1/3SiO_2-1/2CaO$)

$0 \le x_{DO} \le 0.40$

LSODO = 0
XSODO = 83680
TSODO = 83680
LDOSO = -393631+104.6T
XDOSO = -309951+104.6T
TDOSO = -309951+104.6T

$0.40 \le x_{DO} \le 1.0$

LSODO = -195476+41.8T
PSODO = -111796+41.8T
LDOSO = -100416+41.8T
PDOSO = -16736+41.8T

SO-AO ($1/3SiO_2-1/5Al_2O_3$)

LSOAO = 38493
LSOAO = 122173
XSOAO = 122173
TSOAO = 122173
LAOSO = 28451
CAOSO = 112131
XAOSO = 112131
TAOSO = 112131

SO-CO ($1/3SiO_2-1/5Cr_2O_3$)

LSOCO = 68199
CSOCO = 151879
XSOCO = 151879
LCOSO = 68199
CCOSO = 151879
XCOSO = 151879

SO-MO ($1/3SiO_2-1/2MgO$)

$0 \le x_{MO} \le 0.40$

LSOMO = -24267+24.27T
XSOMO = 59413+24.27T
TSOMO = 59413+24.27T
LMOSO = -229283+68.62T
XMOSO = -145603+68.62T
TMOSO = -145603+68.62T

$0.40 \le x_{MO} \le 1.0$

LSOMO = -106274+42.01T
PSOMO = 19246+42.01T
LMOSO = -106274+42.01T
PMOSO = 19246+42.01T

SO-FO ($1/3SiO_2-1/5Fe_2O_3$)

LSOFO = 54392
CSOFO = 138072
XSOFO = 138072
TSOFO = 138072
LFOSO = 163176-83.68T
CFOSO = 246856-83.68T
XFOSO = 246856-83.68T
TFOSO = 246856-83.68T

SO-HO ($1/3SiO_2-1/7Fe_3O_4$)

$0 \le x_{HO} \le 0.70$

LSOHO = 80542-10.46T
XSOHO = 164222-10.46T
TSOHO = 164222-10.46T
LHOSO = 213384-125.52T
XHOSO = 297064-125.52T
THOSO = 297064-125.52T

$0.70 \le x_{HO} \le 1.0$

LSOHO = 0
SSOHO = 83680
LHOSO = 247902-130.0T
SSOHO = 331582-130.0T

SO-WO ($1/3SiO_2-1/2FeO$)

$0 \le x_{WO} \le 0.50$

LSOWO = 29288
XSOWO = 112968
TSOWO = 112968
LWOSO = 324678-225.94T
XWOSO = 408358-225.94T
TWOSO = 408358-225.94T

$0.50 \le x_{WO} \le 1.0$

LSOWO = 162339-112.97T
PSOWO = 246019-112.97T
LWOSO = 191627-112.97T
PWOSO = 275307-112.97T

TABLE 3

SUMMARY OF COMPOUND PARAMETERS
(All units in Joules per gram atom (mole of atoms), Tin Kelvins)

Compound	Stoichiometry	Base	Compound Parameter (Joules/g.atom)
$1/9(2CaO\cdot Fe_2O_3)$	$DO_{0.445}\ FO_{0.555}$	P	9623 - 3.43T
$1/7(CaO\cdot Fe_2O_3)$	$DO_{0.286}\ FO_{0.714}$	S	46861 - 15.48T
$1/32(CaO\cdot 6Al_2O_3)$	$DO_{0.063}\ AO_{0.937}$	C	16736 + 13.18T
$1/12(CaO\cdot 2Al_2O_3)$	$DO_{0.167}\ AO_{0.833}$	C	15481 + 10.46T
$1/7(CaO\cdot Al_2O_3)$	$DO_{0.286}\ AO_{0.714}$	S	38493
$1/11(3CaO\cdot Al_2O_3)$	$DO_{0.546}\ AO_{0.454}$	P	16318 + 13.51T
$1/7(CaO\cdot Cr_2O_3)$	$DO_{0.286}\ CO_{0.714}$	S	101671
$1/5(CaO\cdot SiO_2)$	$DO_{0.40}\ SO_{0.60}$	P	-62383 + 49.29T
$1/7(2CaO\cdot SiO_2)$	$DO_{0.571}\ SO_{0.429}$	P	-56902 + 43.93T
$1/21(2SiO_2\cdot 3Al_2O_3)$	$SO_{0.286}\ AO_{0.714}$	C	41840 + 4.73T
$1/5(MgO\cdot SiO_2)$	$MO_{0.40}\ SO_{0.60}$	P	-66735 + 47.28T
$1/7(2MgO\cdot SiO_2)$	$MO_{0.571}\ SO_{0.429}$	P	-64434 + 41.13T
$1/7(SiO_2\cdot 2FeO)$	$SO_{0.429}\ WO_{0.571}$	P	217986 - 120.5T

$MO = (1/2)MgO$, $DO = (1/2)CaO$, $FO = (1/5)Fe_2O_3$, $AO = (1/5)Al_2O_3$

$SO = (1/3)SiO_2$, $WO = (1/2)FeO$, C = Corundum, P = Periclase

S = Spinel

---

inconsistencies represent cumulative errors which can occur in assessment of thermochemical data when the competition between adjoining phases (i.e. the phase diagram) is not considered. In the present process such competition is considered as a natural part of the evaluation method.

3. Discussion of Computed Phase Diagrams

Binary phase diagrams between CaO and SiO_2 with the oxides Al_2O_3, Cr_2O_3, MgO, FeO, Fe_2O_3 and Fe_3O_4 are provided in the compilation series prepared by Levin, Robbins and McMurdie(5). Although some of the phase diagrams are sketchy and conflicting experimental data are presented the results have been used in concert with the experimental thermochemical data(4) and prior lattice stability values(1) to select the values for the solution and compound parameters which are shown in Tables 2 and 3. Figures 1-13 are the binary phase diagrams which can be generated from the results displayed in Tables 1-3. The calculated Al_2O_3-CaO binary diagram in Figure 1 is in relatively good agreement with the experimental diagrams shown in Figures 231,232,2295,2296 and 4308 of reference 5. Moreover, Table 4 shows that the computed free energies of formation of compounds in this binary system are in relatively good agreement with the "Data Bank Values" derived from thermochemical data. The solution phases in this system are approximated by regular solution descriptions (i.e. LDOAO=LAODO etc.). Figure 2 shows the computed Cr_2O_3-CaO phase diagram

TABLE 4

SUMMARY OF CALCULATED AND ASSESSED (4) FREE ENERGIES OF COMPOUND FORMATION (JOULES, °K)

	DATA BANK ΔG VALUES (4)
$(2/9)CaO + (1/9)Fe_2O_3 \rightarrow 1/9(2CaO \cdot Fe_2O_3)$	-5117 at 300K
$\Delta G = -2714-0.313T$ (calculated)	-7627 at 1400K
$(1/7)CaO + (1/7)Fe_2O_3 \rightarrow 1/7(CaO \cdot Fe_2O_3)$	-3112 at 300K
$\Delta G = -3808 + 0.977T$ (calculated)	-4284 at 1400K
$(1/32)CaO + (6/32)Al_2O_3 \rightarrow (1/32)(CaO \cdot 6Al_2O_3)$	-- --
$\Delta G = -739-0.957T$ (calculated)	-- --
$(1/12)CaO + (2/12)Al_2O_3 \rightarrow (1/12)(CaO \cdot 2Al_2O_3)$	-1916 at 300K
$\Delta G = -1101-1.928T$ (calculated)	-5381 at 1600K
$(1/7)CaO + (1/7)Al_2O_3 \rightarrow (1/7)(CaO \cdot Al_2O_3)$	-3096 at 300K
$\Delta G = -1248-2.219T$ (calculated)	-6720 at 1600K
$(3/11)CaO + (1/11)Al_2O_3 \rightarrow (1/11)(3CaO \cdot Al_2O_3)$	-1632 at 300K
$\Delta G = -947-2.155T$ (calculated)	-5786 at 1600K
$(1/7)CaO + (1/7)Cr_2O_3 \rightarrow (1/7)(CaO \cdot Cr_2O_3)$	-- --
$\Delta G = -4300-2.067T$ (calculated)	-- --

which compares well with Figure 37 of reference 5. Table 2 discloses that this system is computed with regular solution parameters and an ideal liquid phase (i.e. LDOCO=LCODO=0). Figure 3 displays the computed CaO-MgO system which is obtained with assymetric excess free energies (LDOMO≠LMODO) but ideal mixing entropies (dL/dT=0). The latter agrees with Figure 229 of reference 5. Figures 4-6 contain the calculated $CaO-Fe_2O_3$, $CaO-Fe_3O_4$ and CaO-FeO phase diagrams which are in good agreement with those shown in Figures 43-48 of reference(5). Reference to Table 2 shows that the $CaO-Fe_2O_3$ and $CaO-Fe_3O_4$ cases are approximated by regular models (i.e. the latter as an ideal liquid) while the CaO-FeO case is assymetric (LDOWO≠LWODO) with ideal entropies of mixing for solution phases. It should be noted that the computed $CaO-Fe_2O_3$ diagram shown in Figure 4 is metastable since Fe_2O_3 decomposes into Fe_3O_4 and O_2 above 1760K under atmospheric conditions.

In contrast to the results encountered in analysis of the CaO-based systems, reference to Table 2 shows that analysis of the SiO_2-based binary systems proved to be more difficult. In this group, only the $SiO_2-Cr_2O_3$ binary calculated in Figure 9 could be approximated by a regular solution model. The resulting phase diagram compares well with the experimental diagram shown in Figure 332 of reference 5. Figure 8 shows the computed $SiO_2-Al_2O_3$ diagram which is in good agreement with the experimental results which are given in Figures 313,4374 and 4375 of Reference 5. This system is described by assymetric solutions (LSOAO≠LAOSO) and ideal solution entropies (dL/dT etc.=0). Moreover, examination of Table 5 shows that the computed free energy of mullite ($3Al_2O_3 \cdot 2SiO_2$) from the stable forms of Al_2O_3 and SiO_2 is in relatively good agreement with the values listed in the Data Bank(4). The latter are determined by assessment of thermochemical data. The computed $SiO_2-Fe_2O_3$ diagram shown in Figure 11 is metastable above 1760K due to decomposition of Fe_2O_3 into Fe_3O_4 and O_2 at one atmosphere. This diagram is in accordance with Figure 80 of reference 5 and is computed with assymetric solution models

TABLE 5

SUMMARY OF CALCULATED AND ASSESSED (4) FREE ENERGIES OF COMPOUND FORMATION (JOULES,°K)

	DATA BANK ΔG VALUES
$(1/5)CaO + (1/5)SiO_2 \rightarrow (1/5)(CaO \cdot SiO_2)$	
$\Delta G = -19791-2.402T$ (calculated at 300K)	-17970 at 300K
$\Delta G = -20808-1.547T$ (calculated at 1800K)	-18146 at 1800K
$(2/7)CaO + (1/7)SiO_2 \rightarrow (1/7)(2CaO \cdot SiO_2)$	
$\Delta G = -18485-0.954T$ (calculated at 300K)	-19430 at 300K
$\Delta G = -19212-0.343T$ (calculated at 1800K)	-19539 at 1800K
$(2/21)SiO_2 + (3/21)Al_2O_3 \rightarrow (1/21)(2SiO_2 \cdot 3Al_2O_3)$	
$\Delta G = -706-1.254T$ (calculated at 300K)	+397 at 300K
$\Delta G = -1191-0.846T$ (calculated at 1900K)	-2013 at 1900K
$(1/5)MgO + (1/5)SiO_2 \rightarrow (1/5)(MgO \cdot SiO_2)$	
$\Delta G = -6464-1.864T$ (calculated at 300K)	-7273 at 300K
$\Delta G = -7481-1.009T$ (calculated at 1800K)	-5799 at 1800K
$(2/7)MgO + (1/7)SiO_2 \rightarrow (1/7)(2MgO \cdot SiO_2)$	
$\Delta G = -8088-0.216T$ (calculated at 300K)	-8301 at 300K
$\Delta G = -8815 + 0.395T$ (calculated at 1800K)	-7761 at 1800K
$(1/7)SiO_2 + (2/7)FeO \rightarrow (1/7)(SiO_2 \cdot 2FeO)$	
$\Delta G = -7373 + 1.413T$ (calculated at 300K)	-6845 at 300K
$\Delta G = -7849 + 1.880T$ (calculated at 1400K)	-4067 at 1400K

(i.e. LSOFO≠LFOSO) with finite excess entropies of solution(i.e. dL/dT≠0) as shown in Table 2.

Analysis of the remaining binary systems i.e. SiO_2-CaO, SiO_2-MgO, SiO_2-Fe_3O_4 and SiO_2-FeO could only be carried out by segmenting the description of the liquid phase as is illustrated in Table 2. Thus, in the last of the above named cases, the excess free energy of the liquid phase (i.e. the last term in Equation 1) is set equal to $x(1-x)[(1-x)29288+x(324678-225.94T)]$ where $0<x<0.5$ and $x=x_{WO}$=atom fraction of WO. In the range $0.5<x<1.0$ the last term is set equal to $x(1-x)[(1-x)(162339-112.97T)+x(191627)-112.97T)]$. Note that both expressions yield the identical result, 44246-28.24T at $x_{WO}=x_{SO}=0.5$. The calculated SiO_2-FeO phase diagram shown in Figure 13 is in relatively good agreement with the observed diagram in Figure 80 of reference 5 except that liquid monotectic is reported(5) at 1970K and 45 w/o FeO. Examination of Table 5 shows that the computed free energy of formation of Fayalite ($2FeO \cdot SiO_2$) from the stable forms of SiO_2 and FeO is in relatively good agreement with the "assessed values"(4) over the temperature range of its stability. In the SiO_2-Fe_3O_4 case the thermochemical description of the liquid phase shown in Table 2 is divided into two segments corresponding to the composition range $0 \leq x_{HO} \leq 0.70$ (i.e. HO=(1/7)Fe_3O_4) and a second covering the range $0.70 \leq x_{HO} \leq 1.0$. The computed binary phase diagram shown in Figure 12 compares favorably with that shown in Figure 87 of reference 5 except that the observed liquid monotictic is reported (5) to be at 1930K and 90 w/o Fe_3O_4.

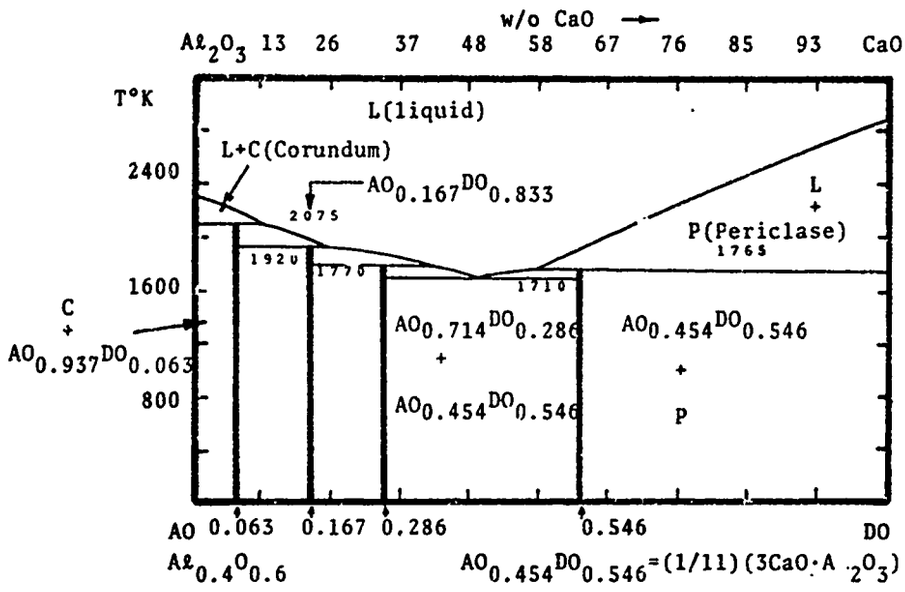

Figure 1. Calculated $Al_{0.4}O_{0.6}$-$Ca_{0.5}O_{0.5}$ Phase Diagram

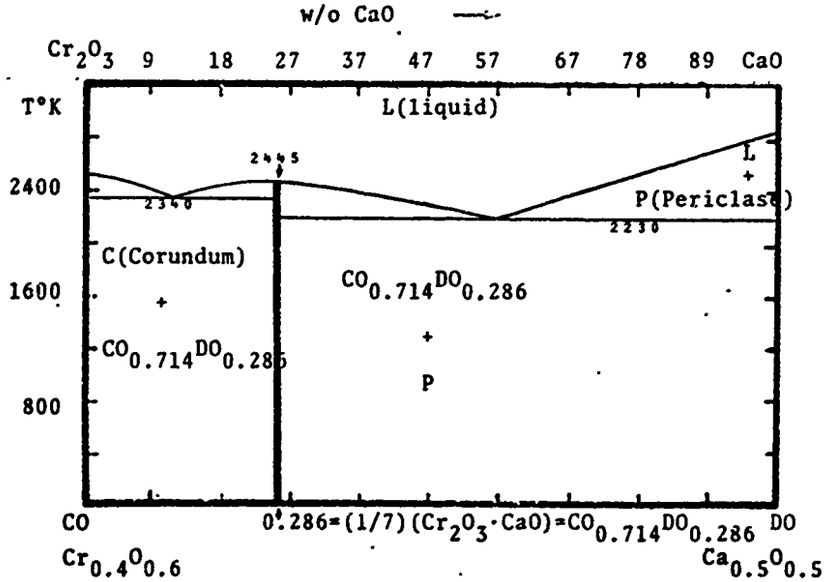

Figure 2. Calculated $Cr_{0.4}O_{0.6}$-$Ca_{0.5}O_{0.5}$ Phase Diagram

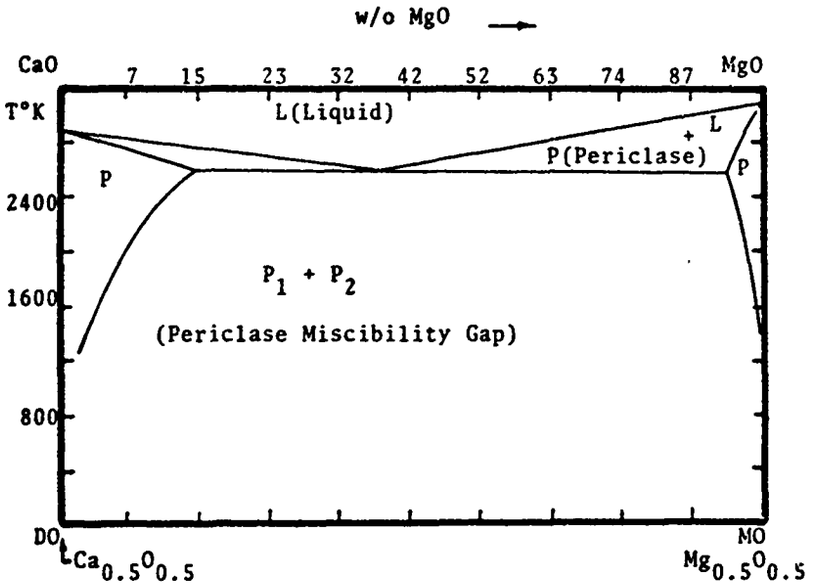

Figure 3. Calculated $Ca_{0.5}O_{0.5}$-$Mg_{0.5}O_{0.5}$ Phase Diagram

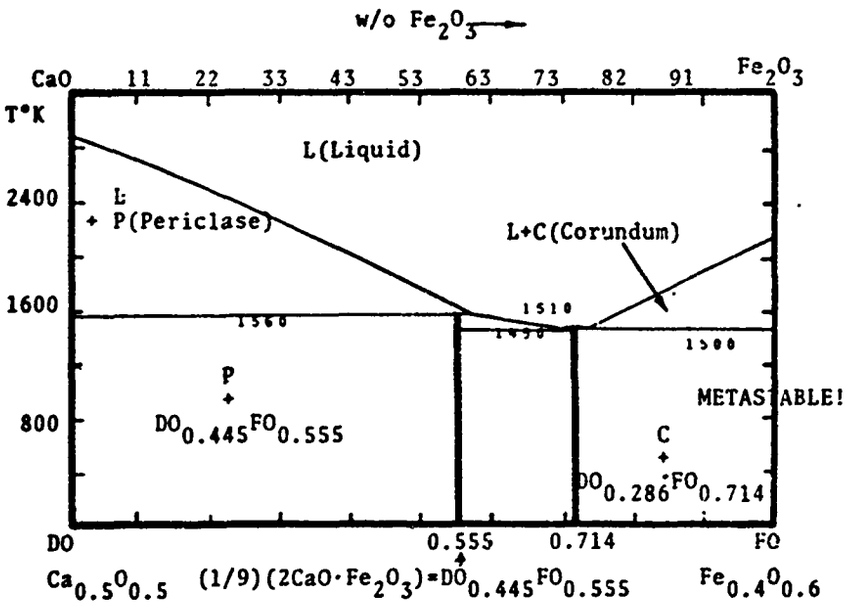

Figure 4. Calculated $Ca_{0.5}O_{0.5}$-$Fe_{0.4}O_{0.6}$ Phase Diagram (Note: $Fe_{0.4}O_{0.6}$ Decomposes into $Fe_{0.429}O_{0.571}$ and $1/2O_2$ above 1760K)

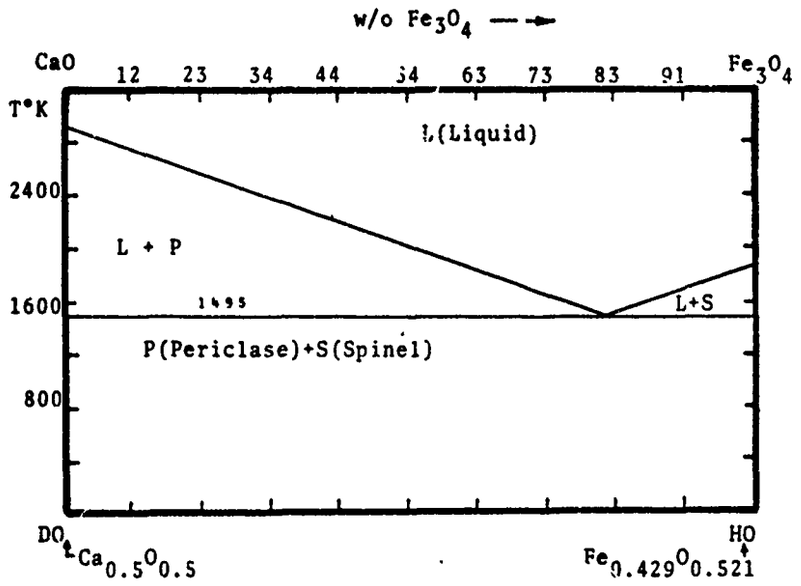

Figure 5. Calculated $Ca_{0.5}O_{0.5}$-$Fe_{0.429}O_{0.571}$ Phase Diagram

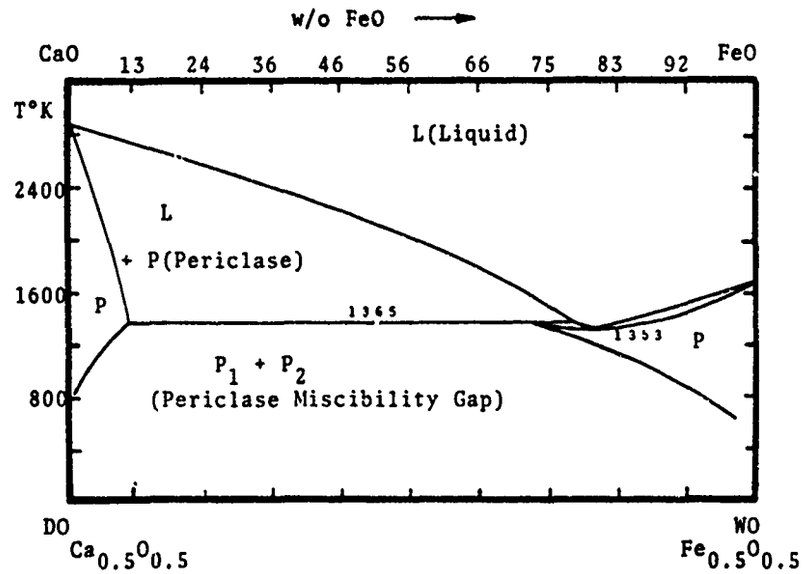

Figure 6. Calculated $Ca_{0.5}O_{0.5}$-$Fe_{0.5}O_{0.5}$ Phase Diagram

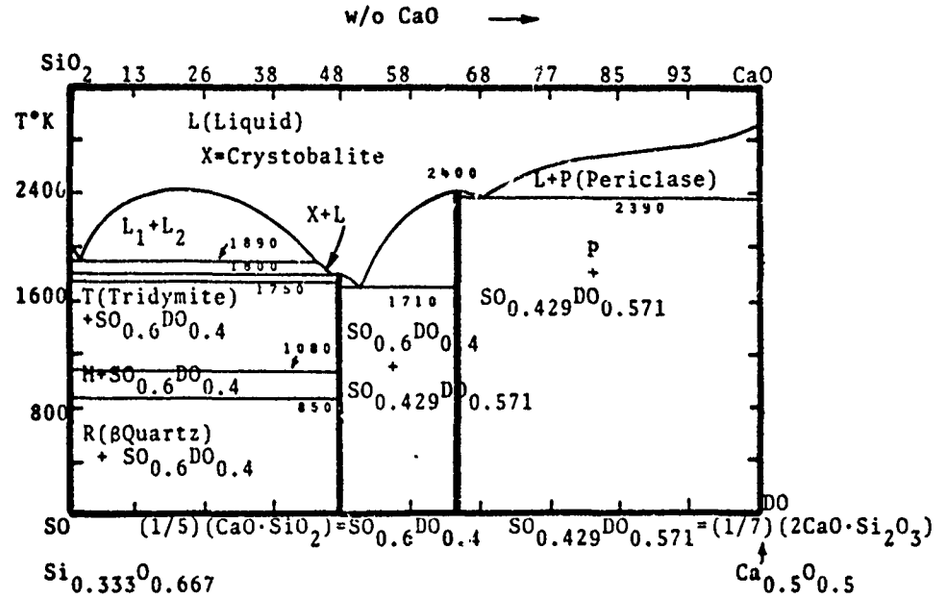

Figure 7. Calculated $Si_{0.333}O_{0.667}$-$Ca_{0.5}O_{0.5}$ Phase Diagram

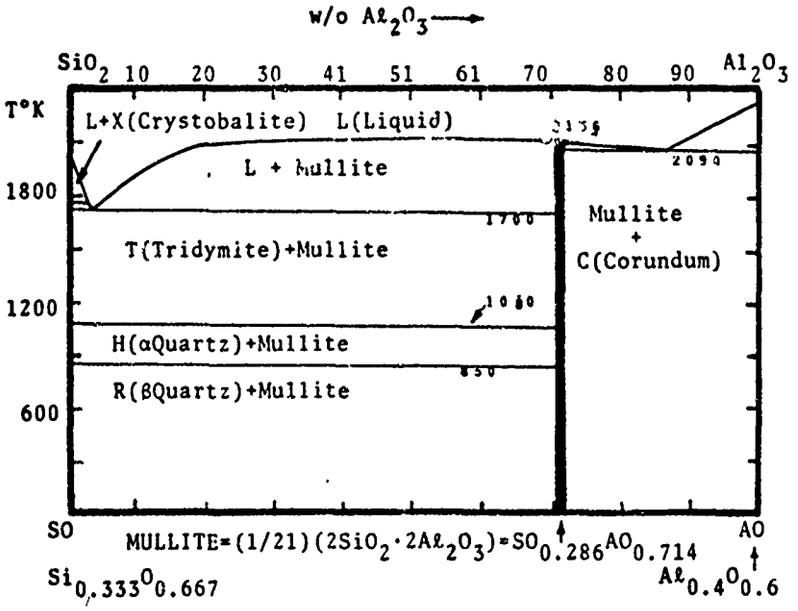

Figure 8. Calculated $Si_{0.333}O_{0.667}$-$Al_{0.4}O_{0.6}$ Phase Diagram

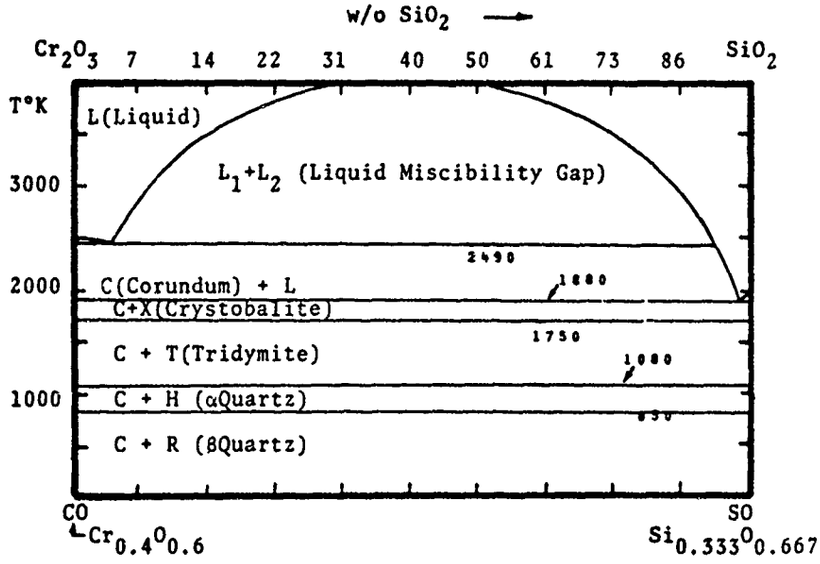

Figure 9. Calculated $Cr_{0.4}O_{0.6}$-$Si_{0.333}O_{0.667}$ Phase Diagram

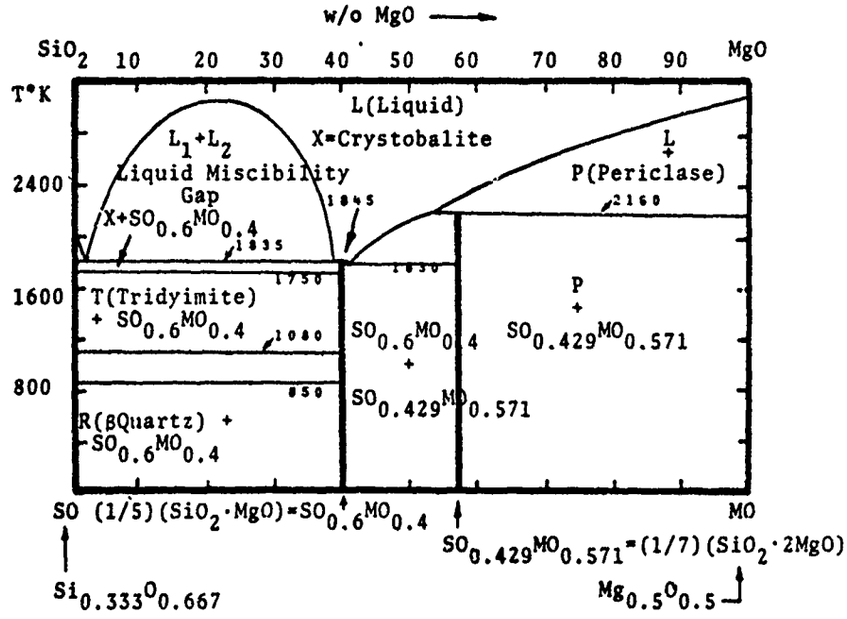

Figure 10. Calculated $Si_{0.333}O_{0.667}$-$Mg_{0.5}O_{0.5}$ Phase Diagram

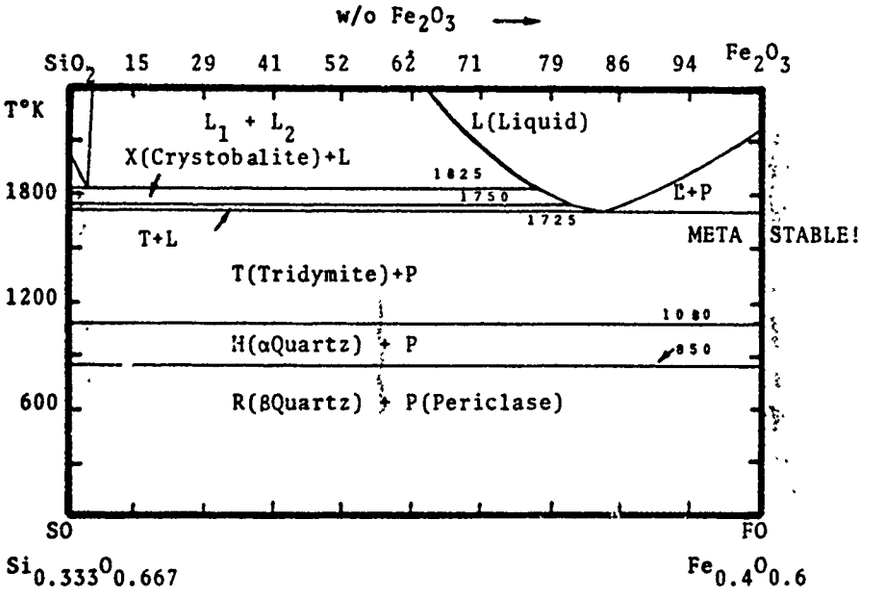

Figure 11. Calculated $Si_{0.333}O_{0.667}$-$Fe_{0.4}O_{0.6}$ Phase Diagram (Note: $Fe_{0.4}O_{0.6}$ Decomposes into $Fe_{0.429}O_{0.571}$ and 1/2 O_2 above 1760K)

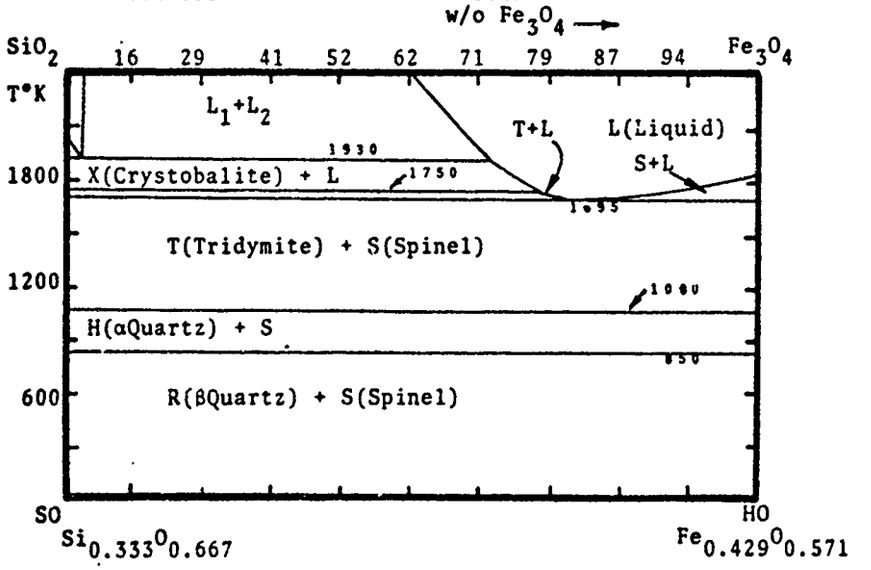

Figure 12. Calculated $Si_{0.333}O_{0.667}$-$Fe_{0.429}O_{0.571}$ Phase Diagram

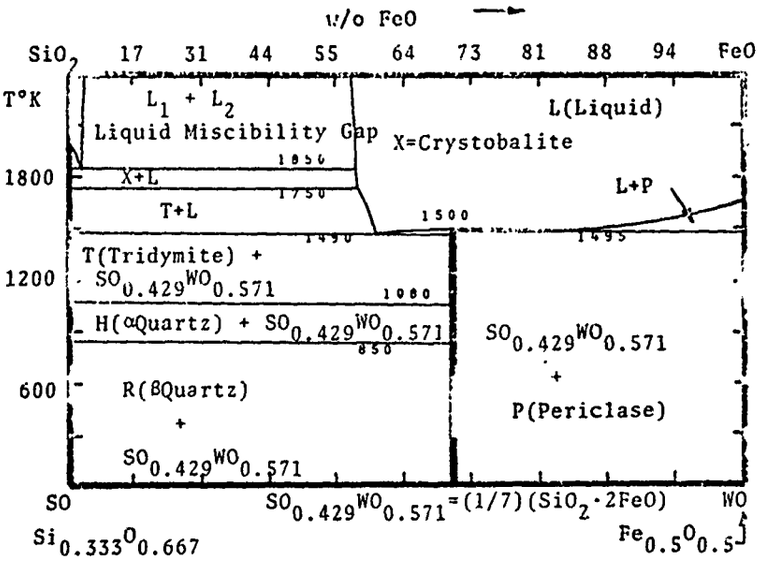

Figure 13. Calculated $Si_{0.333}O_{0.667}$-$Fe_{0.5}O_{0.5}$ Phase Diagram

In the remaining SiO_2-CaO and SiO_2-MgO cases, Table 2 shows that the liquid thermochemistry is described in two composition ranges, from $1.0 \geq x_{SO} \geq 0.6$ and from $0.6 \geq x_{SO} \geq 0$. The resulting computed binary diagrams shown in Figures 7 and 10 compare favorably with those shown in Figures 237, 2331, 2303 and 266, 2331 of reference 5. In these cases the greatest discrepancies are encountered again in the position of the liquid monotectic where the experimental locations are at 1970K and 27 w/o CaO in the SiO_2-CaO case and at 1960K and 31 w/o MgO in the SiO_2-MgO case. Comparison of the computed and "assessed" free energies of compound formation for SiO_2-CaO and SiO_2-MgO compounds listed in Table 5 shows that in both cases excellent agreement is observed for the (1/7)($2MgO \cdot SiO_2$) (i.e. $MO_{0.571}SO_{0.429}$) and (1/7)($2CaO \cdot SiO_2$)(i.e. $DO_{0.571}SO_{0.429}$) cases. However, while the computed low temperature results for the (1/5)($MgO \cdot SiO_2$) (i.e. $MO_{0.4}SO_{0.6}$) and (1/5)($CaO \cdot SiO_2$) (i.e. $DO_{0.4}SO_{0.6}$) agree with the "assessed" values, the computed high temperature values are in poor agreement with the "assessed" high temperature values. Thus, it appears that while the present model can be readily applied to obtain a good description of the CaO based systems difficulity is encountered in its application to some of the SiO_2 based systems.

4. Calculation of Quasi-Ternary Phase Diagrams

The objective of developing the present data base for characterizing quasi-binary ceramic systems is to provede a means for computing stable and meta stable equilibria in quasi-ternary and higher order ceramic systems. Several examples of such systems were presented earlier(1). In these cases the quasi-ternary systems were computed by synthesis of the edge binary characteristic for solutions on the basis of the Koehler equation. Thus for the (1/2)MgO-(1/7)Fe_3O_4-(1/5)Cr_2O_3 (i.e. MO-HO-CO) case the free energy of the liquid is defined as

$$G^L=(1-x-y)\,G^L_{MO}+xG^L_{HO}+yG^L_{CO}+RT((1-x-y)\ell n(1-x-y)+x\ell nx+y\ell ny)$$
$$+x(1-x-y)(1-y)^{-1}[(1-x-y)LMOHO+xLHOMO]$$
$$+y(1-x-y)(1-x)^{-1}[(1-x-y)LMOCO+yLCOMO]$$
$$+xy(x+y)^{-1}[xLHOCO+yLCOHO]$$
$$+TRNL(1-x-y)xy \qquad (4)$$

where x is the atom fraction of HO, y is the atom fraction CO and TRNL is a ternary interaction parameter. Similar equations can be written for the Periclase(P), Corundum(C), Spinel(S) and other solution phases by replacing the L's and TRNL by P's and TRNP etc. If TRNL=0 then all of the terms in Equation(4) have been explicitly defined(1). Thus in this approximation the free energy of ternary solution phases are synthesized from their binary edge components by using Kohler's Equation with a zero ternary interaction parameter. The free energy of ternary compound phases is defined along specific joins As an example, we consider the spinel compound phase in the system MO-HO-CO (see Figure 14). This compound runs between the $Fe_3O_4\cdot MgO$ and $Cr_2O_3\cdot MgO$, compositions designated (Table 7(1)) as $(Fe_{0.306}O_{0.408})\cdot(Mg_{0.143}O_{0.143})$ and $Cr_{0.286}O_{0.428})\cdot(Mg_{0.143}O_{0.143})$: If x is the fraction MO and y is the fraction HO then the free energy of the spinel (SP) compound $CO_{(1-x^1_*)}{}^{MO}x^1_*{}^{-HO}{}_{(1-x_*)}{}^{MO}x_*$ is given by Equation(5) as

$$G^{SP}=(1-x-y)G^S_{CO}+xG^S_{MO}+yG^S_{HO}+RT[y\ell ny+(1-x-y)\ell n(1-x-y)-(1-x)\ell n(1-x)]$$
$$+[1-\frac{y}{1-x}]\Delta G_A+(\frac{y}{1-x})\Delta G_B+\Delta G_E \qquad (5)$$

where

$$\Delta G_E=0,\Delta G_A=(1-x^1_*)x^1_*[(1-x^1_*)\,LCOMO+x^1_*LMOCO-C_A]$$
$$\Delta G_B=(1-x_*)x_*[(1-x_*)\,LHOMO+x_*\,LMOHO-C_B] \qquad (6)$$

and

$$x=x^1_*+yp\ ;\ p=(x_*-x^1_*)/(1-x_*),x^1_*=0.286,\ x_*=0.286,\ p=0$$
$$C_B=0 \text{ and } C_A=38910+16.74T \quad \text{(From Table 7 of reference 1)} \qquad (7)$$

Since all of the parameters required to calculate the free energy of the liquid, spinel, periclase and corundum solution phases in the MO-HO-CO system as well as the free energy of the spinel compound phase, the entire ternary phase diagram can be computed. The results are shown as a series of isothermal sections between 2800K and 1600K in Figures 14 and 15. These results can be employed to locate melting points and liquid decomposition products thus providing a guide for structural studies. Moreover these sections can be employed to locate interesting solid state decomposition reactions which can be employed to produce strengthening reactions attainable via heat treatment. One such example in the present computations is the decomposition of the periclase field indicated on cooling from 1850K to 1600K in Figure 15. Thus an "alloy" composed of 0.7MO-0.25HO-0.05CO (i.e. 88.4 mol percent MgO-9.1 mol percent Fe_3O_4-2.5 mol percent Cr_2O_3) would be expected to be strengthened by solution treatment at 1850K and subsequent aging at 1600K.

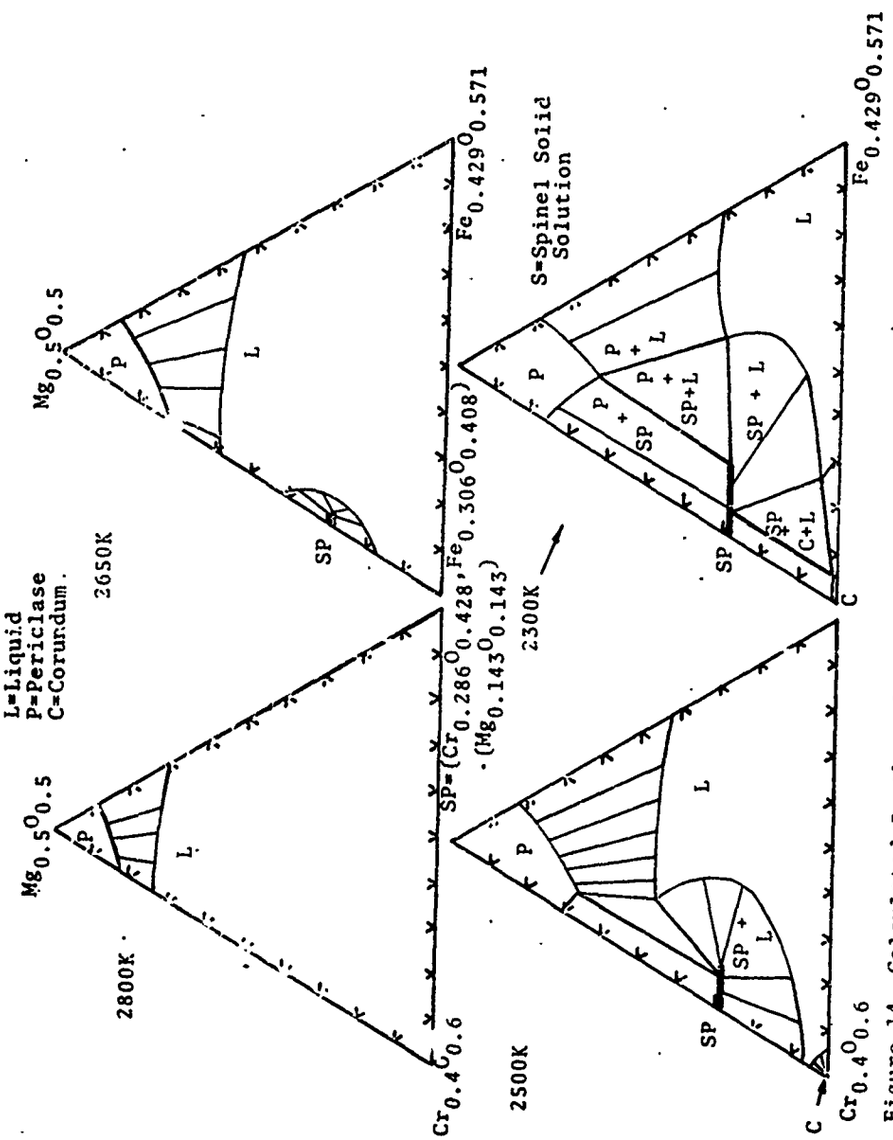

Figure 14. Calculated Isothermal Sections in the $Mg_{0.5}O_{0.5}$-$Fe_{0.429}O_{0.571}$-$Cr_{0.4}O_{0.6}$ System.

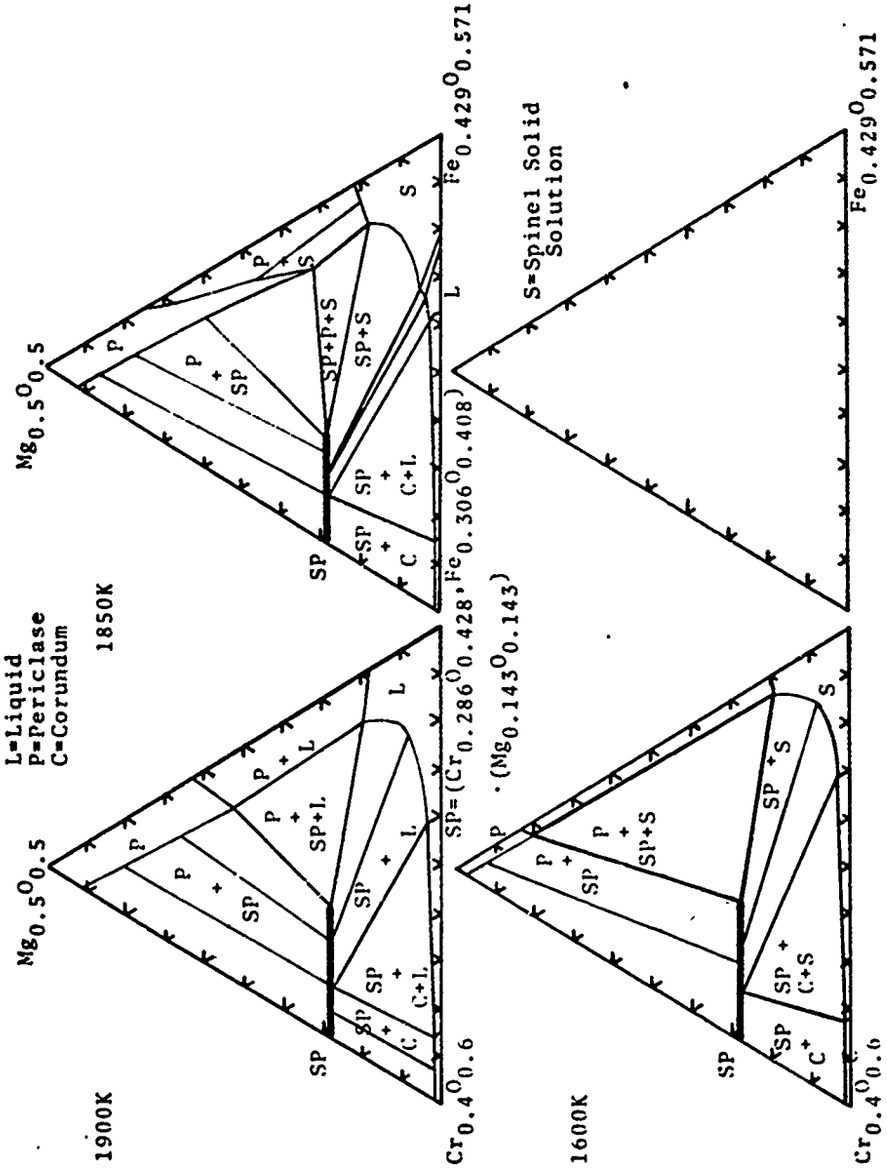

Figure 15 Calculated Isothermal Sections in the $Mg_{0.5}O_{0.5}$-$Fe_{0.429}O_{0.571}$-$Cr_{0.4}O_{0.6}$ System.

References

1. L. Kaufman and H. Nesor, CALPHAD 2 35(1978)
2. G. Kaestle and K. Koch, CALPHAD 2 198(1978)
3. L.J. Gaukler, H.L. Lukas, E. Th. Henig and G. Petzow, (CALPHAD) 2 349(1978)
4. ManLabs-NPL Data Bank, ManLabs, Inc. Cambridge, Massachusetts USA, National Physical Laboratory, Teddington-Middlesex, England
5. E.M. Levin, C.R. Robbins and H.F. McMurdie, Phase Diagrams for Ceramists, American Ceramics Society Columbus, Ohio (1964), First Supplement (Ibid) (1969), Second Supplement Ibid (1975).

Section IV. Calculation of QuasiBinary and QuasiTernary OxyNitride Systems, CALPHAD (1979) 3 pp 273-89

CALCULATION OF QUASIBINARY AND QUASITERNARY OXYNITRIDE SYSTEMS - III*

Larry Kaufman

ManLabs, Inc., 21 Erie Street
Cambridge, Massachusetts 02139 USA

(This paper was presented at CALPHAD VIII, Stockholm, Sweden, May 1979)

ABSTRACT. A data base is being developed for calculation of quasi-binary and quasi-ternary phase diagrams of ceramic systems. Initially the base was restricted to the following oxides: Cr_2O_3, MgO, Fe_2O_3, Fe_3O_4, FeO, Al_2O_3, CaO and SiO_2. Lattice Stability, Solution and Compound Phase Parameters were derived covering the liquid, spinel, corundum, periclase, crystobalite, tridymite and quartz phases which appear in the binary systems composed of these oxides. These parameters were selected in accordance with the observed thermochemical properties and phase diagrams of these binary systems. The usefulness of this analytical description was illustrated by computing isothermal sections for ternary systems composed of these oxides. The above mentioned data base has now been expanded to cover combinations of the oxides with silicon nitride, Si_3N_4, and aluminum nitride, AlN thus permitting computation of oxynitride SIALON ceramic systems which are of current practical interest. The current analysis provides isothermal sections in the Si_3N_4-Al_2O_3-AlN and SiO_2-Al_2O_3-Si_3N_4 systmes as well as computed values for the free energy of formation of the beta sialons in the Si_3N_4-Al_2O_3-AlN system and the X phase in the SiO_2-Al_2O_3-Si_3N_4 system. The former results are compared with independent calculations reported by Doerner et.al. at CALPHAD VIII and published in the current issue of the CALPHAD Journal.

1. Introduction

The utility of computer based methods for coupling phase diagrams and thermochemical data for metallic systems has been well documented in many papers published in this journal. A considerable effort is being applied toward developing an extensive data base for metallic systems. Recently similar efforts have begun with the aim of developing similar data bases for ceramic systems (1-4). Recent development of SIALON composites, combining silicon and aluminum nitrides with oxides of silicon, aluminum, magnesium and other metals has provided additional motivation for developing methods for predicting multicomponent phase diagrams of ceramic systems. The present paper describes work conducted at ManLabs during the past year and compares the results obtained independently at the Max Plank Institute in Stuttgart (4).

2. Description of the Thermochemical System Employed to Describe Solution and Compound Phases

The method utilized for describing solution and compound phases is the same as that employed earlier (1,2) employing some symbolic usage which facilitates data handling as indicated below. The free energy, G^L, of a liquid (solution) phase, L, in the binary system I-J is given by Equation (1) where T is in Kelvins, x is the atomic fraction of J and the mass basis is a mole of atoms (i.e., a gram-atom).

$$G^L = (1-x)^{\circ}G_I^L + x^{\circ}G_J^L + RT(x\ell nx + (1-x)\ell n(1-x)) + x(1-x)[LIJ(1-x) + xLJI] \qquad (1)$$

* This work has been sponsored by the Air Force Scientific Research, Bolling AFB, Washington, D.C., under Contract F44620-76-C-0060.

In this expression, ${}^{\circ}G_i^L$ and ${}^{\circ}G_j^L$ are the free energies of a gram atom of pure liquid I and J, R = 8.314 J/g.at. °K, and LIJ and LJI are functions of temperature (but not of composition). The composition, x, is the atom fraction of J. Similar equations can be written for each solution phase with ${}^{\circ}G_i^L$ replaced by ${}^{\circ}G_i^P$, ${}^{\circ}G_i^C$, etc., for the P=Periclase, C=Corundur phases, etc., and with LIJ replaced by PIJ and CIJ etc. In the present symbolism, one uses the symbol SNSNLB to designate the free energy of pure liquid Si_3N_4 minus the free energy of the beta form of Si_3N_4. Reference to Tables 1 and 2 show SNSNLB=33949-12.51T Joules/g.at., and that the liquid phase of the SN-AO, $(1/7)Si_3N_4$-$(1/5)Al_2O_3$ system (i.e. SN-AO with i=SN, j=AO and x=atom fraction of AO) is described by LSNAO=29288 and LAOSN=29288. The free energy, G^{Ψ}, of a compound phase ${}_{(1-x_*)}i^{j}{}_{x_*}$ is defined by Eq.(2) as

$$G^{\Psi} = (1-x_*)\ {}^{\circ}G_i^{\theta} + x_*\ {}^{\circ}G_j^{\theta} + x_*(1-x_*)[(1-x_*)LIJ + x_*\ LJI-C[T]] \qquad (2)$$

where θ refers to the base phase selected for the compound and C[T] (which is a temperature dependent function) is the compound parameter. Table 2 lists the compound parameters and base phases assigned to compounds in the systmes of interest. Thus the free energy of one gram atom of the compound $AlN{\cdot}Al_2O_3$ which is defined as $(1/7)(AlN{\cdot}Al_2O_3)$ or ${}^{AN}_{0.286}{}^{AO}_{0.714}$ is defined as

$$G^{\Psi} = 0.286\ {}^{\circ}G_{AN}^{B} + 0.714\ {}^{\circ}G_{AO}^{B} + (0.286)(0.714)[(0.286)LANAO+0.714\ LAOAN-C] \qquad (3)$$

Reference to Table 2 shows that LANAO=LAOAN=29288 and the compound parameter C in this case is equal to 146440. Thus the free energy of formation of ${}^{AN}_{0.286}{}^{AO}_{0.714}$ from the beta Si_3N_4 forms of AN and AO is equal to -23922 Joules. In order to compute the free energy of formation of ${}^{Al}_{0.286}{}^{AO}_{0.714}$ from the stable N(hexagonal) form of AN (i.e. AlN) and the stable C(Corundum) form of AO (i.e. Al_2O_3) it is necessary to include the lattice stability terms ANANBN and AOAOBC. The former is contained in Table 1 (ANANBN=ANANLN-ANANLB=42593-0.80T) while the latter AOAOBC=AOAOLC-AOAOLB=23640+2.30T. With this additional information the free energy of formation of ${}^{AN}_{0.286}{}^{AO}_{0.714}$ from the N form of AN and the C form of AO can be computed as is shown in Table 3. Here the free energy of formation of (1/7)$(AlN{\cdot}Al_2O_3)$ from (1/7)AlN (i.e. 0.286AN) and $(1/7)(Al_2O_3)$(i.e. 0.714 AO) with AN in the hexagonal, N, form and AO in the Corundum form as illustrated by Equation 4.

$$\Delta G = 0.286\ ({}^{\circ}G_{AN}^{B} - {}^{\circ}G_{AN}^{N}) + 0.714\ ({}^{\circ}G_{AO}^{B} - {}^{\circ}G_{AO}^{C}) - 23922 \qquad (4)$$

$$= 0.286\ (ANANBN) + 0.714\ (AOAOBC) - 23922 \qquad (5)$$

$$= 5138 + 1.418T \text{ Joules/g.at.} \qquad (6)$$

Tables 1 and 2 summarize the lattice stabilities, solution phase and compound phase parameters for the quasi-binary oxynitride systems of interest while Table 3 displays the free energy of formation of the compound phases which form in the subject binary systems. The quasi-binary systems computed on the basis of Tables 1 and 2 in combination with the lattice stability values presented earlier are shown in Figures 1-7 which are all computed at one atmosphere pressure! Thus these diagrams represent metastable equilibria at temperatures above the decomposition points of AN and SN. This matter will be taken up in Section 3. Reference to Table 3 shows that several metastable phases are described in the AN-AO system. These phases designated, ${}^{AN}_{0.706}{}^{AO}_{0.294}$(G) and ${}^{AN}_{0.286}{}^{AO}_{0.714}$(B) display positive free energies of formation of 1.121T Joules/g.at. and 5138+1.418T Joules/g.at. respectively. Indeed the latter was discussed in Equations (3-6) above. In equation 2 it was shown that the free energy of formation of this ${}^{AN}_{0.286}{}^{AO}_{0.714}$(B) phase from AN(B) and AO(B) was negative i.e. -23922 Joules/g.at. However Equations (3-6) which compute the free energy of formation of this phase from AN(N) and AO(C) yield the positive value in Table 6. Thus this phase does not appear on the AN-AO diagram shown in Figure 3. Reference to Figure 3 shows that neither the above mentioned ${}^{AN}_{0.706}{}^{AO}_{0.294}$(G) nor the ${}^{AN}_{0.286}{}^{AO}_{0.714}$(B) phase

TABLE 1

SUMMARY OF LATTICE STABILITY PARAMETERS
(All units in Joules per gram atom (mole of atoms), T in Kelvins)

AO = (1/5)Al_2O_3, SO = (1/3)SiO_2, MO = (1/2)MgO, AN = (1/2)AlN, SN = (1/7)Si_3N_4

P = Periclase, C = Corundum, S = Spinel, X = Crystobalite, T = Tridymite

H = α quartz, R = β quartz, B = beta Si_3N_4, N = hexagonal AlN, L = Liquid

SNSNLB* = (1/7) Si_3N_4(Liquid) - (1/7) Si_3N_4(beta)

ANANLN = (1/2) AlN (Liquid) - (1/2) AlN (hex) etc.

SNSNLB = 33949 - 12.51T		ANANLN = 42593 - 13.31T	
SNSNLN = - 13.31T		ANANLB = - 12.51T	
SNSNLP = - 12.55T		ANANLP = - 10.21T	
SNSNLC = - 10.21T		ANANLC = - 10.21T	
SNSNLX = - 1.67T		ANANLX = - 1.67T	
SNSNLS = - 8.37T		ANANLS = - 8.37T	
MOMOLP = 47698 - 15.40T	(reference 1)		
MOMOLB = - 12.51T		AOAOLB = - 12.51T	
MOMOLN = - 13.31T		AOAOLN = - 13.31T	
SOSOLC = - 2.09T	(reference 2)	AOAOLC = 23640 - 10.21T	(reference 1)
SOSOLB = -2.09T			
SOSOLN = -2.09T			
SOSOLX = 3347 -1.674T	(reference 2)		

* These differences specify the free energy of one phase (i.e. liquid) minus the free energy of the second phase (i.e. beta) for a given compound.

---

is stable. Indeed these phases are the unstable counterphases for the stable $SN_{0.412}AN_{0.588}$(G) and the $SN_{0.980}AN_{0.020}$(B) phases which appear in the SN-AN system shown in Figure 2. This definition of the metastable $AN_{0.706}AO_{0.294}$(G) and $AN_{0.286}AO_{0.714}$(B) phases are required for calculation of the SN-AO-AN ternary system described in Section 5. Tables 1 and 2 permit computation of the melting points of these metastable compounds. In particular subtraction of equation 2 from equation 1 provides the description of the free energy of fusion of compound phase ϕ when $x=x_*$.
Thus

$$\Delta G^{\phi\to L} = G^L - G^\phi = (1-x_*)[{}^\circ G_i^L - {}^\circ G_i^\theta] + x_*[{}^\circ G_j^L - {}^\circ G_j^\theta] + RT(x_* \ell n x_* + (1-x_*)\ell n(1-x_*)) + x_*(1-x_*)C \quad (7)$$

The free energy change on fusion for the $AN_{0.286}AO_{0.714}$(B) phase with θ=B and C=146440 is given by

$$G^L - G^B = 0.286(\text{ANANLB}) + 0.714(\text{AOAOLB}) - 4.977T + 2990? \quad (8)$$

$$= 29904 - 17.487T \quad \text{Joules/g.at} \quad (9)$$

yielding a melting point of 1710°K which lies below the stable 2200°K eutectic in Figure 3. A similar calculation can be performed for the $AN_{0.706}AO_{0.294}$(G) phase with θ=N and C=62760 from Table 2.

TABLE 2

SUMMARY OF SOLUTION AND COMPOUND PARAMETERS
(All units in Joules per gram atom (mole of atoms), T in Kelvins)

Solution Parameters

LANSO = LSOAN = LSNAN = LANSN = LANAO = LAOAN = LANMO = LMOAN = 29288
LSNSO = LSOSN = LSNAO = LAOSN = LMOSN = LSNMO = 29288

NANSO = NSOAN = XANSO = XSOAN = TANSO = TSOAN = HANSO = HSOAN = RANSO = RSOAN = 125520
BSNAN = BANSN = NSNAN = NANSN = 125520
NANAO = NAOAN = CANAO = CAOAN = 125520
NANMO = NMOAN = PANMO = PMOAN = 125520
BSNSO = BSOSN = XSOSN = XSNSO = TSNSO = TSOSN = HANSO = HSOAN = RANSO = RSOAN = 125520
BSNAO = BAOSN = CSNAO = CAOSN = 125520
BSNMO = BMOSN = PSNMO = PMOSN = 125520

Compound Parameters

Compound	Name	Stoichiometry	Stability	Base	Compound Parameter Joules/g.at.
(1/50)($7Si_3N_4$·(1/2)AlN)	B	$SN_{0.980}{}^{AN}{}_{0.020}$	Stable	B	83680 + 4.184T
(1/17)(Si_3N_4·5AlN)	G	$SN_{0.412}{}^{AN}{}_{0.588}$	Stable	N	96232
(1/17)(6AlN·Al_2O_3)	G	$AN_{0.706}{}^{AO}{}_{0.294}$	Metastable	N	62760
(1/ 7)(AlN·Al_2O_3)	B	$AN_{0.286}{}^{AO}{}_{0.714}$	Metastable	B	146440
(1/17)(AlN·3Al_2O_3)	SP	$AN_{0.118}{}^{AO}{}_{0.882}$	Stable	S	120081 − 12.678T
(1/12)(5AlN·MgO)	Q	$AN_{0.833}{}^{MO}{}_{0.167}$	Stable	N	104600 − 8.368T
(1/50)($7Si_3N_4$·(1/3)SiO_2)	B	$SN_{0.980}{}^{SO}{}_{0.020}$	Stable	B	71128 + 4.184T
(1/10)(Si_3N_4·SiO_2)	R	$SN_{0.700}{}^{SO}{}_{0.300}$	Stable	B	115060 − 25.104T
(1/50)($7Si_3N_4$·(1/5)Al_2O_3)	B	$SN_{0.980}{}^{AO}{}_{0.020}$	Stable	B	65270 + 4.184T
(1/50)((1/2)MgO·$7Si_3N_4$)	B	$MO_{0.020}{}^{SN}{}_{0.980}$	Stable	B	112968 + 4.184T

Here

$$G^L - G^G = 0.706(ANANLN) + 0.294(AOAOLN) - 5.036T + 13027 \quad (10)$$

$$= 43098 - 18.346T \text{ Joules/g.at.} \quad (11)$$

yielding a melting point of 2349°K which is unstable since it lies within the two phase L+N field shown in Figure 3.

Finally mention should be made of the $Sn_{0.980}{}^{AN}{}_{0.020}$(B), $Sn_{0.980}{}^{SO}{}_{0.020}$(B) $Sn_{0.980}{}^{AO}{}_{0.020}$(B) and $MO_{0.020}{}^{Sn}{}_{0.980}$(B) compound phases shown in Tables 2 and 3 and in Figures 2,5,6 and 7. These "compound" phases are defined for mathematical convenience only so that the extension of the Si_3N_4 or SN(B) phase into a ternary system can be made along the lines used previously for metallic systems(5). Examination of the free energy of formation of these compounds show very small negative values which could be representative of a dilute solution phase.

TABLE 3

SUMMARY OF CALCULATED FREE ENERGIES OF COMPOUND FORMATION
(JOULES, °K)

REACTION	ΔG
$(7/50)Si_3N_4(B) + (1/100)AlN(N) \rightarrow (1/50)(7Si_3N_4 \cdot (1/2)AlN)(B)$	-213 - 0.098T
$(1/17)Si_3N_4(B) + (5/17)AlN(N) \rightarrow (1/17)(Si_3N_4 \cdot 5AlN)(G)$	-2234 + 0.326T
$(6/17)AlN(N) + (1/17)Al_2O_3(C) \rightarrow (1/17)(6AlN \cdot Al_2O_3)(G)$	+ 1.121T
$(1/7)AlN(N) + (1/7)Al_2O_3(C) \rightarrow (1/7)(AlN \cdot Al_2O_3)(B)$	5138 + 1.418T
$(1/17)AlN(N) + (3/17)Al_2O_3(C) \rightarrow (1/17)(AlN \cdot 3Al_2O_3)(SP)$	-515 - 0.259T
$(5/12)AlN(N) + (1/12)MgO(P) \rightarrow (1/12)(5AlN \cdot MgO)(Q)$	-2510 + 0.815T
$(7/50)Si_3N_4(B) + (1/150)SiO_2(R) \rightarrow (1/50)(7Si_3N_4 \cdot (1/3)SiO_2)(B)$	-720 - 0.102T
$(1/10)Si_3N_4(B) + (1/10)SiO_2(R) \rightarrow (1/10)(Si_3N_4 \cdot SiO_2)(R)$	-16495 + 4.971T
$(7/50)Si_3Ni_4(B) + (1/5)Al_2O_3(C) \rightarrow (1/50)(7Si_3N_4 \cdot (1/5)Al_2O_3)(B)$	-234 - 0.036T
$(1/100)MgO(P) + (7/50)Si_3N_4(B) \rightarrow (1/50)((1/2)MgO \cdot 7Si_3N_4)(B)$	-686 - 0.140T

3. Calculation of the Melting and Decomposition Temperatures of AlN and Si_3N_4

Examination of Figures 1-7 shows that the decomposition temperatures for AlN and Si_3N_4 are computed to be 2850K and 2129K respectively at one atmosphere. These temperatures are below the computed melting points of AN and SN which are defined by ANANLN and SNSNLB in Table 1 at 3200K and 2714K respectively. Calculation of the melting and decomposition temperatures of AN and SN was carried out along the lines developed previously (1,6-12) by defining Equations 1 and 2 for the liquid and $Al_{0.50}N_{0.50}$ phase in the Al-N system and the liquid and $Si_{0.429}N_{0.571}$ phase in the Si-N system. Table 4 shows the results in terms of Lattice Stability Parameters (4.1), Solution Phase Parameters (4.2), Compound Parameters (4.3) and Free Energy changes on Fusion 4.4. The latter provides the basis for the values of ANANLN and SNSNLB in Table 1. The equations displayed earlier in connection with the melting point of $AN_{0.286}AO_{0.714}(B)$ and $AN_{0.706}AO_{0.294}(G)$ and derived by subtraction of equations 1 and 2 (i.e. Eqs. 7-11) are used in defining the results in (4.4). The Table 4 description can also be employed to compute the free energy of formation of AN and SN from nitrogen and liquid or solid forms of aluminum and silicon. The results shown in 4.5 are in good agreement with the assessed Data Bank values (8). These results yield the predicted one atmosphere decomposition points. Finally, the solubility of nitrogen in liquid silicon and liquid aluminum can be computed (4.6) and are found to be in good agreement with observed values (9,10).

4. Calculation of the SiO_2-Al_2O_3-Si_3N_4 Ternary System

The isothermal section at 2200K in the SiO_2-Al_2O_3-Si_3N_4 system was computed and is shown in Figure 8. The ternary liquid(L), corrundum(C) and B(beta) solution phases were described by means of Kohler's equation with zero values for the ternary interaction parameters. The mullite(M) and silicon oxynitride(R) compounds were defined as shown in Figure 8 with the counterphase parameters CB=0 and CAB=0 along the lines previously set forth in Equations 4-6 of reference (2). In addition a ternary X phase was included corresponding to $SO_{0.20}AO_{0.65}SN_{0.15}$ (3,4). The compound parameter for this phase

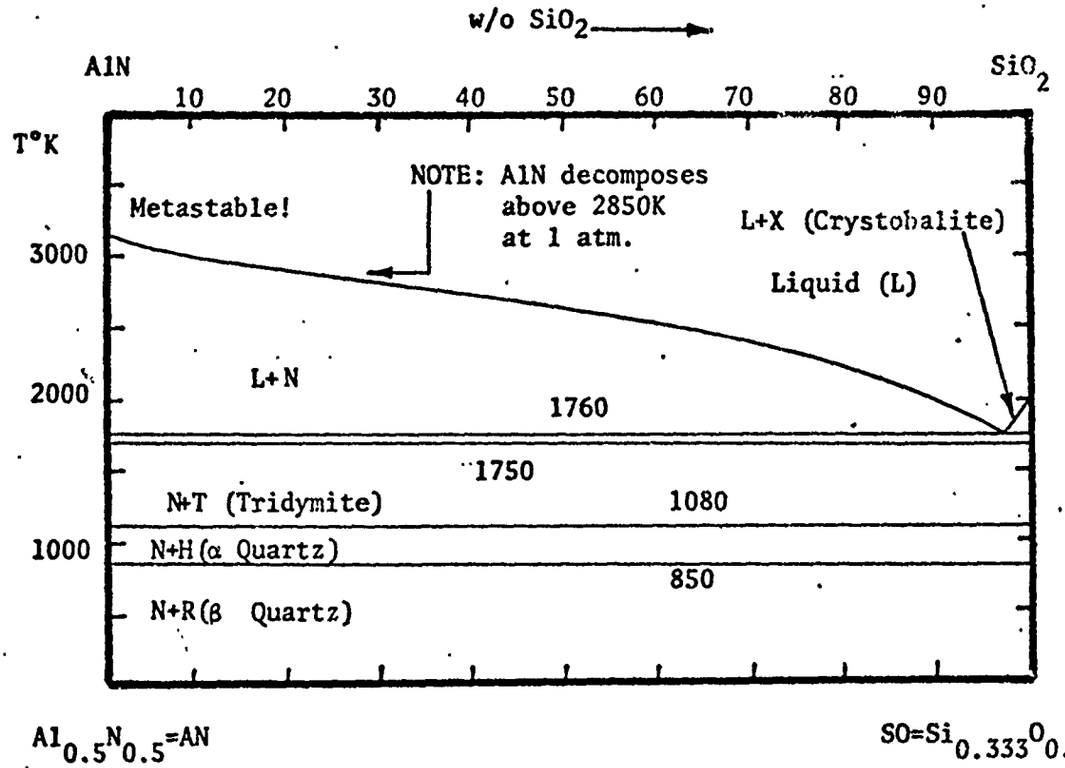

Figure 1. Calculated $Al_{0.5}N_{0.5}$-$Si_{0.333}O_{0.667}$ Phase Diagram at one atmosphere

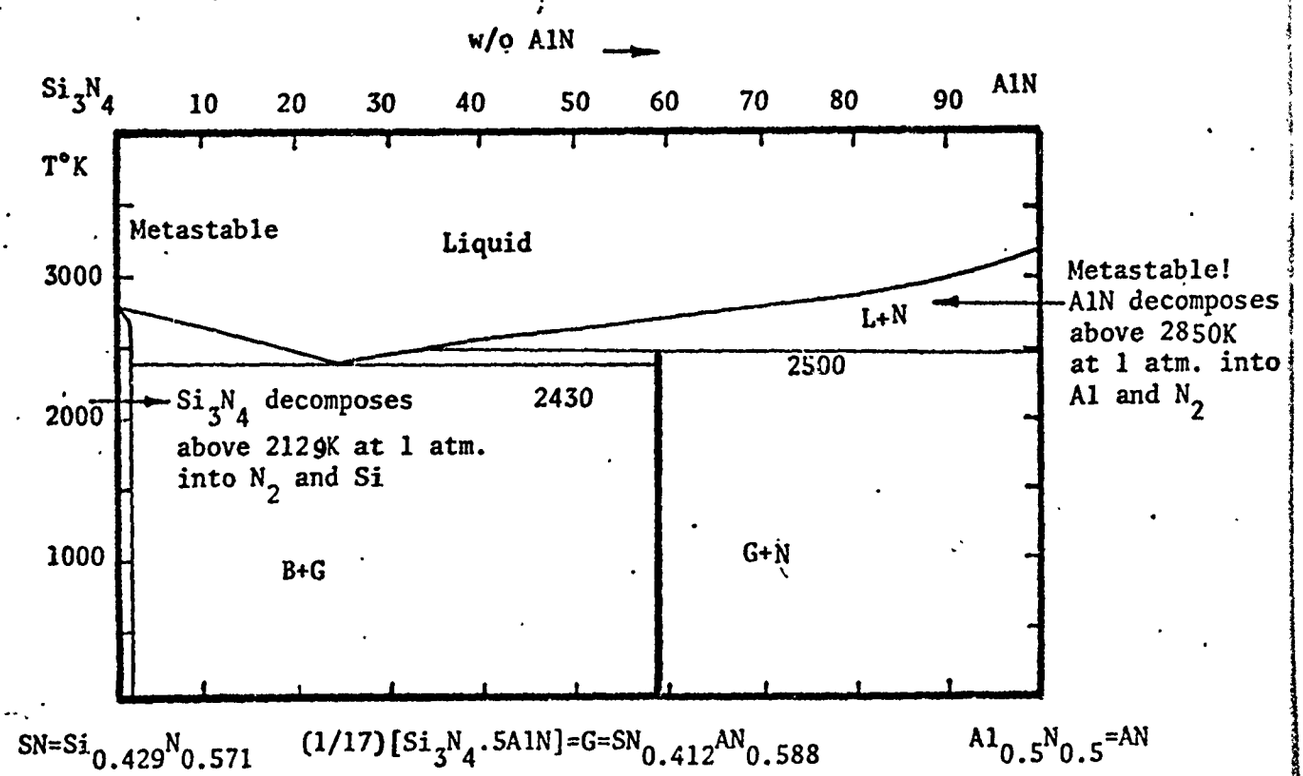

Figure 2. Calculated $Si_{0.429}N_{0.571}$ -$Si_{0.333}O_{0.667}$ Phase Diagram at one atmosphere

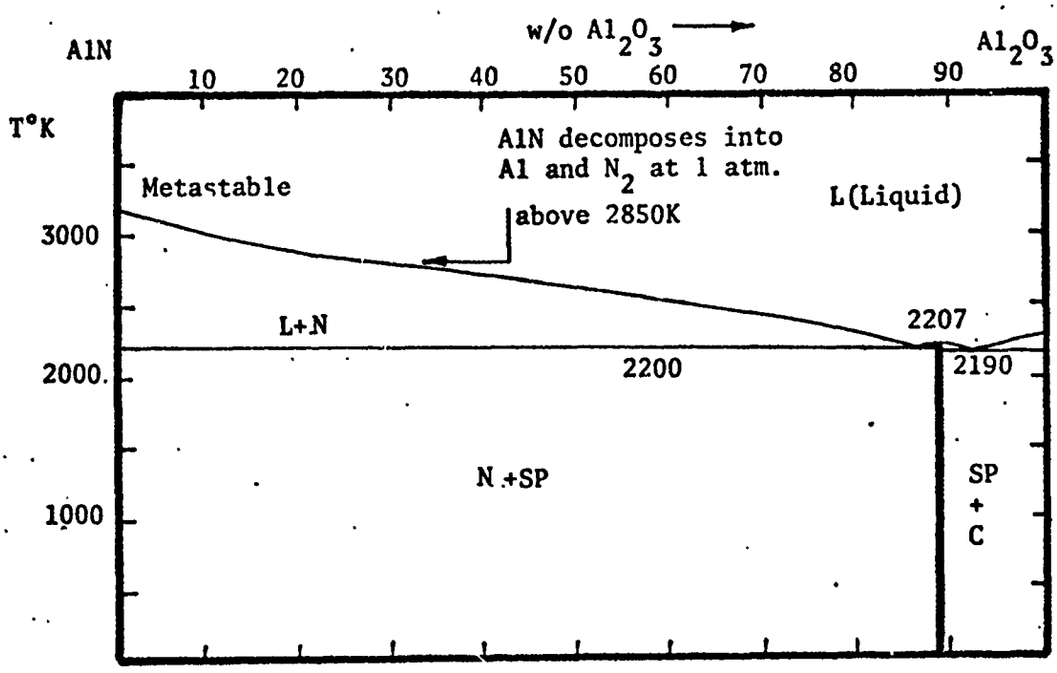

Figure 3. Calculated $Al_{0.5}N_{0.5}$ -$Al_{0.4}O_{0.6}$ Phase Diagram at one atmosphere

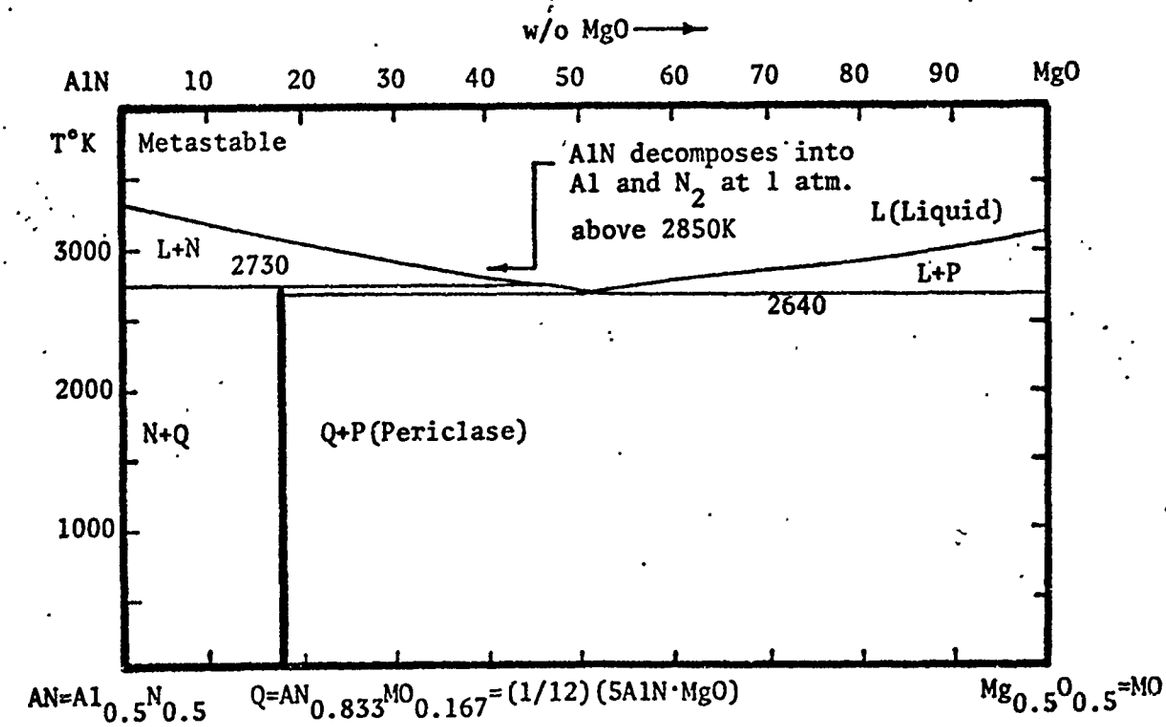

Figure 4. Calculated $Al_{0.5}N_{0.5}$ -$Mg_{0.5}O_{0.5}$ Phase Diagram at one atmosphere

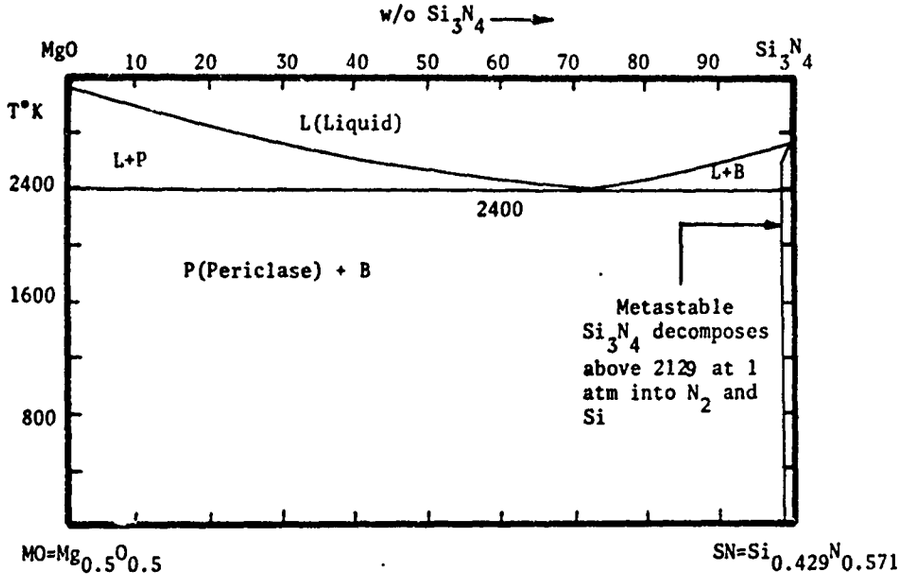

Figure 5. Calculated $Mg_{0.5}O_{0.5}$ -$Si_{0.429}N_{0.571}$ Phase Diagram at one atmosphere

(i.e. C=47,700) shown in Figure 8 is defined on the basis of Table VIII of reference 12 which defines the free energy of a ternary compound by means of Equation (12) as

$$G^X = 0.20\ {}^{\circ}G^C_{SO} + 0.65\ {}^{\circ}G^C_{AO} + 0.15\ {}^{\circ}G^C_{SN} + (0.20)(0.65)(0.85)^{-1}[0.20LSOAO + 0.65LAOSO - C]$$
$$+ (0.20)(0.15)(0.35)^{-1}[0.20LSOSN + 0.15LSNSO - C] + (0.65)(0.15)(0.80)^{-1}[0.65LAOSN + 0.15LSNAO - C] \quad (12)$$

Since LAOSO=28451 and LSOAO=38492 from reference (2)

$$G^X = 0.20\ {}^{\circ}G^C_{SO} + 0.65\ {}^{\circ}G^C_{AO} + 0.15\ {}^{\circ}G^C_{SN} - 9460 \quad \text{Joules/g.at.} \quad (13)$$

or the free energy change for the reaction

$$0.067SiO_2(x) + 0.13Al_2O_3(C) + 0.0214Si_3N_4(B) \rightarrow [0.067SiO_2 \cdot 0.13Al_2O_3 \cdot 0.0214Si_3N_4](X) \quad (14)$$

$$\Delta G = 0.20(SOSOCX) + 0.15(SNSNCB) - 9460 = -3700 - 0.261T \quad \text{Joules/g.at.} \quad (15)$$

5. Calculation of the Si_3N_4-Al_2O_3-AlN Ternary System

The ternary isothermal section for the SN-AO-AN system shown in Figure 6 was calculated along lines similar to those described in Section 4. The solution phases covered included the liquid, L, corundum, C, hexagonal, N, and Beta, B, phases described by Kohler's equation with zero valued ternary interaction parameters. In addition, the spinel $AN_{0.118}AO_{0.882}(SP)$, $SN_{0.412}AN_{0.588}$-$AN_{0.706}AO_{0.294}(G)$ and $SN_{0.980}AO_{0.020}$-$AN_{0.286}AO_{0.714}(B)$ compound phases are included. The spinel compound phase is described with a $SN_{0.118}AO_{0.882}(SP)$ counterphase with θ=S, CB and CAB equal to zero. The base phases and the compound parameters for the B and G compound phases are shown in Figure 9. The prior discussion in Section 2 described the metastable counterphases $AN_{0.706}AO_{0.294}(G)$ and $AN_{0.286}AO_{0.714}(B)$. These metastable phases are described with base phases of N and B respectively and with compound parameters which are 62760 and 146440 Joules/g.at. respectively as shown in Table 2. Panels (a) through (c) in Figure 9 show the computed equilibrium between the N/L, B/L and G/L pairs at 2200K. The B/L equilibrium shown in Panel (b) was computed with a value of CAB=-83862 in order to extend the B (beta Si_3N_4)

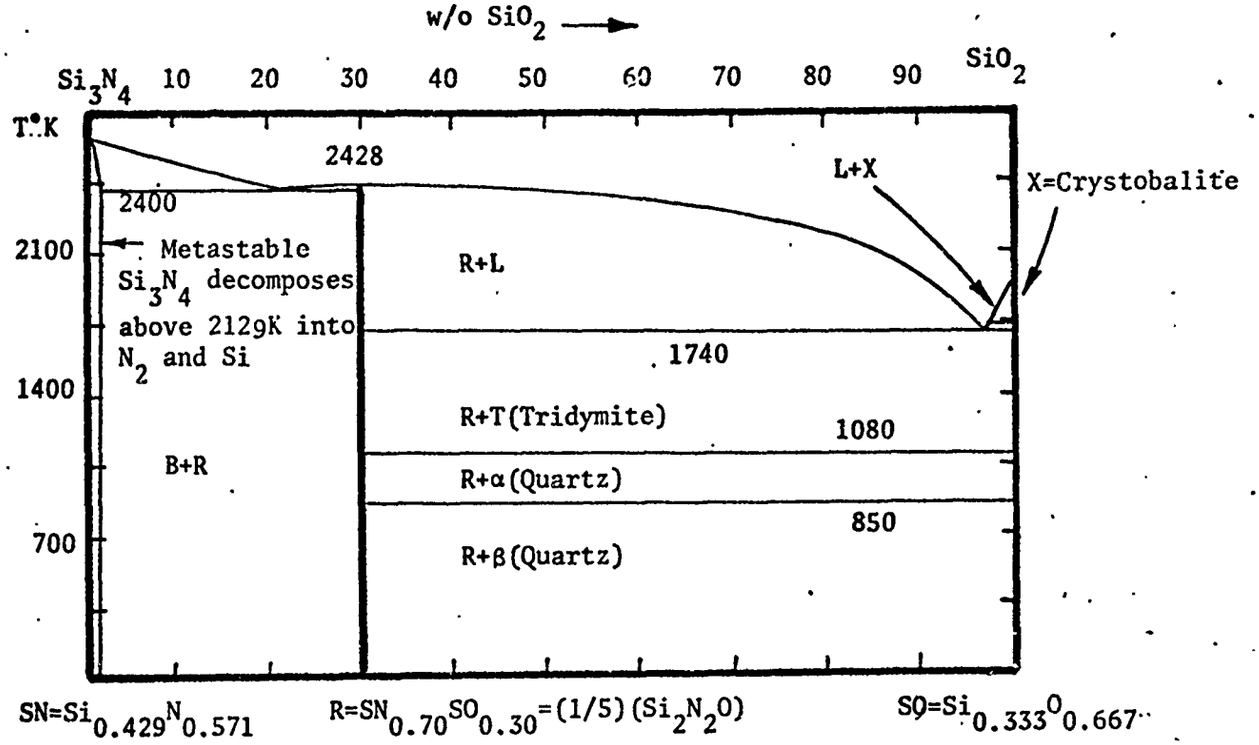

Figure 6. Calculated $Si_{0.429}N_{0.571}$ -$Si_{0.333}O_{0.667}$ Phase Diagram at one atmosphere

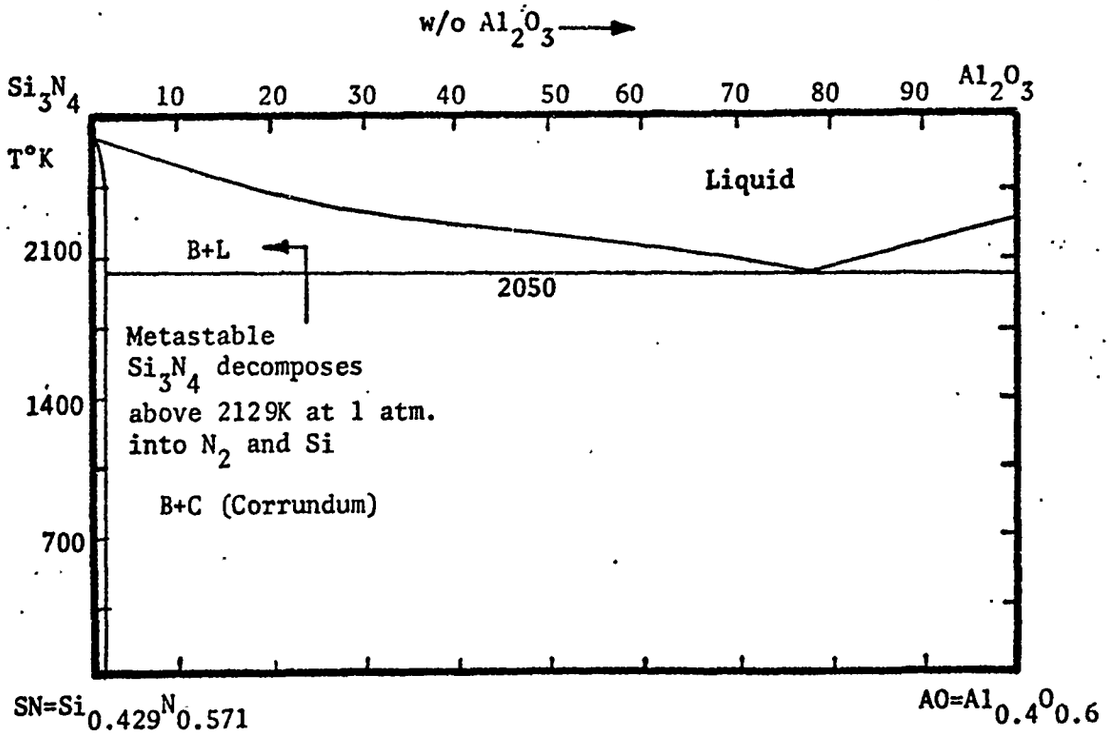

Figure 7. Calculated $Si_{0.429}N_{0.571}$ -$Al_{0.4}O_{0.6}$ Phase Diagram at one atmosphere

TABLE 4

SUMMARY OF ALUMINUM-NITROGEN AND SILICON-NITROGEN SYSTEM ANALYSES FOR ESTIMATION OF THE MELTING TEMPERATURES AND HEATS OF FUSION OF AlN and Si_3N_4 (Joules, g.at. °K)

V=Vapor, L=Liquid, D=Diamond Cubic, A=fcc, B=bcc

1. Lattice Stability Parameters

ALALLB= 628- 6.69T	(reference 6)	NNNNLB= 879-1757T
ALALLA=10711-11.51T	"	NNNNBV=-3682+53.64T
ALALBA=10083-4.82T	"	NNNNLV=-2803+36.07T
SISIBD=44350-19.54T	(reference 5)	
SISILD=50626-30.00T	"	
SISILB= 6276-10.46T	"	

2. Solution Phase Parameters

LALNN=-50208, LNNAL=-912112+256.48T, LSINN=14644, L=-674879+235.14T

3. Compound Phase Parameters

$(Al_{0.5}N_{0.5})$; C=167360+18.41T base=bcc

$(Si_{0.429}N_{0.571})$; C=125520+31.38T base=bcc

4. Free Energy Change on Fusion

$Al_{0.5}N_{0.5}$:

$\Delta G = 0.5(628-6.69T)+0.5(879-17.57T)-5.77T+0.25(167360+18.41T)$

$= 42593-13.31T$ = ANANLN(Table 1) ; Melting Point=3200°K

$Si_{0.429}N_{0.571}$:

$\Delta G = 0.429(6276-10.46T) + 0.571(879-17.57T) - 5.68T+0.245(125520+31.38T)$

$= 33949-12.51T$ = SNSNLB(Table 1) ; Melting Point=2713°K

5. Free Energy of Formation

$0.5\ Al(L) + 0.25N_2(V) \rightarrow Al_{0.5}N_{0.5}$

$\Delta G = 0.50(-628+6.69T) + 0.5(-3682+53.64T)$

$+ 0.25(0.50(-50208)+0.50(-912112+256.48T)-167360-18.41T)$

$= -164285 + 57.625T$; Decomposition at 1 atmosphere at 2850°K

$0.5\ Al(fcc) + 0.25N_2(V) \rightarrow Al_{0.5}N_{0.5}$

$\Delta G = 0.50(10083-4.82T) + 0.5(-3682+53.64T)$

$+ 0.25(0.50(-50208)+0.50(-912112+256.48T)-167360-18.41T)$

$= -158929 + 51.87T$

TABLE 4 (concluded)

$0.429\ Si(L) + 0.2855N_2(V) \rightarrow Si_{0.429}N_{0.571}$

$\Delta G = 0.429(-6276+10.46T) + 0.571(-3682+53.64T)$

$+ 0.245(0.429(14644) + 0.571(-674879+235.14T)-125520-31.38T)$

$= -128420+60.32T$; Decomposition at 1 atmosphere at 2129°K

$0.429\ Si(D) + 0.2855N_2(V) \rightarrow Si_{0.429}N_{0.571}$

$\Delta G = 0.429(44350-19.54T) + 0.571(-3682+53.64T)$

$+ 0.245(0.429(14644) + 0.571(-674879+235.14T)-125520-31.38T)$

$= -106702+47.44T$

6. Calculation of Nitrogen Solubility in Liquid Aluminum and Silicon

Al-N (Solubility of nitrogen in liquid aluminum)

$RT\ln x = ALALBL + NNNNBL - LALNN$

$+ 0.50(0.5(-50208)+0.50(-912112+256.48T)-167360-18.41T)$

$= -275559 + 79.18T$; x=0.0001=0.01 atomic percent at 1773K

Si-N (Solubility of nitrogen in liquid silicon)

$RT\ln x = (0.429)(0.571)^{-1}\ SISIBL+NNNNBL-LSINN$

$+ 0.429[0.429(14644)+0.571(-674879+235.14T)-125520-31.38T)$

$= -236701+69.55T$; x=0.00017=0.017 atomic percent at 1673K.

---

compound phase out into the ternary system (3,4). Panel (d) shows a composite of the B/L, G/L, N/L and S/L equilibrium. This composite constitutes the ternary section at 2200K and should provide a picture of the phase constitution at lower temperatures. Calculation of ternary sections at lower temperatures, (wher. the liquid disappears) can be readily carried out on the basis of the parameter values developed here. It should be noted that the isothermal sections shown in Figures 8 and 9 are metastable with respect to the one atmosphere decomposition of Si_3N_4 at 2129°K (see Section 3).

6. Calculation of the Free Energy of Formation of Beta SIALONS and Comparison with the Computed Results of the Stuttgart Group(4)

The foregoing results can be compared directly with those presented earlier (3,4) by the Stuttgart group with respect to phase equilibria and the free energy of formation of the beta SIALONS. Figures 8 and 9 should be compared with Figure 7 of reference 3 and Figure 16 of reference 4. With respect to the former comparison Figure 8 covering the SN-SO-AO ternary section should be compared with the upper left portion of the SiO_2-Al_2O_3-AlN-Si_3N_4 square in Figure 7 of reference 3 which corresponds to the Si_3N_4-SiO-Al_2O_3 right isosceles triangle. Here the X_1 phase shown in Figure 7 of reference 3 corresponds to the current X phase in Figure 8. Figure 9 should be compared with the lower right isoceles triangle Si_3N_4-Al_2O_3-AlN shown in Figure 7 of reference 3. The present diagram includes the "beta Si_3N_4" phase and the G phase. The latter corresponds to the X_7 phase in reference 3. The phases labeled X_2,X_4,X_5 and X_6 in reference 3 are not included in Figure 9. The next step in the comparison is computation of the free energy of formation of beta sialons. This calculation is detailed in Table 5 starting with the expression for G^B given by Equation (16) in Table 5. Reference to Equation (16) and the succeeding relations through Equation (21) shows that the free energy of the beta sialon phase which projects into the Si_3N_4-Al_2O_3-AlN ternary from the Si_3N_4 corner toward the AlN·Al_2O_3 or Al_3O_3N composition can be defined explicitly in terms of the compound parameter for the

(a)=R/L and M/L

SO=(1/3(SiO_2)

AO=(1/5)(Al_2O_3)

SN=(1/7)(Si_3N_4)

L=Liquid

C=Corrundum

R=(1/5)(Si_2N_2O) Silicon Oxy Nitride

$R=SO_{0.3}SN_{0.7}=R$

$SO_{0.3}SN_{0.7}$ - $SO_{0.3}AO_{0.7}$

θ=B

CB=0

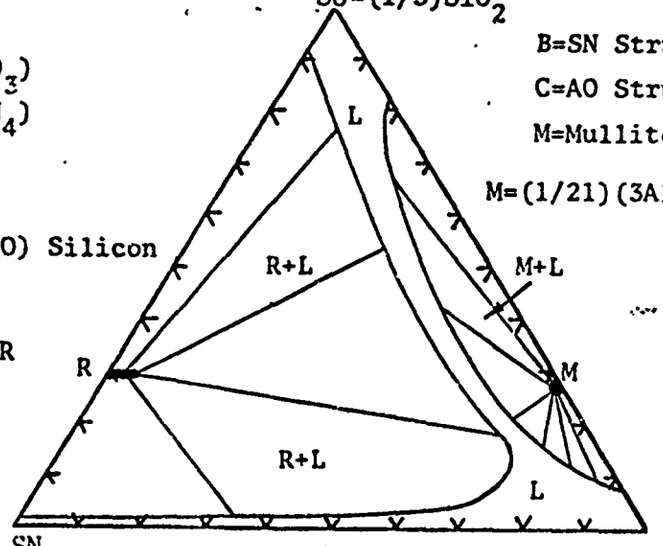

(b)=B/L and C/L

B=SN Structure

C=AO Structure

M=Mullite=$SO_{0.286}AO_{0.714}$

$M=(1/21)(3Al_2O_3-2SiO_2)$

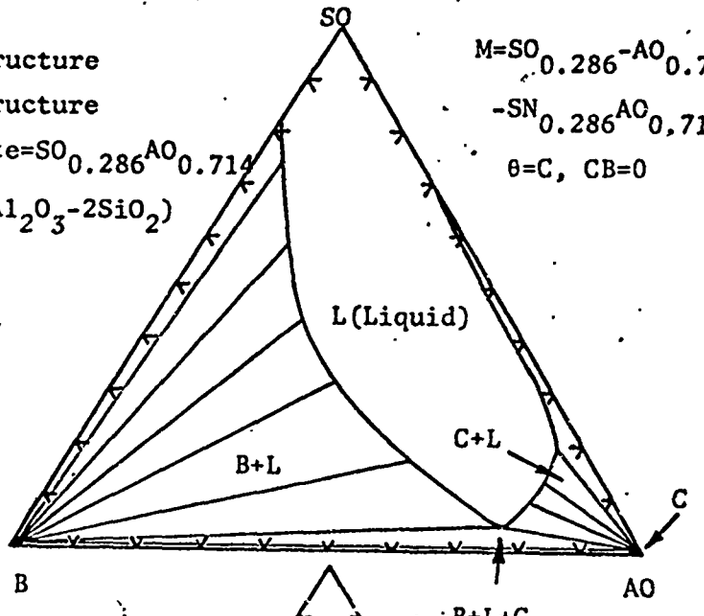

$M=SO_{0.286}-AO_{0.714}$

$-SN_{0.286}AO_{0.714}$

θ=C, CB=0

(c)=X/L

$X=SO_{0.20}AO_{0.65}SN_{0.15}$

θ=C, C=47,700

ΔG_f (from Corrundum)

=-9460 J/g.at.

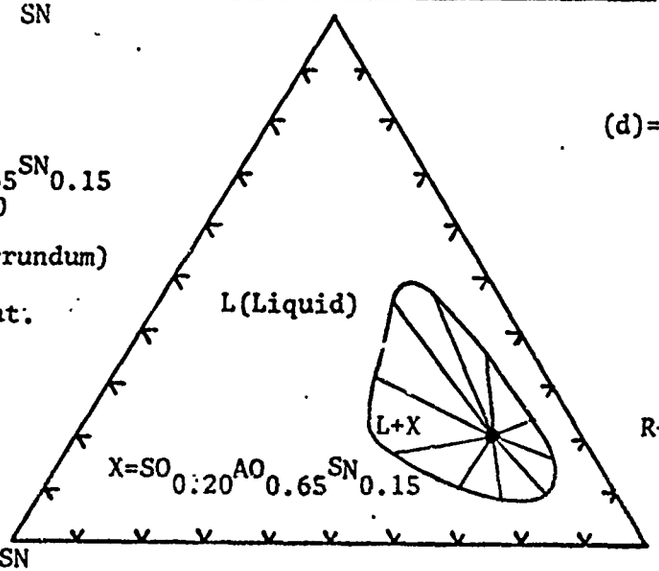

(d)=Composite

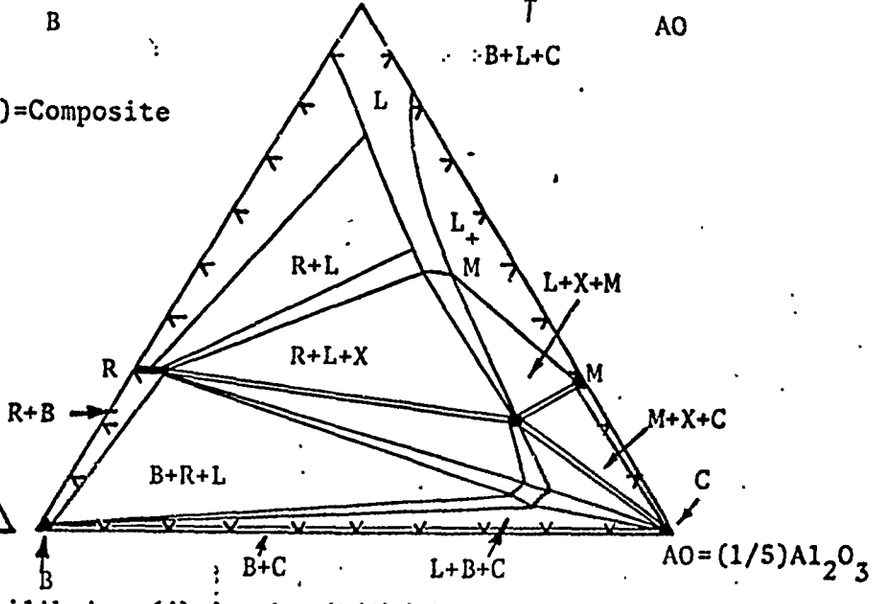

Figure 8. Calculated Pairwise (a-c) and Composite Equilibrium (d) in the $(1/3)(SiO_2)$ - $(1/7)(Si_3N_4)$-$(1/5)Al_2O_3$ System at 2000K and one atmosphere

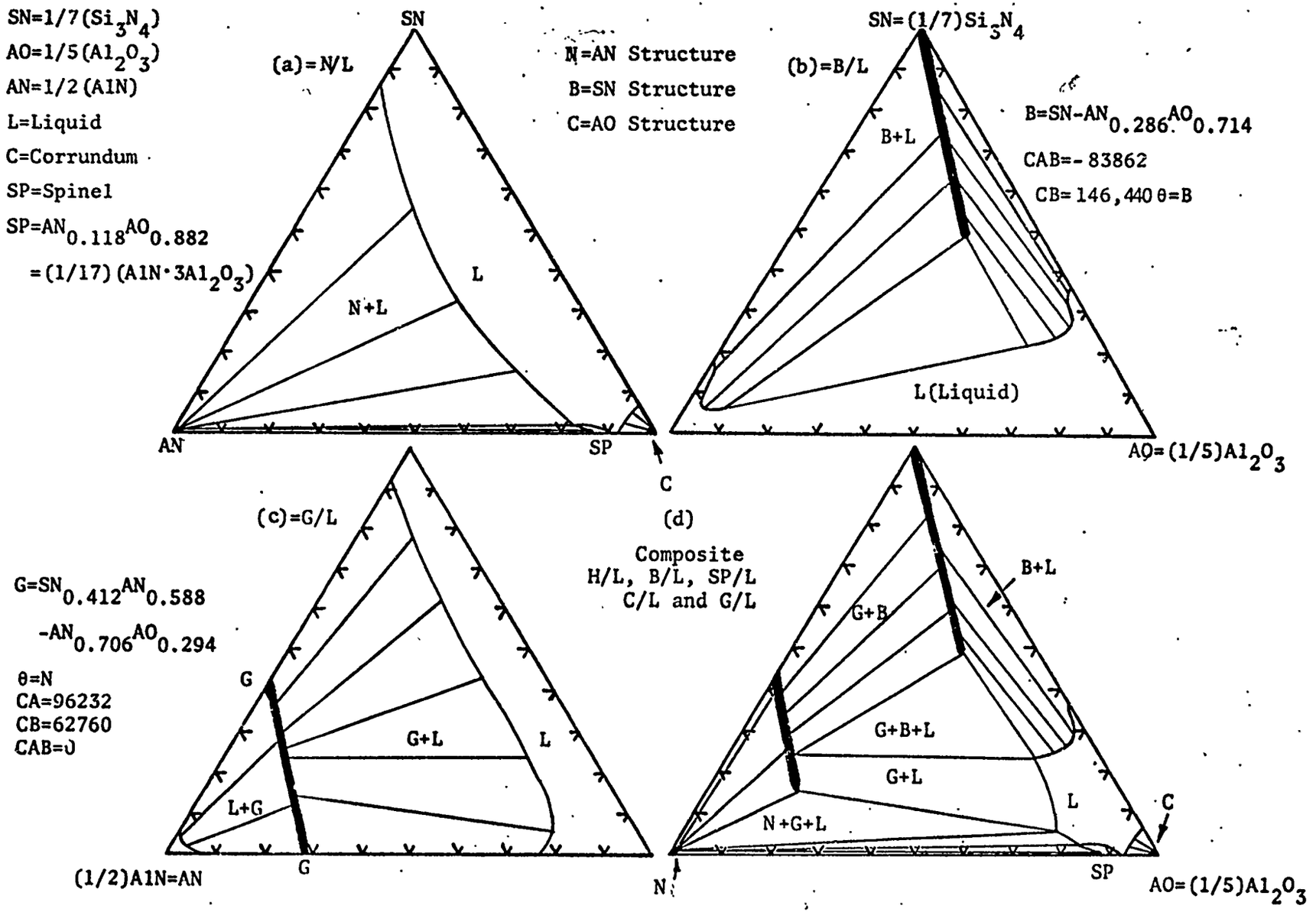

Figure 9. Calculated Pairwise (a-c) and Composite Equilibrium(d) in the $(1/7)Si_3N_4$-$(1/5)Al_2O_3$-(1/2)AlN system at2200K and one atmosphere.

TABLE 5

CALCULATION OF THE FREE ENERGY OF FORMATION OF BETA SILICON NITRIDE - ALUMINUM OXYNITRIDE SOLID SOLUTIONS
(Joules, °K)

$$G^B = z\ {}^\circ G^B_{SN} + x\ {}^\circ G^B_{AO} + y\ {}^\circ G^B_{AN} + (1-(y/(1-x)))\Delta G_A + (y/(1-x))\ \Delta G_B$$

$$+ RT(y\ln y + z\ln z - (1-x)\ln(1-x)) + \Delta G_E \quad \text{(from reference 5)} \tag{16}$$

where $x=x_{AO}$ and $y=y_{AN}$ and $z=z_{SN}=1-x-y$ as in Figure 9

Since the solid solution runs from $Sn_{0.980}{}^{AO}{}_{0.020}$ to $AN_{0.286}{}^{AO}{}_{0.714}$ then $x_*=0.714$, $x^1_*=0.020$ and $p=(x_*-x^1_*)/(1-x_*)=2.426$. Thus

$$x=x_*+yp = 0.02 + 2.46y \quad \text{(from reference 5)} \tag{17}$$

$$z=1-x^1_* - y(1+p) = 0.98 - 3.426y \tag{18}$$

with $\Delta G_A = (0.02)(0.98)[0.02LSNAO+0.98LAOSN-C]=0.0196[29288-65270-4.184T]$

$$= -705 - 0.082T \tag{19}$$

and $\Delta G_B = (0.286)(0.714)[0.286LANAO+0.714LAOAN-C]=0.2042[29288-146440]$

$$= -23922 \tag{20}$$

since the compound parameters, C, in these equations refer to the values listed in Table 2 for $SN_{0.980}{}^{AO}{}_{0.020}$ and $AN_{0.286}{}^{AO}{}_{0.714}$ respectively
Thus

$$G^B = (0.98-3.426y)\,{}^\circ G^B_{SN} + (0.02+2.426y)\,{}^\circ G^B_{AO} + y\ {}^\circ G^B_{AN}$$

$$+ (1-y(0.98-2.426y)^{-1})(-705-0.082T) + y(0.98-2.426y)^{-1}(-23922)$$

$$+ RT(y\ln y+(0.98-3.426y)\ln(0.98-3.426y)-(0.98-2.426y)\ln(0.98-2.426y))$$

$$+ CABy(0.98-3.426y)(0.98-2.426y)^{-1} \tag{21}$$

The free energy change for the reaction

$$(0.14-0.490y)Si_3N_4(B)+(0.004+0.485y)Al_2O_3(C)+0.5y\ AlN(N) \rightarrow$$

$$[(Si_3N_4)_{(0.14-0.409y)}(Al_2O_3)_{(0.004+0.485y)}(AlN)_{0.5y}](B) \tag{22}$$

is

$$\Delta G = G^B - (0.98-3.426y)\,{}^\circ G^B_{SN} - (0.02+2.426y)\,{}^\circ G^C_{AO} - y\ {}^\circ G^N_{AN} \tag{23}$$

or since ${}^\circ G^B_{AO} - {}^\circ G^C_{AO} = AOAOBC=AOAOLC-AOAOLB=23640+2.30T$ (24)

from Table 1 and Reference 1 and

$${}^\circ G^B_{AN} - {}^\circ G^N_{AN} = ANANBN=42593-0.80T \text{ from Table 1} \tag{25}$$

TABLE 5 (concluded)

Then Equation (23) yields the following result when CAB=-83862 J/g.at.

$$\Delta G = (0.02+2.426y)(23640+2.30T) + y(42593-0.80T)$$
$$+ (1-y(0.98-2.426y)^{-1})(-705-0.082T) + y(0.98-2.426y)^{-1}(-23922)$$
$$+ RT(y\ln y+(0.98-3.426y)\ln(0.98-3.426y)-(0.98-2.426y)\ln(0.98-2.426y))$$
$$-83862y(0.98-3.426y)(0.98-2.426y)^{-1} \qquad (26)$$

for $0 \leq y \leq 0.286$. Thus Eq. (26) permits explicit calculation of the free energy of formation of the beta silicon nitride-aluminum oxynitride solid solution as a function of concentration along the join between SN$((1/7)Si_3N_4)$ and $AN_{0.286}AO_{0.714}((1/7\ AlN \cdot Al_2O_3)$ or $(1/7)Al_3N_3O$. If Y is the mole fraction of Al_3N_3O along the Si_3N_4-Al_3N_3O join then Y and y (the atom fraction of AN in the SN-AO-AN ternary shown in Figure 9)are simply related by

$$Y = (0.98/0.286)y+0.02 = 3.426y+0.02 \qquad (27)$$

---

metastable $AN_{0.286}AO_{0.714}$ phase, C=146440, given in Table 2 and the value for CAB=-83862 Joules/g.at. which was used to compute Figure 9. Equations 21 through 26 show how the free energy of formation of the beta sialon phase can be computed as a function of composition when the compounds— beta Si_3N_4, the corundum form of Al_2O_3 and the hexagonal form of AlN are considered to be reactants. Thus equations (26) and (27) can be employed to compute the free energy of formation of beta sialons according to equation 22 as a function of composition. Figure 10 shows the result of such a calculation which was kindly carried out by Dr. H.L. Lukas (3,4) as a function of the mole percent Al_3O_3N. The mole percent is 100 times the mole fraction, Y, given in Equation 27. In Figure 10, the curve labeled L. Kaufman is that given by Equation 26 while the curve labeled P. Doerner et al is the identical free energy change as computed by the Stuttgart group from a completely different starting point using an entirely different model for the liquid and beta sialon phase. The differences between the two curves are less than 4KJ/g.at. (i.e. 1 kcal/g.at.) which is quite remarkable. If the values of CAB-83862 and C=146400 Joules/g.at. employed in Table 5 to develop Equation 26 are reconsidered,the difference between the two curves can be reduced to less than 1600 J/g.at. (i.e. 400 cal/g.at.). Thus the current value of C=146440 yields a positive free energy of formation for the metastable compound $AN_{0.286}AO_{0.714}$ as noted in Section 2, Equations 4-6 and Tables 2 and 3. Moreover the melting point of this compound, based on C=146,400 Joules/g.at. is 1710K according to Eq. 9. If the value of C were increased to C=167,360 Joules/g.at. Equations 4-6 and 9 would lead a free energy of formation (from hexagonal AlN and Al_2O_3(C)) of 866+1.418T Joules/g.at. as compared with the current value of 5138+1.418T listed in Table 3. Thus the increase in C would make the free energy of $An_{0.286}AO_{0.714}$ more negative than it is currently, but still positive. Finally alteration of C from 146,400 to 167,360 would increase the melting point of $AN_{0.286}AO_{0.714}$ from 1710°K to 1956°K, which is still below the 2200K eutectic in Figure 3. Thus if C=167,360 Joules/g.at. for $AN_{0.286}AO_{0.714}$ the upper curve in Figure 10 would be sheared downward until it coincided with the lower curve at 100 mole percent Al_3O_3N. Conversely one could inquire as to the accuracy of the lower curve at 100 mole percent Al_3O_3N since the latter phase is unstable! The final step in bringing the upper curve close to the lower curve is decreasing CAB from -83862 Joules/g.at. to -92048 Joules/g.at. The effect of such a change on the computed phase diagram (along with the aforementioned change in C from 146400 to 167360) is shown in Figure 11. The net result is an increase in the field of stability of beta Si_3N_4.

6. Conclusions

The current extension of the quasibinary synthesis of oxynitride ceramic systems has provided a means for synthesizing the thermochemical properties and the phase diagrams of complex multicomponent systems. The utilization of metastable phase descriptions as a means for assessing phase stability has been shown to be of value in deriving information on the stability of beta sialons. The current description has also been applied to compute the free energy of formation of the X phase in the SiO_2-Si_3N_4-Al_2O_3 system and could be applied to calculation of other oxynitride solid solution phases (i.e. the G phase in the Si_3N_4-Al_2O_3-AlN system). It is hoped that the future development of this interesting and inportant CALPHAD area will provide future opportunities to perform comparison of independent comparisons along the lines of Figure 10 with increasing levels of agreement!

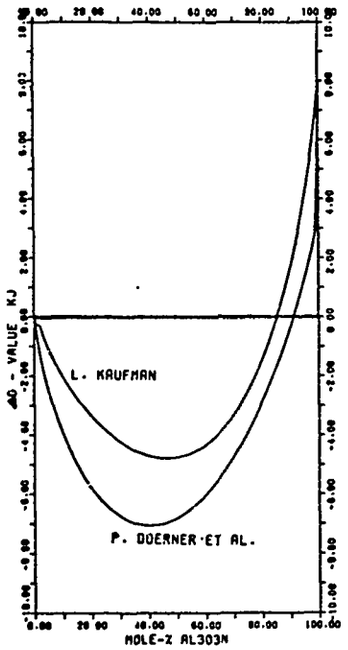

Figure 10. Comparison of Current Computed Free Energies of Formation of Beta Si_3N_4 Solid Solutions at 2000K with those due to Doerner et al (4).

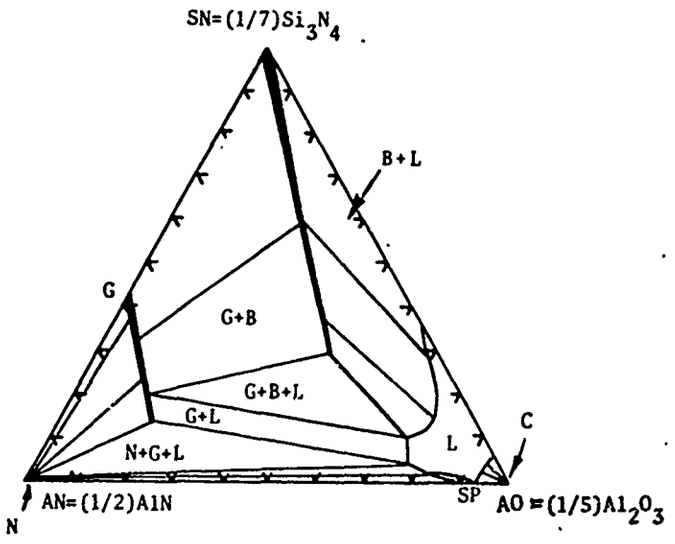

Figure 11. Recalculated Composito Equilibrium in the $(1/7)Si_3N_4$-$(1/5)Al_2O_3$-(1/2)AlN System at 2200K with CAB=-92048 Joules/g.at. and C=167360 Joules/g.at.

References

1. L. Kaufman and H. Nesor, CALPHAD 2 35 (1978)
2. L. Kaufman, CALPHAD 3 27 (1979)
3. L.J. Gaukler, H.L. Lukas, E.Th. Henig and G. Petzow, CALPHAD 2 349 (1979)
4. P. Doerner, L.J. Gaukler, H. Krieg, H.L. Lukas, G. Petzow and J. Weiss CALPHAD 3 239 (1979)
5. L. Kaufman and H. Nesor, Met. Trans. 6A 2115 (1975)
6. L. Kaufman, CALPHAD 3 45 (1979)
7. L. Kaufman and H. Nesor, CALPHAD 2 325 (1979)
8. ManLabs-NPL Data Bank
9. M Hansen and K. Anderko, Constitution of Binary Alloys, McGraw Hill, N.Y. (1958)
10. R.P. Elliot and F. Shunk, First and Second Supplements (Ibid)(1965) and (1968)
11. L. Kaufman and H. Nesor, Titanium Science and Technology, R.I. Jaffee and H. Burte, Eds. Plenum Press, New York 2 773 (1973)
12. L. Kaufman and H. Nesor, Met. Trans. 5 1623 (1975)
13. L. Kaufman, Summary of the Proceedings of the Eighth CALPHAD MEETING, CALPHAD 3 160 (1979)

Section V. Utilization of Data Bases and Computer Techniques for Solving Metallurgical Problems (to be published in the) Proceedings of a Joint National Physical Laboratory/Chemical Society CONFERENCE ON INDUSTRIAL USE OF THERMOCHEMICAL DATA (September 1979)

Joint
National Physical Laboratory Chemical Society
CONFERENCE ON INDUSTRIAL USE OF THERMOCHEMICAL DATA

held at the

University of Surrey-Guildford, Surrey
England

11-15 September 1979

"Utilization of Data Bases and Computer Techniques for Solving Metallurgical Problems"

by

Larry Kaufman
ManLabs, Inc.
21 Erie Street
Cambridge, Massachusetts
U.S.A. 01239

telephone 617-491-2900

20 illustrations

UTILIZATION OF DATA BASES AND COMPUTER TECHNIQUES FOR SOLVING METALLURGICAL PROBLEMS*

by

Larry Kaufman
ManLabs, Inc.
Cambridge, Massachusetts 02139
U.S.A.

ABSTRACT

Documentation of specific instances in which thermochemical data have been employed successfully to economic advantage is difficult because of the secrecy and confidentiality restrictions which of necessity limit publication of such information. Nevertheless, such examples come to light over a period of years and have been properly documented. Moreover, development or computational facility can be assessed as providing a vehicle for evaluating, guiding and synthesizing potential economic projects. The CALPHAD group is an international association of practicing thermochemists devoted to fostering technological advances in thermochemical knowledge and its application to real problems. The fourth meeting of the CALPHAD group held in August 1975 at the National Bureau of Standards in Gaithersburg, Maryland provided a list of examples demonstrating the importance of phase diagram and thermochemical data in developing industrial processes. The proceedings of this meeting were published in the CALPHAD Journal. Succeeding meetings of the CALPHAD group, as well as subsequent journal papers have provided many more situations. The current paper will review these cases in the fields of: in situ columbium, nickel and cobalt base superalloys, sigma phase formation in high temperature alloys, multicomponent semiconductors for electro-optical devices, SIALON ceramics, molten salt, sulfide and oxide slags for ore reduction and refining, high temperature battery electrodes, hardenability calculations in alloy steels, synthesis of hydrogen storage alloy compounds, grain refinement in aluminum alloys, metatectic reactions in hafnium alloys and the growth of HEM silicon solar cell material.

Introduction

The symposia and publications of the CALPHAD group[1-5] which have taken place during the past five years have provided many examples of the application of thermochemical data bases to the solution of industrial problems The CALPHAD Journal, published regularly by Pergamon Press of Oxford, England provides a vehicle for timely exposition of information and instances and such applications. Nevertheless, it is useful to compile additonal illustrations from time to time in order to demonstrate the wide range of applications and to review examples presented in other publications. Accordingly, the present paper will cover recent cases related to the topics listed in the abstract which demonstrate how data bank thermochemical data can be applied to the solution of real problems.

* This work has been sponsored by the Air Force Office of Scientific Research Bolling AFB, Washington, D.C. under Contract F 44620-76-C-0060 and the Metallurgy Program, Metallurgy and Materials Section, Division of Materials Research, National Science Foundation, Washington, D.C. under Grant DMR76-08453

1. Calculation of Superalloy Phase Diagrams. Today there is strong interest in the development of directionally solidified eutectic alloys for the blades and vanes of the gas turbine engine which are being subjected to increasingly higher temperatures and stresses. These alloys derive their superior high temperature strength from the directional solidification of an alloy of eutectic composition in a high temperature gradient producing aligned high strength microdimensional fibers or lamellae in a relatively ductile matrix. The potential for increases in average operating metal temperatures of over 100°C have already been domonstrated for the $\gamma/\gamma'+\delta$ and carbide reinforced superalloy in situ composites. Limitations in terms of oxidation resistance, ductility, and/or castability in these first generation alloys indicate the need for discovering other eutectic alloy systems. These may be ternary or higher order systems, so there is a requirement for systematically and efficiently identifying promising multi-element eutectics. A substantial number of publications are devoted to displaying methods for computing ternary isothermal sections of superalloy systems[6-10]. Detailed computations of the Cb-Al-Cr system[10] published in 1973 and shown in Figure 1 predicted a eutectic with a minimum melting point at 1317°C and a composition of 41Cr-25Cb-34Al (wt.%) within the region of the Cr-Cb-$CbAl_3$-Cr_2Al_3 composition space. This investigation suggested that directional solidification of an alloy of this composition should result in an in situ composite having a $CbAl_3$ reinforcing phase in a matrix of 64Cr-10Cb-26Al (wt.%), providing a combination of good high temperature strength and oxidation resistance. Subsequent experimental investigation of this system by M.K. Thomas[11] shown in Figure 2 verified the eutectic and matrix compositions and disclosed a melting point at 1350°C within 33°C of the predictions[10]. Extensive data bases covering binary metallic systems are being developed in the U.S.[12], France[9,13], Germany[13], England[14,15], Sweden[16], and Japan[17,18] which can be employed to compute ternary superalloy systems. Figures 3 and 4 present recent ternary calculations for the Co-Cr-Zr system which are part of a systematic and integrated program of work being carried out at the National Physical Laboratory, aimed at identifying and characterizing eutectic behaviour in ternary and quaternary Co + Cr or Ni + Cr based alloys. Calculations of the analogue systems Co-Cr-Nb and Co-Cr-Ta, of the corresponding Ni-Cr-X systems, and of some quaternary modifications to these systems have also been made. The phase diagram calculations have been made using the well established CALPHAD approach using a newly developed NPL system "ALLOYDATA" which stores critically assessed thermodynamic and structural data for elements, binary and ternary alloys, retrieves relevant data for a chosen multicomponent system and calculates a wide range of types of two and three-phase equilibria in ternary and quaternary systems. The unusual feature of the sections shown in Figures 3 and 4 is the

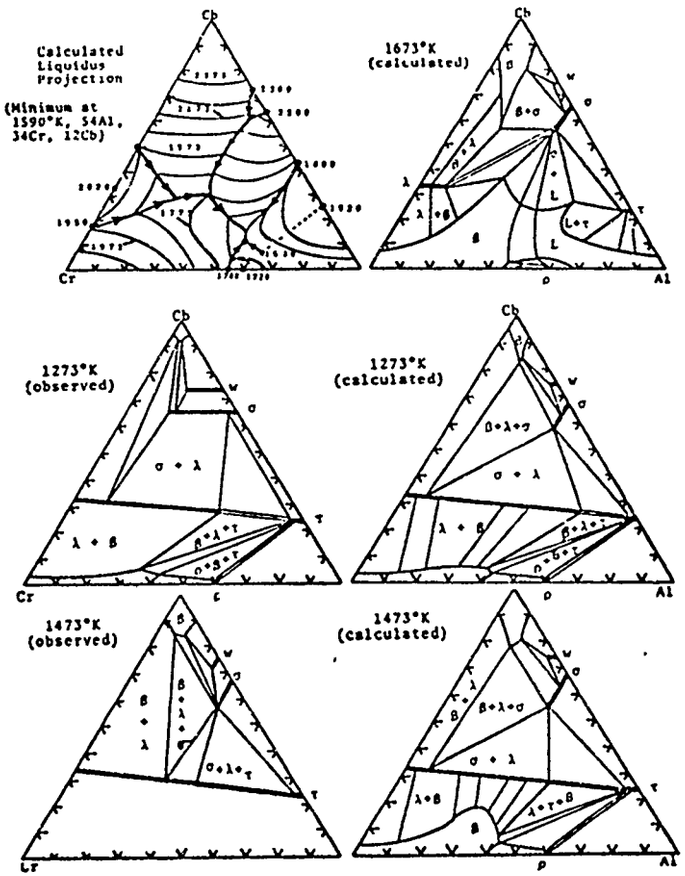

Figure 1. Calculated Cb-Al-Cr Isothermal Sections[10]
(Atom Percent)

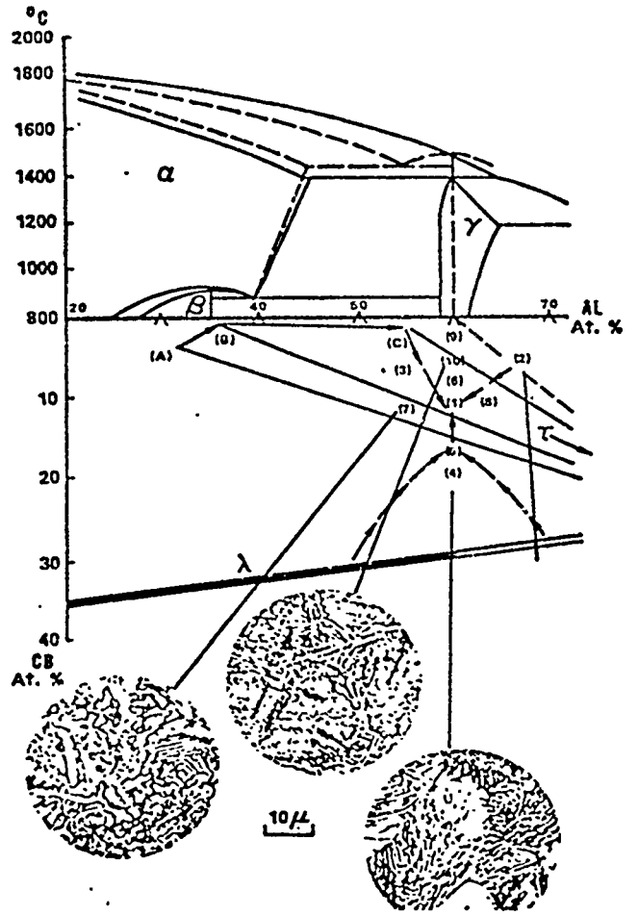

Figure 2. Experimental phase diagram and microstructures of the Cr-Cb-Al system[11].

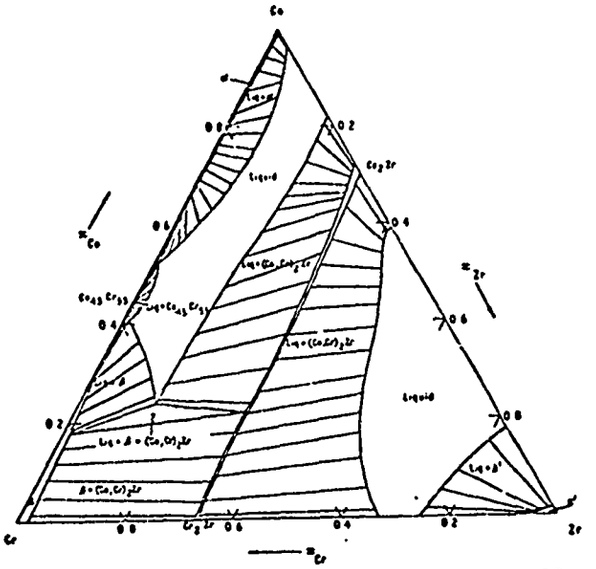

Figure 3. Calculated 1700°K Co-Zr-Cr Section [15]

stability of the $(Co,Cr)_2Zr$, Laves phase clear across the ternary section. The computed isothermal sections for 1300-1900K indicate the composition and temperature ranges over which a number of eutectic troughs exist, and also summarize the composition ranges over which the embrittling sigma phase, $Co_{.4}Cr_{.6}$, is calculated to exist[15]. Of particular relevance to the aim of the calculations is the eutectic valley between fcc Co-based solutions (α) and the $(Co,Cr)_2Zr$ Laves phase which may be of potential use for turbine blade applications. The isothermal sections indicate the solidification path along this valley, and demonstrate how the detailed calculation of phase diagrams can assist in the understanding of fairly complex solidification processes. The calculated compositions of this eutectic valley have been verified by subsequent experimental studies to be within 0.5-2 mol %, although the calculated eutectic temperatures are somewhat higher than the experimentally determined values. Bearing in mind the lack of experimental thermodynamic data for the Co-Zr system, and the uncertain nature of the liquidus and solidus curves for the Co-Cr system, the agreement is very satisfactory[15].

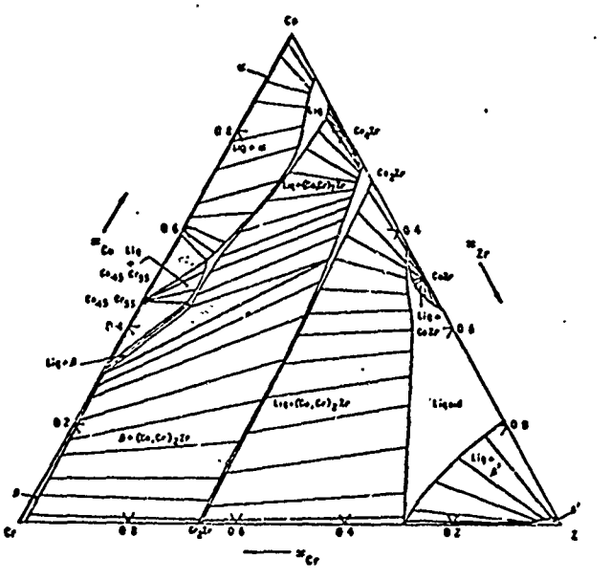

Figure 4. Calculated 1600°K Co-Zr-Cr Section [15]

2. Sigma Phase. Due to the wide range of applicability of nickel and cobalt base superalloys and of high chromium stainless steels substantial effort has been directed toward computing ternary diagrams establishing the stability range of the sigma phase[8,9,13,17]. Figure 5 shows a recent result by Chart,

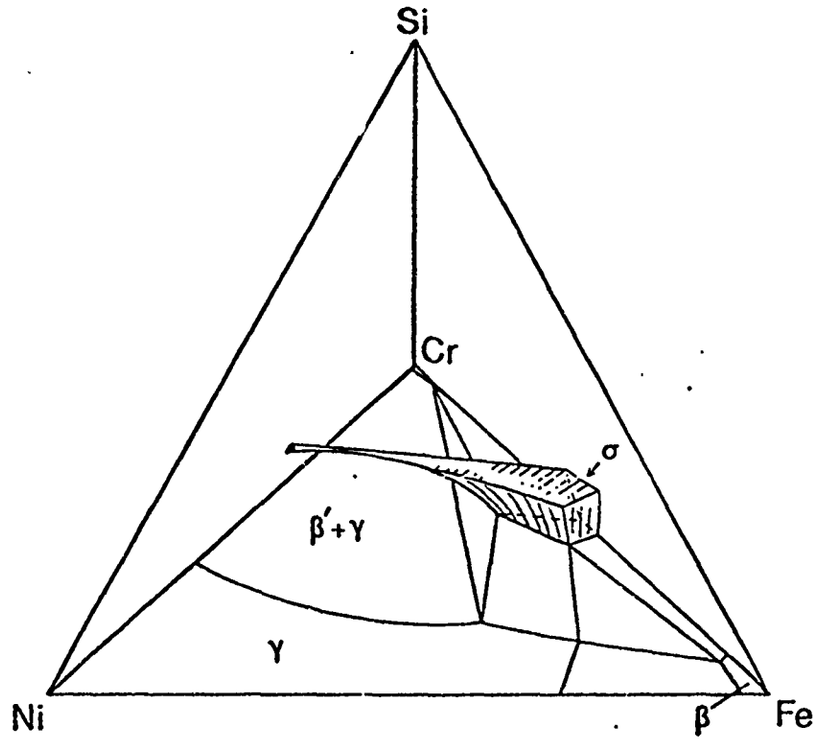

Figure 5. Calculated Stability Range of the Sigma Phase in the Cr-Fe-Ni-Si System at 800K, for Alloys Containing up to 0.08 Mole Fraction Si. Phase Relationships in the Ternary Cr-Fe-Ni Systems are Indicated [14]

Putland and Dinsdale[14] for quarternary section in the Fe-Cr-Ni-Si system at 800K. This system is of particular interest in the development of stainless steel tubing for nuclear reactors which is resistant to void swelling under irradiation[19,20]. A new procedure for evaluating the sigma phase precipitation tendency of superalloys has been developed by Machlin and Shao[21]. It is called SIGMA-SAFE. Phase diagrams were used to determine the degree of supersaturation with respect to precipitation of the sigma phase as a function of temperature and alloy compositions. It was found that this supersaturation number, Δ, distinguishes between 24 superalloys according to their known tendency to precipitate or not to precipitate the sigma phase, except for one superalloy. This capability of predicting the sigma phase precipitation tendency of an arbitrary new superalloy composition is not shared by PHACOMP. It was shown that Δ correlates quantitatively to wt pct sigma precipitated in a specific alloy. SIGMA-SAFE also yields the multicomponent phase diagram applicable to each superalloy[21]. The method depends upon fixing the geometry of the two and three phase fields bounding the γ,γ' and σ fields in multicomponent nickel base superalloys as illustrated in Figure 6. Machlin and Shao carried this out with the help of computed isothermal ternary sections[8] and have demonstrated excellent agreement as illustrated in Table 1.

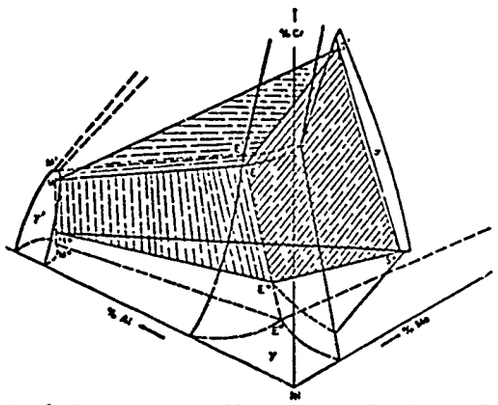

Fig.6—Perspective view of high Ni region of Ni-Cr-Mo-Al quaternary. Cross-hatched region defines $\gamma + \gamma' + \sigma$ 3 phase region. Below and above the cross-hatched region the respective 3 phase regions each contain $\gamma + \gamma' + \alpha$.[21]

Table I. Comparison of SIGMA-SAFE Predictions with Observations[21]

Alloys Observed to Be			
Sigma Prone		Sigma Free	
INCO 713 C	(0 248)	INCONEL 700	
IN 100	(Borderline)	MAR M 200	
PDRL 163	(0 901)	MAR M 246	
IN 728 NX	(1.333)	TRW 1900	
TRW 1800	(0.465)	NICROTUNG	
U 500	(0 393)	TRW NASA IV Y	
U 700	(0 652)	TRW NASA VI A	
Nimonic 115	(Borderline)	WASPALOY	
U 520	(0.98)	UNITEMP AF 21D	
RENE 41	(1.562)	UNITEMP AF 21DA	
		NIMONIC 80	
		NIMONIC 90	
		B1900	
		M252	(0.8)

Value in parenthesis is the supersaturation number, defined to equal the minimum value of $((\text{pct } \overline{Al}) + (\text{pct } \overline{Mo}))_{alloy} - ((\text{pct } \overline{Al}) + (\text{pct } \overline{Mo}))_{\sigma \text{ solvus}}$, where the arrows denote the vectors parallel to the (pct Al) and (pct Mo) coordinates in the constant Cr section of the quaternary corresponding to the Cr content of the superalloy.

The assessment of their SIGMA-SAFE proposals shows that for the 10 superalloys known to be prone to precipitation of the sigma phase at 875°C, SIGMA-SAFE correctly predicts all to be supersaturated with respect to precipitation of the sigma phase. Out of a total of 14 superalloys reported to have been held at 875°C for long time and in which no sigma phase was found 13 were predicted by SIGMA-SAFE to be in equilibrium phase fields that do not contain sigma while one was predicted to lie in a $\gamma+\sigma$ field (M252). The supersaturation number predicted by SIGMA-SAFE correlates to wt pct sigma quantitatively, as well as does the N_v number predicted by PHACOMP. The critical composition for precipitation of sigma in IN 100 is correctly predicted by SIGMA-SAFE. The boundaries between the γ, $\gamma+\sigma$, $\gamma+\gamma'$ and $\gamma+\gamma'+\sigma$ phase fields in the multicompnent phase diagrams corresponding to Ni base superalloy compositions are predicted by SIGMA-SAFE as a function of temperature. The γ' solvus temperature predicted by SIGMA-SAFE agrees with those observed for 4 superalloys within a 100°C maximum deviation. The predictions of PHACOMP and SIGMA-SAFE for the effects of specific alloying elements in promoting sigma differ quantitatively, and for some elements, qualitatively. This difference can be important for certain superalloys.

3. High Temperature Battery Electrodes. Solid Li-Al alloys appear to be one of the leading candidates for the negative electrode of high temperature batteries. Nevertheless a loss of capacity, accompanied by changes in morphology of the Li-Al components has been encountered after cyclic operation. Modification of cell design and alteration of the electrode composition is being considered in an effort to overcome the above noted shortcomings and improve Li diffusion in the α-Al solution[22]. Addition of Mg has been considered as a viable solution, however such a route requires knowledge of the Al-Li-Mg phase diagram. To fill the gap in experimental data, computations of the component binary systems and the ternary sections between 648 and 773K

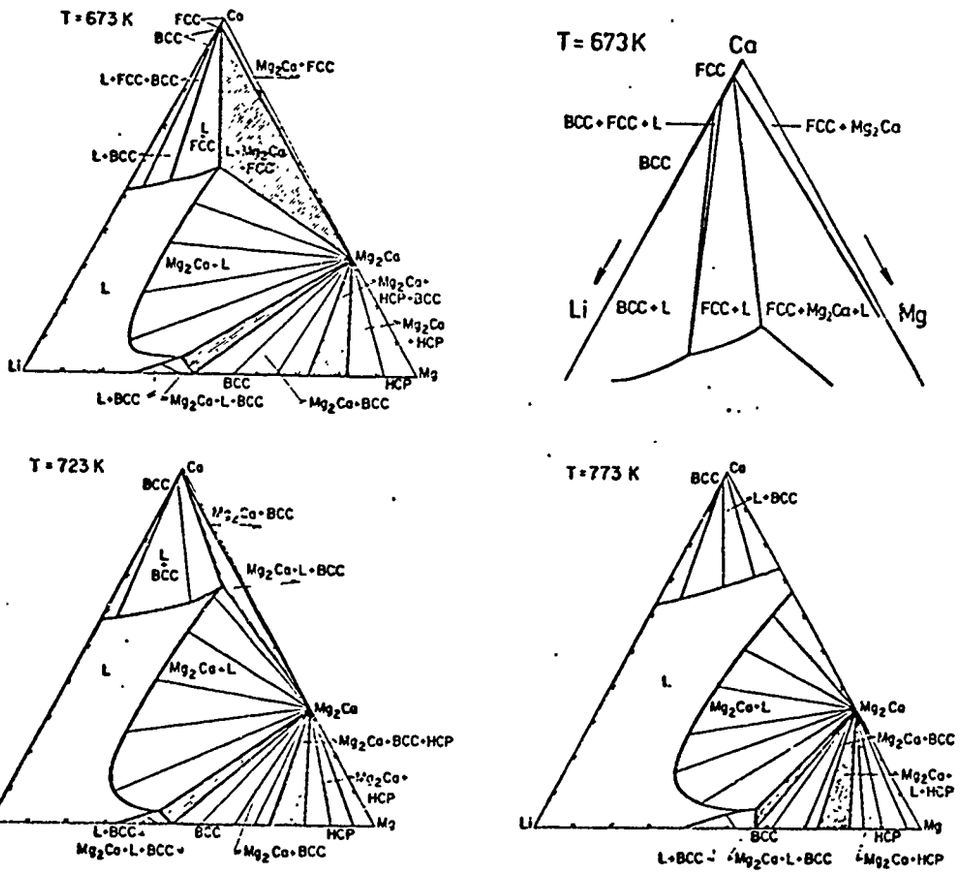

Figure 7. Calculated Isothermal Sections in the Ca-Mg-Li System[23].

were performed[22]. These computations define the field of temperatures-composition stability for alloys in this system. Recently these computations have been extended to cover the binary components and ternary sections in the Ca-Mg-Li system[23], Figure 7 shows the results obtained by Hsu and Saboungi between 673 and 773K in order to define the composition range of stability of the solid and liquid phases. This system is of interest in the development of high-temperature batteries in which iron sulfide is the positive electrode, calcium-magnesium alloys are the negative electrode and mixtures of LiCl-KCl-$CaCl_2$ salts serve as electrolytes. Thus, reaction of the lithium from the electrode with the Ca-Mg alloy can lead to formation of ternary Ca-Mg-Al alloys whose field of stability can be specified by Figure 7 for 673-773°K.

4. Hydrogen Storage Compounds. The intermetallic compound FeTi is most likely to be the first to undergo commercial development for energy storage purposes. It can be hydrided at room temperature under a few atmospheres pressure; the hydrogen can subsequently be released at a few tens of atmospheres by heating to 50-100°C. This range of pressure and temperature make iron-titanium hydride a natural energy storage medium for peak-shaving systems, solar energy

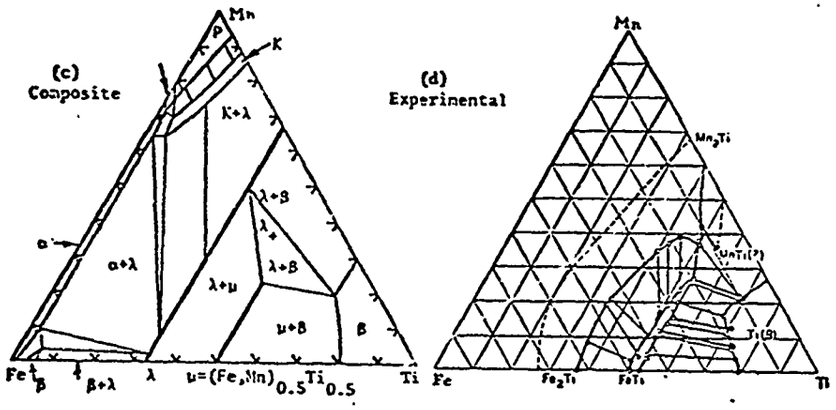

Figure 8. Recalculated (Left Panel) Composite (c) and Experimental Equilibrium(d) in the Manganese-Titanium-Iron System at 1273K[24].

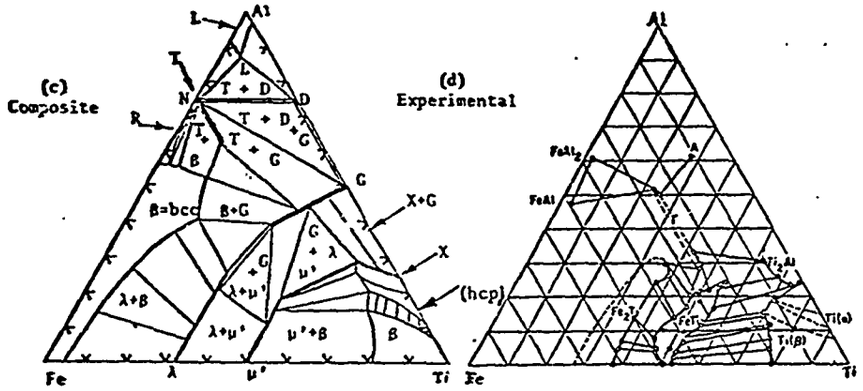

Figure 9. Recalculated (Left Panel), Composite (c) and Experimental(d) Equilibrium in the Aluminum-Titanium-Iron System at 1273K[24].

conversion and storage, and fuel for transportation systems.

The hydriding characteristics of the FeTi intermetallic can be manipulated by addition of a third element. Replacement of iron by manganese improves the stability of the compound hydride, making it more suitable for peak-shaving applications. It is important to have single phase FeTi. Excess iron yields Fe_2Ti Laves phase, which does not hydride. Excess titanium leads to solid solution phase, whose hydride is so stable that the hydrogen is not recoverable. The presence of either reduces the hydriding capacity and efficiency, of the alloy. Knowledge of the iron-titanium-manganese ternary phase diagram is necessary for producing single phase material. In addition, the alloy cost is high, directly melted from sponge titanium and scrap iron, the cost is estimated to be from $2.50-3.00 per lb. The compound could be produced by direct reduction from ilmenite (an ore which contains Fe and Ti

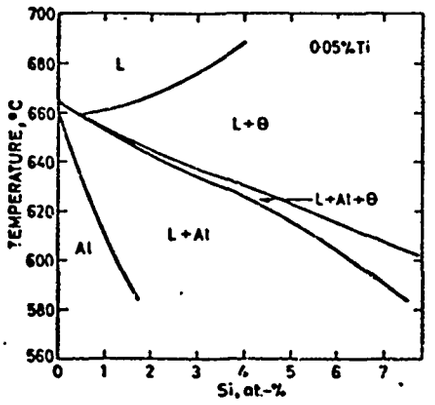

Partial vertical section at 0·05%Ti for the calculated Al–Ti–Si system (L–liquid, θ–$TiAl_3$).

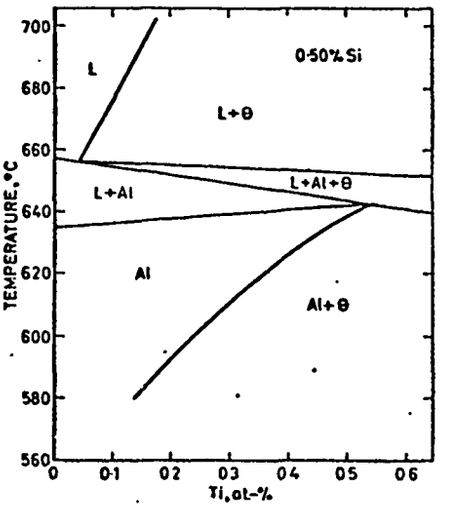

Partial vertical section at 0·50%Si for the calculated Al–Ti–Si system (L–liquid, θ–$TiAl_3$).

Figure 10. Calculated Vertical Sections in the Al-Ti-Si System[25].

in about equal proportions) at a lesser cost. Presently only aluminothermic reduction is thought to offer cost reductions below $2.00 per lb. However, this process will lead to aluminum in the alloy. Again single phase material is desirable, and a knowledge of the iron-titanium-aluminum phase diagram is essential. To provide such information, synthesis of the manganese-titanium-iron and aluminum-titanium-iron systems were carried out by using the analytical descriptions developed for the Fe-Ti, Fe-Mn, Ti-Mn, Al-Ti and FeAl binary systems and combining these to generate ternary sections[24]. To provide additional experimental information a study of selected portions of the Mn-Ti-Fe and Al-Ti-Fe system were carried out at 1000°C(1273K). These sections are shown in Figures 8 and 9 with a recalculation of the Mn-Ti-Fe and Al-Ti-Fe systems to provide closer agreement with the experimental results[24].

5. Grain Refinement of Aluminum. Grain refinement of Al by Ti increases markedly when the Ti concentration exceeds 0.08 a/o resulting from the onset of a peritectic reaction. Evaluation of the role of Si additives has been carried out by Youdelis[25] by constructing the vertical sections shown in Figure 10 from computed Al-Ti-Si isothermal sections generated between 700 and 1000K from binary descriptions. These results show that silicon additions tend to move the liquidus line defining the two phase (L+θ) field to lower Ti concentrations thus lowering the critical Ti concentration (for the onset of the peritectic) to lower levels. This calculated result agrees with the observation that enhanced grain refinement is observed at silicon levels as low as 0.05 a/o.

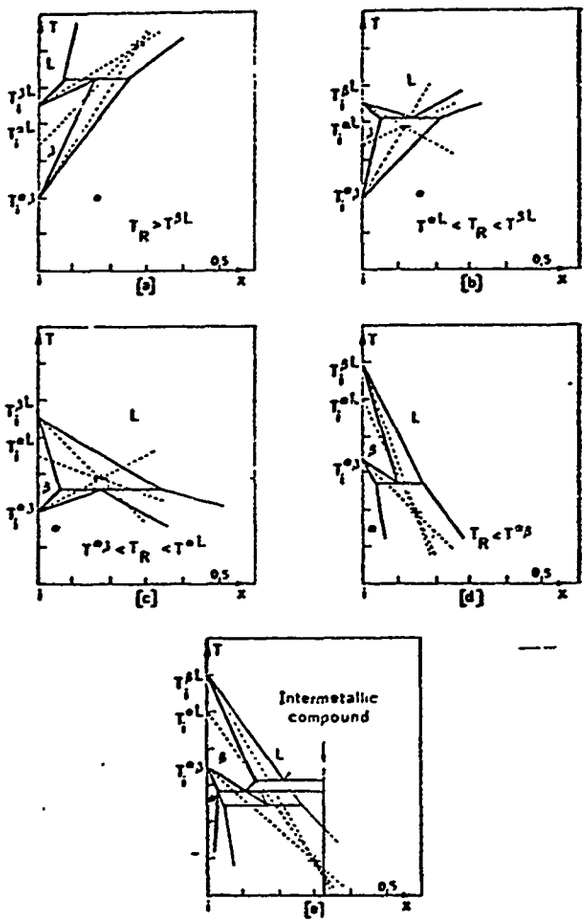

Figure 11. Different types of three-phase equilibrium between α,β and L phases in relationship to the position of the intersection point of the (x_o, T_o) curves[26].

6. Metatectic Reactions in Hafnium Alloys. The metatectic reaction in which β→α+L on cooling has a deleterious effect on the high temperature properties of alloys. This transformation can cause excessive segregation during solidification, welding or heat treatment. Moreover, when there is limited solubility between low temperature phases, a eutectic or peritectic results at lower temperatures, which reduces the capability of the alloy for high temperature service. Pieraggi and Dabosi[26] have used a regular solution model to predict the occurence of this reaction in hafnium base alloys as illustrated in Figure 11. In particular they have related the tendency for metatectic formation to the difference between melting and transformation temperatures of the solvent element and to the strain energy contribution to the interaction parameters.

7. Hardenability of Alloy Steels. Kirkaldy, Thomson and Baganis[27] have coupled thermochemical and kinetic data for alloy steels to develop an efficient method for computing CCT and TTT diagrams illustrated in Figures 12 and 13. This has been carried out by using free energy changes and activity data for iron and its binary and ternary alloys which are used to evaluate the general linear series (Wagner) expansion of the activity coefficient. The latter have been employed in turn for the accurate thermodynamic determination of the liquidus line and the γ field in steels with additions of Mn, Si, Ni, Cr, Mo, Cu, V, Nb, W and Co. A computer program based on several derived analytic formulae is accurate for total additions up to 5 wt.%. Indeed, the predictions compare favorably with observations on over 200 steels from international compendia. The predicted Ae_3 temperatures and diffusion data have been incorporated into a Zener-type expression for the transformation kinetics of ferrite and a semi-empirical formula has been optimized to adequately predict the ferrite start line of the TTT diagrams of low alloy steels. The TTT diagrams are converted in turn to CCT diagrams via the Avrami rule. Comparisons of the predictions with the CCT curves for a representative set of commercial steels show good agreement[27].

8. Growth of HEM Silicon Solar Cell Material. The heat exchanger method (HEM) developed to grow large sapphire crystals (25 cm diam. x 25 cm. high) has been applied to the growth of silicon solar cell materials. In this method the seed is placed at the bottom of the crucible and the temperature in the melt increases upwards. This suppresses convection that causes temperature and concentration fluctuations at the solid-liquid interface.

Early experiments indicated that SiC particles were found in crystals solidified by the HEM. However, even with the presence of SiC particles, large grains have been grown with limited interface breakdown during solidification. This observation differs from Czochralski (CZ) growth where interface breakdown due to SiC is followed by twin/polycrystalline growth.

The basic elements of the HEM and the CZ growth furnaces and the processes are quite similar (heaters, crucibles, insulation,etc.). A silica crucible loaded with the charge and set in a graphite retainer is placed in the furnace. The chamber is evacuated, and after melting the charge crystal growth is achieved. In the HEM process, the chamber is typically evacuated during growth to 0.1 Torr. For CZ growth an argon blanket is used and the chamber pressure can vary from 10 Torr to 1 atm. In early experiments with HEM growth it was quite surprising that high carbon concentrations were found in the silicon ingots. A thermochemical analysis was conducted to assess the source of the problem[28]. This analysis, illustrated in Figure 14, was subsequently confirmed experimentally. Analysis of the equilibrium between C, CO, CO_2, Si, SiO and SiO_2 over the temperature and pressure range of interest shows

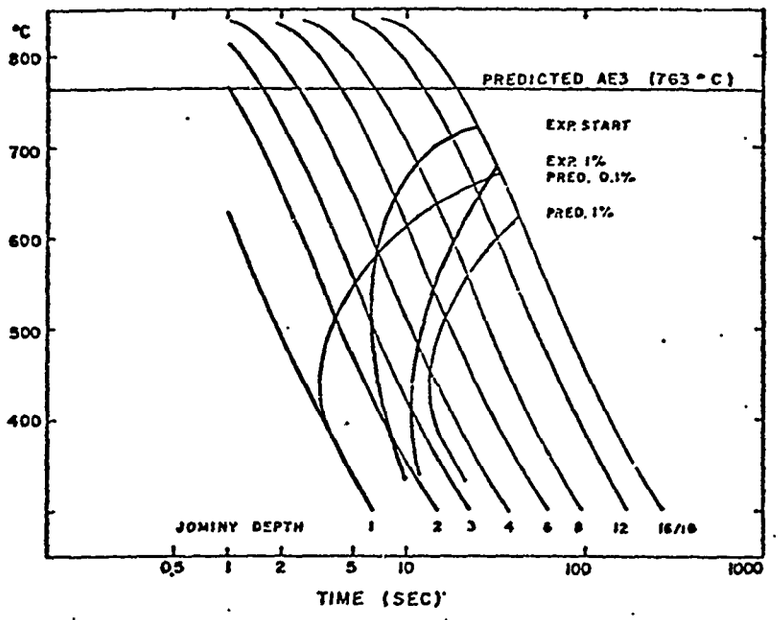

Figure 12. Comparison of predicted and experimental CCT start (0.1% and 1%) curves — for steel type 5140[27].

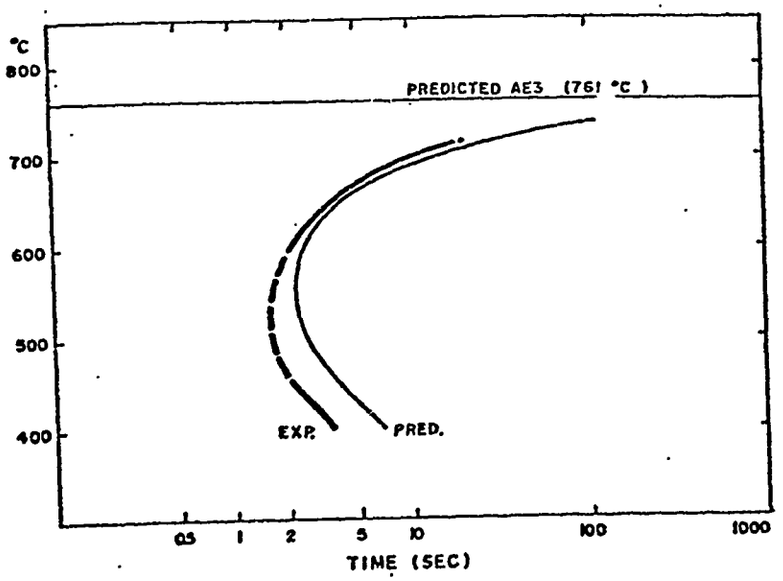

Figure 13. Comparison of predicted and experimental TTT start (0.1%) curves — for steel type 5140[27].

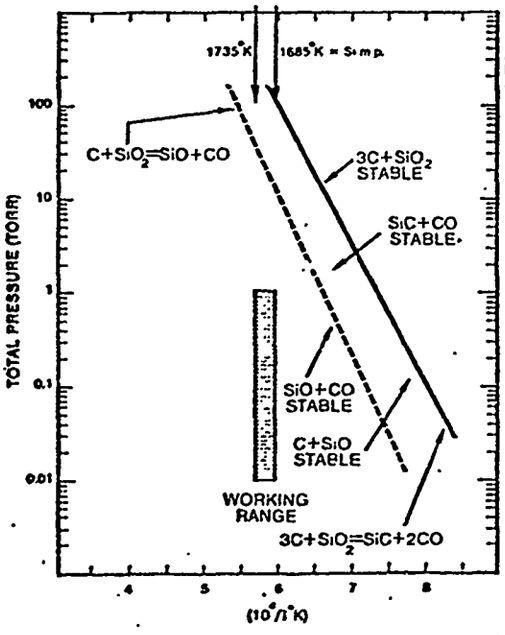

1. Calculated pressure-temperature relations for reaction of graphite and silica to form silicon carbide, silicon monoxide, and carbon monoxide.

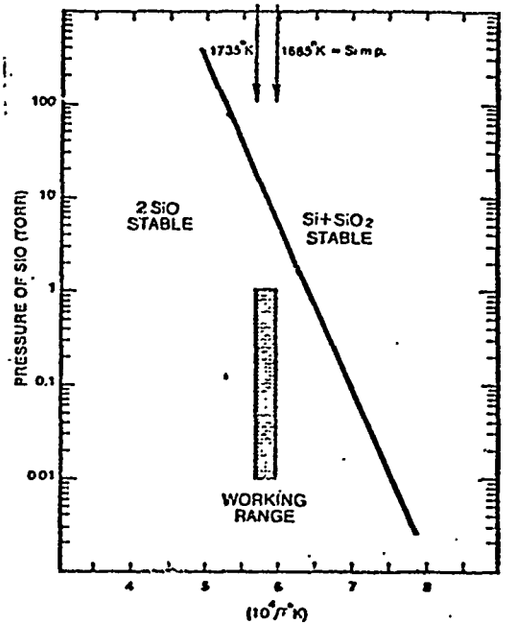

2. Equilibrium vapor pressure of gaseous SiO as a function of temperature for the reaction Si (condensed) + SiO_2 (condensed) → 2SiO (gas).

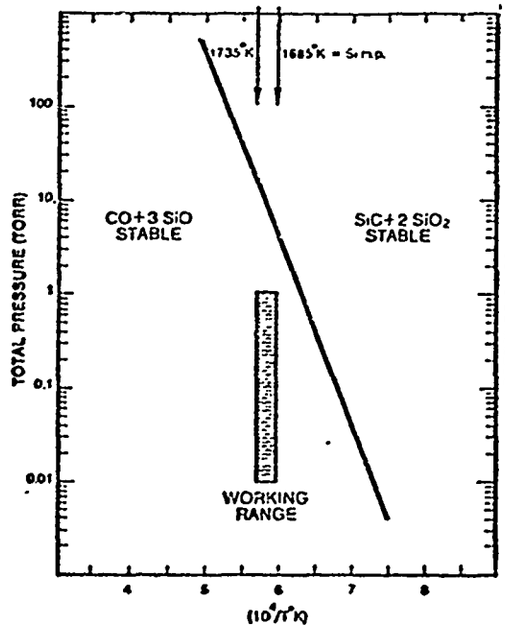

3. Equilibrium total pressure of CO and SiO as a function of temperature for the reaction CO + 3SiO → SiC + $2SiO_2$.

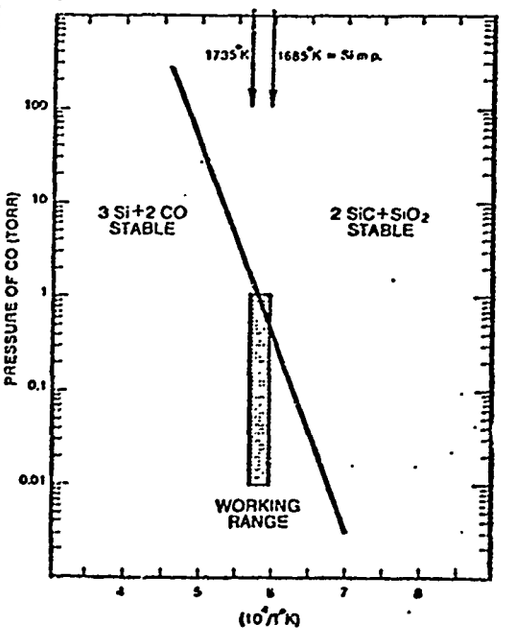

4. Equilibrium pressure of CO as a function of temperature for the reaction 2CO + 3Si → 2SiC + SiO_2.

Figure 14. Calculated Pressure-Temperature Fields of Stability for SiC Stability During HEM Growth of Silicon Solar Cell Materials in the Presence of Graphite[28].

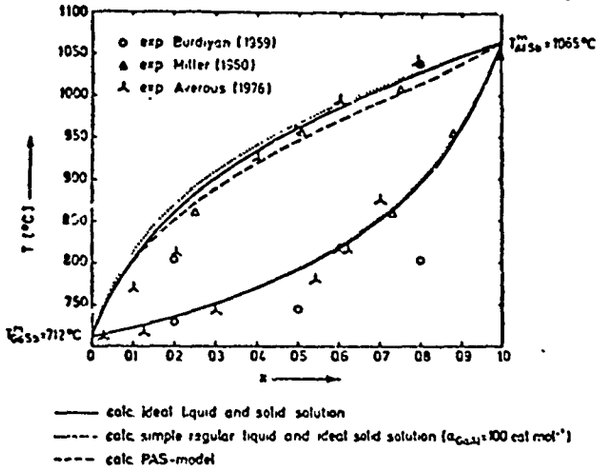

Figure 15. Calculated Pseudobinary system $(GaSb)_{1-x}(AlSb)_x$[30]

that CO is present in the working range. The reaction of carbon monoxide with silicon to yield silicon carbide and silicon monoxide is the source of the silicon carbide. One source of CO is the reaction of SiO_2 crucible with the graphite retainer. Reduction of the CO, effected by switching to a Mo retainer reduced the carbon concentration in the silicon[28].

9. Multicomponent Semiconductors. Simple solution models, generally based on regular solutions are applied successfully to compute the phase diagrams for alloy semiconductors, III-V compounds and a variety of multi-component systems which are important for electro-optical and light emitting diode applications[1]. The location of the liquidus phase boundaries is critical to successful growth of such compositions from the melt[29]. Such calculations also provide insight into the distribution of impurities likely to be developed in a crystal grown from the melt. Recently, Linnebach[30] has considered the effect of using a partially associated solution (PAS) model in defining the solutions in the pseudobinary system GaSb-AlSb. The results of these computations are shown in Figure 15.

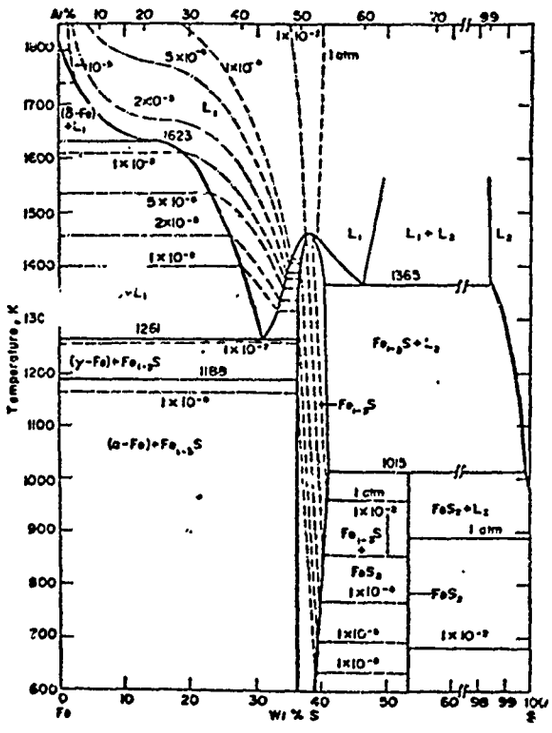

Figure 16. The calculated Fe-S diagram with isobar values of $S_2(g)$ up to 1 atm[31].

10. Sulfide, Molten Salt, Oxide and Ceramic Systems. During the past ten years, substantial progress has been made in developing data bases, models

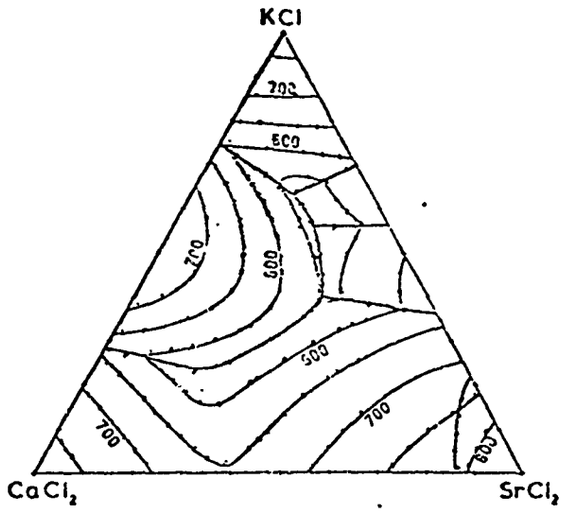

Figure 17. Calculated Liquidus Contours in the $KCl-SrCl_2-CaCl_2$ System[35].

and computational methods for calculating the phase diagrams and thermochemical properties of metallic systems. The development of similar data bases and models for dealing with non-metallic systems has proceeded at a lower pace. Nevertheless, measurable advances have been made and it is likely that the next few years will see even more rapid development of this non-metallic field than the "metallic" field. This is due to the fact that the "non-metallic" group covers a very broad spectrum of materials where development of accessible data bases and models for estimating properties can be quickly translated into new solutions for important industrial problems. Indeed the development of data bases for the "non-metallic" systems has begun and prior CALPHAD symposia[1-5] as well as current publications[31-40] provide a measure of this development. Figure 16 shows a recent example of a computed Fe-S phase diagram developed by Sharma and Chang[31]. Chang and Hu[32] have been developing a description of Metal-Metal-Oxygen and Metal-Metal-Sulphur systems covering associated solution, defect thermodynamic and "Wagner" models for dealing with these "mixed" metal-non-metal systems. Similar studies have been carried out by Schwerdtfeger and Pitsch[33].

Pelton, Bale and co-workers[34-37] have been developing data bases covering molten salt and oxide systems. Figures 17 and 18 show some of their recent results[35] for fused salt systems. The thermodynamic properties of all phases in the fifteen binary systems

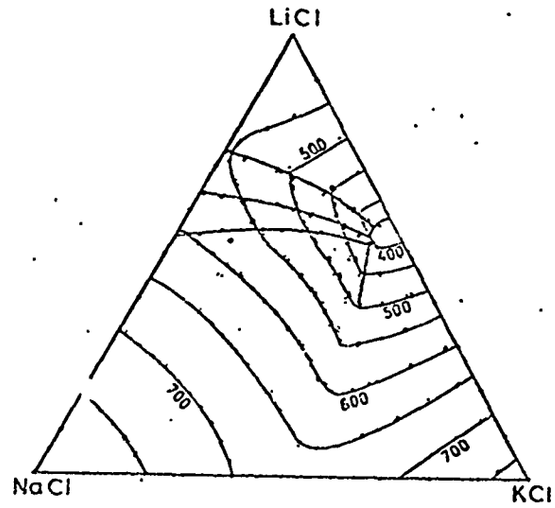

Figure 18. Calculated Liquidus Contours in the LiCl-KCl-NaCl System[35].

can be expressed as differences of single-ion site preference energies. The site preference energies and redox energies, used to give the best agreement with the high temperature phase diagrams are in reasonable agreement with values predicted by earlier analyses of thermodynamic and spectral data as well as with calculations from crystal field theory. In the case of the Fe_3O_4-Co_3O_4 spinel phase, it was necessary to propose a small additional positive regular solution term to obtain quantitative agreement between the measured and calculated phase diagrams at all compositions. In the other systems, the simple model with no additional terms was found to be sufficient[36].

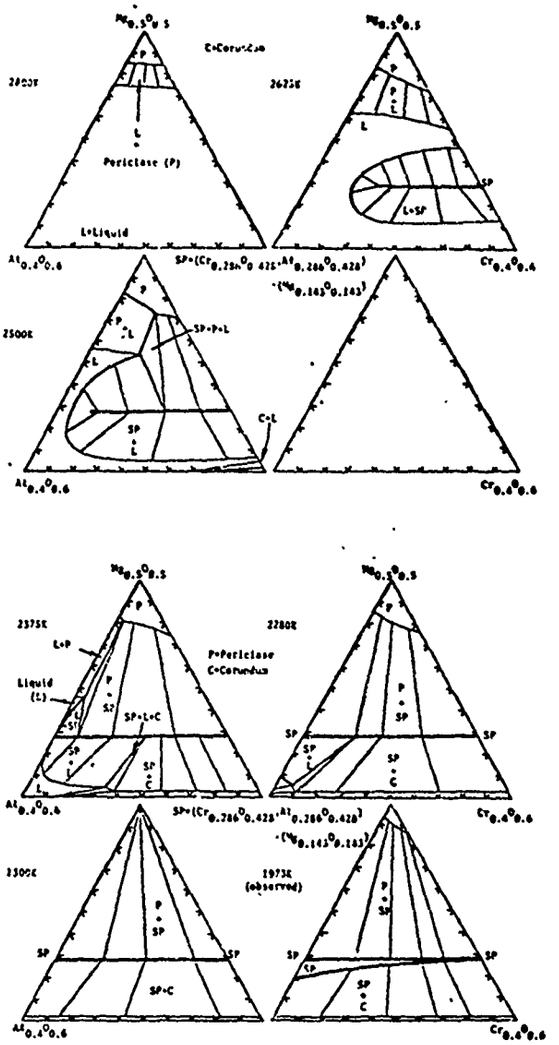

Figure 20. Calculated $Mg_{0.5}O_{0.5}$-$Cr_{0.4}O_{0.6}$-$Al_{0.4}O_{0.6}$ System[38].

Additional efforts[38-43] have been directed toward development of data bases capable of computing ternary and higher order phase diagrams from the thermochemical properties of oxide, nitride and mixed systems which have direct application in slag-metal equilibria, high temperature refractories and (SiO_2-Al_2O_3-Si_3N_4-AlN) synthesis of SIALON ceramics. Figure 20 shows an example of calculated and observed isothermal sections in the MgO-Cr_2O_3-Al_2O_3 system.[38] One of the chief advantages which this effort will provide is the ability to generate metastable equilibria data which can provide information on supercooled liquids and the nature of the phase diagram when one or more of the competing phases is suppressed. Such information is of great practical value when dealing with oxide ceramics and glass forming systems.

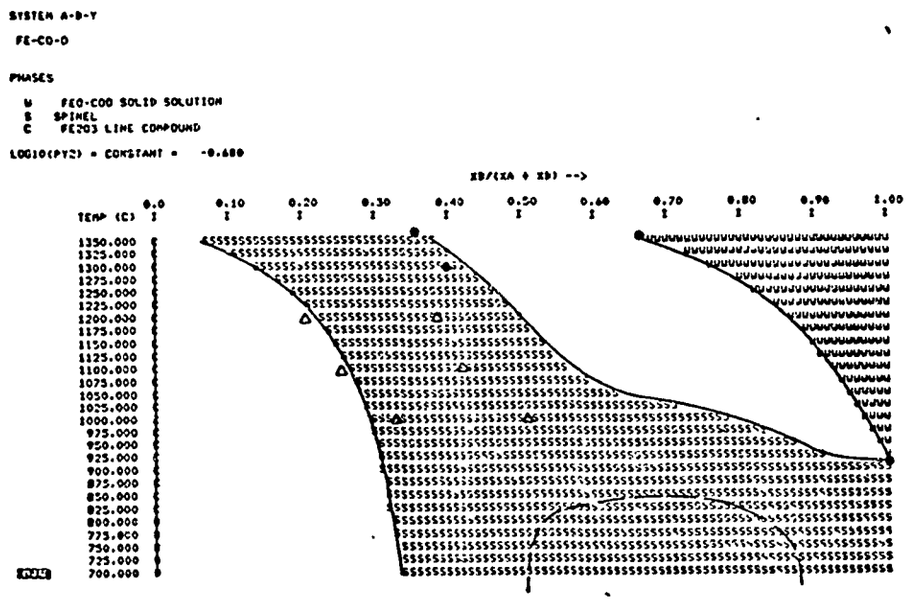

Figure 19. Calculated Phase Diagram for the Fe-Co-O System in Air[36]. Points are Experimental.

formed among the six salts LiCl, NaCl, KCl, $MgCl_2$, $CaCl_2$, and $SrCl_2$ were obtained and expressed in mathematical form by a critical analysis of the measured binary phase diagrams and of published binary thermodynamic data. Interpolation precedures were then used to estimate the thermodynamic properties of the twenty ternary systems formed among the six salts, and all twenty ternary phase diagrams were calculated using a computer program designed for the purpose. Good agreement with the measured phase diagrams for the eight ternary systems for which measured diagrams are available was obtained[35].

Synthesis of thermochemical properties and phase diagram data has also been performed[36,37] for the Fe-Cr-O, Fe-Ni-O, Cr-Ni-O, Mn_3O_4-Co_3O_4, Fe_3O_4-Mn_3O_4 and Fe_3O_4-Co_3O_4 systems. Figure 19 shows an example of a section in the latter system computed at an oxygen pressure corresponding to air at one atmosphere. In the former study[36] high temperature phase equilibrium data was compiled and assessed to evaluate the thermodynamics and structural models of the spinel phases. The thermodynamics of the spinel phases was determined in terms of the distribution of the cations between the tetrahedral and octahedral sites. The phase diagram analysis approach to examining this cation distribution has the advantage that a true high temperature equilibrium is being examined. The high temperature phase diagram data was shown to be consistent with the assumption that the equilibrium constants for the exchange and redox reactions are independent of composition and that the free energies of the three site exchange reactions, but not of the redox reaction, are independent of temperature. Furthermore, the free energies of the site exchange reactions

Conclusion

The foregoing set of examples show how far the utilization of data bases and computer methods for solving industrial problems has progressed in just the past five years. Not too long ago it was a difficult task to consider computing a ternary system. Moreover, there were very few systems for which sufficient data existed which would permit a realistic computation to be carried out. By contrast, the current situation is such that computation techniques for routine calculation of ternary systems (at reasonable cost) are available and are being applied to a very wide spectrum of real problems. Higher order systems are also being computed where necessary. Moreover, data bases covering a wide range of materials systems are developing. The community of effort which has achieved this progress must be continued and attention should be paid to educating the technical and scientific community at large to the efficacy of this development.

References

1. L. Kaufman, "Proceedings of the Fourth CALPHAD Meeting", August 1975 CALPHAD 1977,1,7.
2. W. Pitsch and G. Inden "Project Meeting CALPHAD V", MPI-Dusseldorf, West Germany, June 1976.
3. L. Kaufman, G. McHugh, A.P. Miodownik and M.H. Rand, "Summary of the Proceedings of the Sixth CALPHAD Meeting", Harwell-Oxford England, April 1977, CALPH 1977, 1, 293.
4. G. Petzow, E. Th. Henig and H. Lukas, "Project Meeting CALPHAD VII", MPI-Stuttgart, West Germany, April 1978, Summary-P.J. Spencer and T. Chart, CALPHAD, 1978, 2, 197.
5. B. Uhrenius and M. Hillert, CALPHAD VIII, Royal Institute of Technology-Stockholm, Sweden, May 1979, Summary-L. Kaufman, CALPHAD, 1979, 3, 159.
6. L. Kaufman and H. Nesor, Zeit. f. Metallkunde, 1973, 64, 249.
7. L. Kaufman and H. Nesor, Annual Reviews of Materials Science, 1973, 3, 1.
8. L. Kaufman and H. Nesor, Met. Tr., 1974, 5, 1617, 1623, 1975, 6A, 2115, 2123.
9. I. Ansara, International Metals Review, 1979, No. 1, p.20, (Review No. 238).
10. L. Kaufman and H. Nesor, Conference on In-Situ Composites-II, M.R. Jackson et al Editors, Xerox Publishing, Lexington, Mass., 1976, p.11.
11. M.K. Thomas, Ibid p.37.
12. L. Kaufman, CALPHAD 1978, 2, 55, 81, 117, 295, 325; CALPHAD, 1979, 3, 45.
13. C. Allibert, C. Bernard, H.D. Nussler and P.J. Spencer, reference 5, p.207.
14. T. Chart, F. Putland and A. Dinsdale, reference 5, p.183.
15. T. Chart and F. Putland, CALPHAD, 1979, 3, 9.
16. B. Sundman, reference 5, p.102.
17. T. Nishazawa, M. Hasebe and M. Ko, reference 5, p.113.
18. M. Hasebe and T. Nishazawa, "Application of Phase Diagrams in Metallurgy and Ceramics", NBS Special Publication 496-Symposium of January 1977, 1978, 2, 911.
19. L. Kaufman, J.S. Watkin, J.H. Gittus and A.P. Miodownik, CALPHAD, 1977, 3, 281.
20. J.S. Watkin, reference 5, p.161.
21. E.S. Machlin and J. Shao, Met. Trans., 1978, 9A, 561.
22. M.L. Saboungi and C.C. Hsu, CALPHAD, 1977, 1, 237.
23. C.C. Hsu and M.L. Saboungi, Zeit.f. Metallkunde, 1978, 69, 581.
24. D. Dew-Hughes and L. Kaufman, CALPHAD, 1979, 3, 180.
25. W.V. Youdelis, Metal Science, 1978, (August), p.363.
26. B. Pieraggi and F. Dabosi, J. Materials Science, 1979, 14, 416.
27. J.S. Kirkaldy, B.A. Thompson, and E.A. Baganis, "Hardenability Concepts with Applications in Steel", A.I.M.E., 1978.
28. F. Schmid, C.P. Khattuk, T.G. Diggs and L. Kaufman, J. Electrochem. Soc., 1979, 126, 935.
29. M. Illegems, reference 4, p.60.
30. R. Linneback, reference 4, p.61 and reference 5, p.278.
31. R.C. Sharma and Y.A. Chang, reference 4, p.178.
32. Y.A. Chang and D.C. Hu, reference 4, p.175.
33. K. Schwerdtfeger and W. Pitsch, reference 2, pII. 2-1.
34. M.L. Saboungi, Perisei and M. Blander, reference 4, p.164.
35. P.L. Lin, A.D. Pelton and C.W. Bale, J. Ceramics Soc., 1979, (In Press).
36. A.D. Pelton, H. Schmalzried and J. Sticher, Ber. Bunsenges. Phys. Chem., 1979, 83, 241.
37. A.D. Pelton, H. Schmalzried and J. Sticher, J. Phys. Chem. Solids, 1979, (In Press).
38. L. Kaufman and H. Nesor, CALPHAD, 1978, 2, 35.
39. G. Kaestle and K. Koch, reference 4, p.6.
40. L. Kaufman, CALPHAD, 1979, 3, 27.
41. L.J. Gaukler, H.L. Lukas, E.Th. Henig and G. Petzow, CALPHAD, 1978, 2, 349.
42. L. Kaufman, reference 5, p.11.
43. P. Dorner, L.J. Gaukler, H. Krieg, H.L. Lukas, G. Petzow and J. Weiss, reference 5, p.12.

VI. Thermochemistry of Doped Germanium Borosilicate Glasses for Communications Fibers

Recent efforts at RADC/ET-Hanscom Field, Massachusetts have led to the development of the only fiber drawing tower in the DoD capable of producing multikilometer lengths of jacketed fiber by a process which involves drawing the 150 micron diameter fibers from a glass preform which has been passed through an annular hot zone. The preforms from which fibers are drawn are prepared by the CVD process such that the layers (and the distribution of elements providing a refractive index variation) can be deposited in a controlled manner. This insures light guiding of the communications signal. One current objective is improvement of the induced transmission loss due to exposure to ionizing irradiation. At present the evidence in hand indicates that doping the preforms with multivalent ions and/or ions providing deep energy band levels in the silicate glass may provide the best route to radiation resistance improvement. The ratio of oxidation/reduction levels of the various dopant ions such as Ce^{+3}/Ce^{+4} or Sb^{+3}/Sb^{+5} as a function of oxidation/reducing atmosphere has proven to be critical in some of the glasses. The preforms are fabricated in a thin-walled fused silica reaction tube which will serve as a cladding material for the fiber which is supported on both ends in a glassworking lathe. While rotating, it is heated with an oxygen-hydrogen burner which traverses along its length. Electronic grade chemicals ($SiCl_4$, $GeCl_4$, $POCl_3$) are kept in separate containers at controlled temperatures and ultra-pure oxygen is bubbled through these liquids. The chemical vapors entering the reaction tube are controlled using a mass flow control system incorporating a feedback loop to control the desired quantity of oxygen and chloride vapors. Ultra-pure BCl_3 vapors from a pressurized tank are also monitored and controlled by the system, since B_2O_3 can be used in chemical vapor deposition as an

intermediate cladding or core component. The mixture of oxygen and reactants is passed through the fused quartz tube continuously, the heat for the reaction being provided by the traversing burner. The temperature of the tube (1600-1650°C) is continuously monitored and controlled using an optical pyrometer. In the reaction zone, both the heterogeneous reaction at the tube wall and a homogeneous gas phase reaction take place. The homogeneous reaction produces fine solid particles of oxide glass product, some of which are driven to the tube wall. At the high temperature employed, they are fused to a bubble-free glassy film as the burner passes along the tube. After the desired number of passes has been made, tne burner temperature is increased in excess of 1800°C, and the tube is collapsed to form a waveguide preform.

Since the CVD process is largely empirical, ManLabs, Inc. has initiated application of the computer based thermochemical and data bank analysis of the CVD problem in support of the RADC effort. The most expeditious route to provide this support is to utilize the methods described in Sections II-V with specific consideration of the phase diagrams composed of B_2O_3-SiO_2-GeO and additions of P_2O_5, Sb_2O_5 and CeO_2.

The current effort will attempt to generate state diagrams for the glass CVD process which can be applied to a variety of materials of current interest in optical wave guides. These state diagrams should specify the temperature-pressure-concentration ranges where specific products can be formed starting with known reactants. These systems should be representative of those of current interest in the doped silicate glass preform technology. Thus, the best state diagram information may consist of free energy-temperature-oxygen (or chlorine) pressure information which is capable of being combined to deal with mixtures or solutions of components in the gaseous or condensed state. The particular glass systems of interest will cover

the GeO_2-SiO_2-B_2O_3 system with the following dopants: P_2O_5, Sb_2O_5, Sb_2O_3, Ce_2O_3 and CeO_2. The current study will examine the CVD process as it relates to fabrication of doped germanium-borosilicate glass preforms used for optical communication fibers with special emphasis on the current RADC/ET mixing chamber design employed to investigate introduction of a variety of dopants. In this configuration the dopants are introduced as chloride compounds which are decomposed and oxidized to be finally deposited as oxides at 1550 to 1650°C. The decomposition and reformulation steps will be treated separately and then combined so as to simulate the oxide configuration of the final preform. Special attention will be given to the oxidation state of the dopants in the germanium-borosilicate glass.

In order to illustrate how the current technique can be applied to generate such information it is instructive to consider the following examples:

a. Utilization of the ManLabs-NPL Data Bank to Define Vapor Pressure of Dopants

Thermochemical data on over 2000 inorganic compounds are held in the data bank. Many of the halides of the dopants of interest are included. The chlorides of antimony, $SbCl_5$ and $SbCl_3$ in the gaseous and condensed state, are included. Figure 1 and Table 1 illustrate how the bank can be employed to compute the vapor pressure of $SbCl_5$ over solid $SbCl_5$ as a function of temperature. Table 1 shows the reaction -C15SB + C15SB(G), which is the computer language for the vaporization of solid $SbCl_5$ displayed in Figure 1. Entry of this notation in the ManLabs-NPL system causes the computer to output the specific heat, entropy, enthalpy and free energy change for the reaction as a function of temperature as shown in Table 1. In addition LOG10KP is tabulated. The latter can be employed to compute the vapor pressure of $SbCl_5$ since

$$K_p = P(SbCl_5)(atm) = P(SbCl_5)(torr)/760 \qquad (1)$$

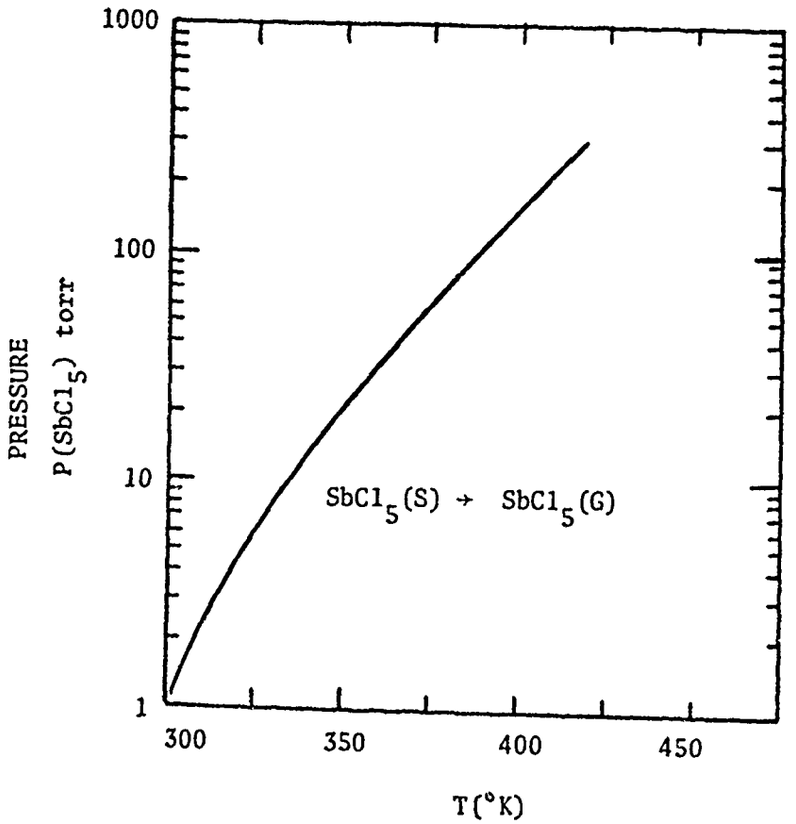

Figure 1. Calculated Vapor Pressure-Temperature Relations for $SbCl_5$

TABLE 1

DATA BANK OUTPUT FOR VAPORIZATION OF $SbCl_5$

790126 THERMODYNAMIC FUNCTIONS

-CL5SB+CL5SB(G)

T K	DELTACP CAL/K MOL	DELTAS CAL/K MOL	DELTAH CAL/MOL	DELTAG CAL/MOL	LOG10KP
298.15	-12.245	27.000	11900	3850	-2.822
300.00	-12.190	26.924	11877	3800	-2.768
325.00	-11.528	25.976	11581	3139	-2.111
350.00	-11.000	25.142	11300	2500	-1.561
375.00	-10.572	24.398	11030	1881	-1.096
400.00	-10.219	23.727	10771	1280	-0.699
425.00	-9.923	23.117	10519	694	-0.357

The vapor pressure of $SBCl_5$ in torr calculated from Eq.(1) and the data in Table 1 is displayed in Figure 1. This shows that at 350°K(i.e. 77°C) the vapor pressure of $SbCl_5$ is 20.8 torr while at 300°K (i.e. 27°C) it is only 1.6 torr which is too low for practical use. In fact, the 20.8 torr pressure is used by maintaining the $SbCl_5$ feed lines at 77°C.

b. Calculation of the Relative Proportion of $SbCl_3$ and $SbCl_5$ as a Function of Temperature and Pressure

The foregoing example illustrates how the data bank can perform a simple problem. A second example of a more complex problem can be illustrated by considering the decomposition of $SbCl_5$ into $SbCl_3$ and Cl_2 which can be written as

$$SbCl_3 + Cl_2 \rightleftarrows SbCl_5 \qquad (2)$$

Table 2 shows the Data Bank results for the forward reaction. The fifth column tabulates $\Delta G°$ for the forward reaction, thus at equilibrium

$$\Delta G=0=\Delta G° + RT\ln P_{SbCl_5}/(P_{Cl_2})(P_{SbCl_3}) \qquad (3)$$

Since $P_{Cl_2} = P_{SbCl_3} = P_t\, x$ (where P_t is the total pressure and x is the fraction of $SbCl_3$) and $P_{SbCl_5} = P_t(1-2x)$. Equation(3) can be recast as

$$-\Delta G°=RT\ln (1-2x)/x^2P_t$$

thus permitting solution of x (and 1-2x) as a function of temperature and pressure. Figure 2 displays the results for P_t=1 atm and P_t=0.1 atm (76 torr). The results show that at 1 atmosphere and 300K the mixture consists largely of $SbCl_5$ with very little $SbCl_3$. As the temperature is increased the $SbCl_3$ fraction increases substantially. Lowering the pressure to 76 torr has a very marked effect on the ratio. Thus control of the pressure could be an easy way to vary the ratio of

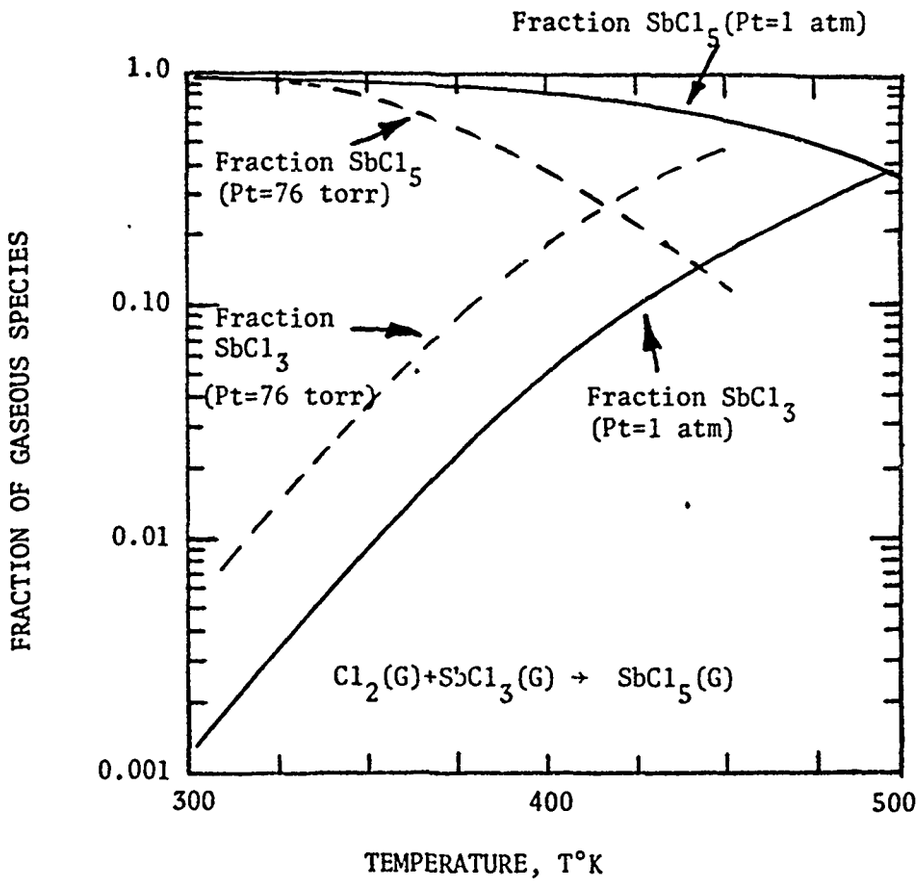

Figure 2. Calculated Fraction of $SbCl_3$ and $SbCl_5$ as a Function of Temperature and Total Pressure in Chlorination of $SbCl_3$

TABLE 2

DATA BANK OUTPUT FOR CHLORINATION OF $SbCl_3$

-CL2(G)-SBCL3(G)+SBCL5(G)

T K	DELTACP CAL/K MOL	DELTAS CAL/K MOL	DELTAH CAL/MOL	DELTAG CAL/MOL	LOG10KP
298.15	0.170	-35.290	-18450	-7928	5.812
300.00	0.199	-35.289	-18450	-7863	5.728
325.00	0.550	-35.259	-18440	-6981	4.695
350.00	0.830	-35.207	-18423	-6100	3.809
375.00	1.057	-35.142	-18399	-5221	3.043
400.00	1.244	-35.068	-18370	-4343	2.373
425.00	1.400	-34.987	-18337	-3468	1.783
450.00	1.532	-34.903	-18300	-2594	1.260
475.00	1.645	-34.818	-18261	-1722	0.792
500.00	1.742	-34.731	-18218	-853	0.373
525.00	1.827	-34.644	-18174	14	-0.006
550.00	1.901	-34.557	-18127	879	-0.349
575.00	1.967	-34.471	-18079	1742	-0.662
600.00	2.026	-34.386	-18029	2603	-0.948

Sb^{+3}/Sb^{+5} ions entering the reaction chamber.

Thus the data bank offers a means for investigating the stability of Sb^{+3}/Sb^{+5} interchanges in the reaction

$$6SbCl_5(G) + 5Sb_2O_3(S) \rightarrow 10SbCl_3(G) + 3Sb_2O_5(S) \qquad (5)$$

as a function of temperature and pressure. Similar investigation can be undertaken for chloride and oxides of phosphorous, and cerium in order to evaluate their tendency to yield a predominate valence state in the glass.

Although the CVD process is controlled by kinetic factors as well as by thermodynamic factors and the former may prevent attainment of equilibrium, the equilibrium calculations can still serve as a useful guide in outlining the field in which certain species predominate (i.e. Figure 2).

Since the dopants finally are deposited in the glass phase it is proposed that the techniques developed in the present program for computing multicomponent oxide phase diagrams be applied in dealing with the condensed state reactions which take place during the preform synthesis at high temperatures.

As the first step in this analysis the GeO_2-SiO_2, B_2O_3-SiO_2 and B_2O_3-GeO_2 binary systems have been analysed along the lines described in Sections II-IV. The results are shown in Table 3 and Figures 3-5. The binary solution phases in these systems are described by equations similar to Equation 1 on page 27. These results can be employed to compute ternary sections of the B_2O_3-GeO_2-SiO_2 system between 1600K and 1000K which are shown in Figures 6 and 7. The latter are computed by employing the description contained in Table 3 and ternary solution phase free energies similar to those depicted by Equation 4 on page 40 with a zero valued ternary interaction parameter for each phase. The current program will next consider effects on this system due to additions of P_2O_5, CeO_2 and Sb_2O_5.

TABLE 3

SUMMARY OF LATTICE STABILITY AND SOLUTION PHASE PARAMETERS
FOR GERMANIUM BOROSILICATE SYSTEMS

(All Units in Joules per gram atom (mole of atoms), T in Kelvins)

$BO = (1/5)B_2O_3$, $SO = (1/3)SiO_2$, $GO = (1/3)GeO_2$

$Q=B_2O_3$ structure, R=low temperature GeO_2 structure, X=Crystobalite, T=Tridymite, H=α quartz, B=β quartz structure, U=low temperature GeO_2

GOGOLH* = $(1/3)GeO_2$ (Liquid) - $(1/3)GeO_2$ (α quartz)

SOSOLQ=	-6.15T	BOBOLQ=	4448-6.15T
SOSOHU=	-4791-5.69T	BOBOLX=	-1.67T
GOGOLH=	3891-2.80T	BOBOLT=	-2.01T
GOGOHU=	7443-5.69T	BOBOLH=	-2.80T
GOGORU=	7109-5.40T	BOBOLR=	-3.10T
GOGOLX=	-1.67T	BOBOLU=	-8.49T
GOGOLT=	-2.01T		
GOGOLQ=	-6.15T		

LBOSO=64852-41.84T, LSOBO=-4184+20.92T
XBOSO=XSOBO=TBOSO=TSOBO=HBOSO=HSOBO=83680
RBOSO=RSOBO=QBOSO=QSOBO=33472

LGOSO=LSOGO=HGOSO=HSOGO=RGOSO=RSOGO=4184+12.552T
TGOSO=TSOGO=XGOSO=XSOGO=83680; UGOSO=USOGO=41840

LBOGO=LGOBO=12552, QBOGO=QGOBO=33472, HGOBO=HBOGO=83680
RBOGO=RGOBO=83680

* These differences specify the free energy of one phase (i.e. liquid) minus the free energy of the second phase (i.e. for a given compound).

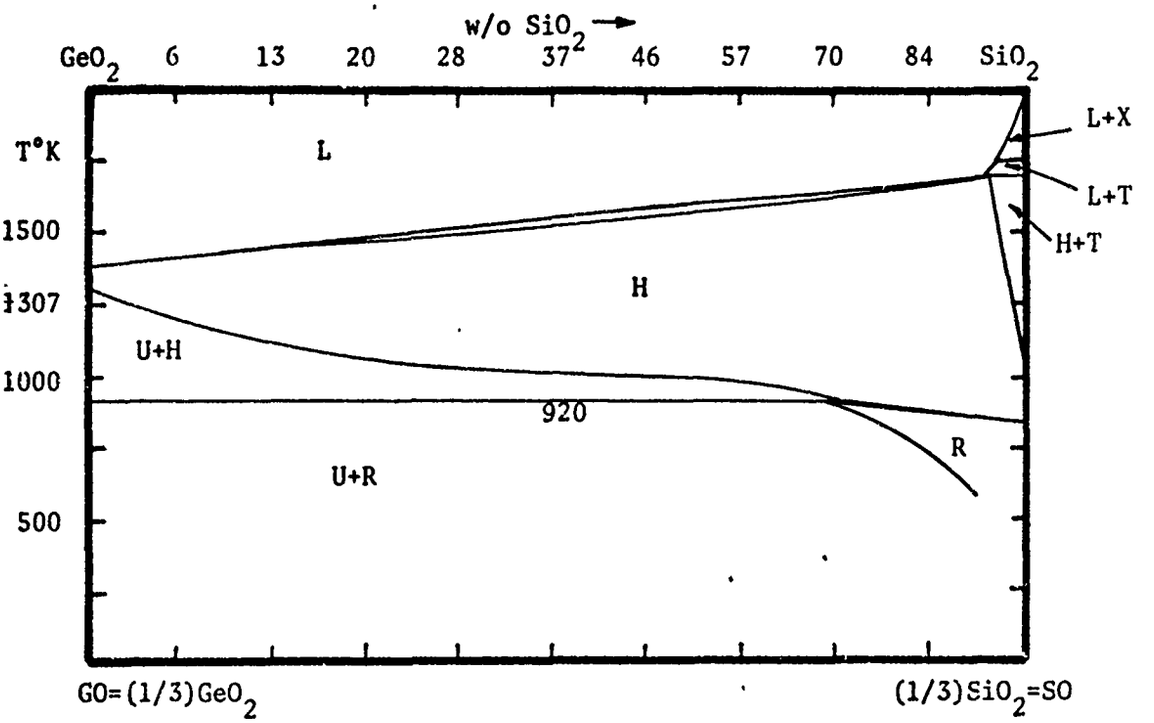

Figure 3. Calculated GeO_2 - SiO_2 Phase Diagram

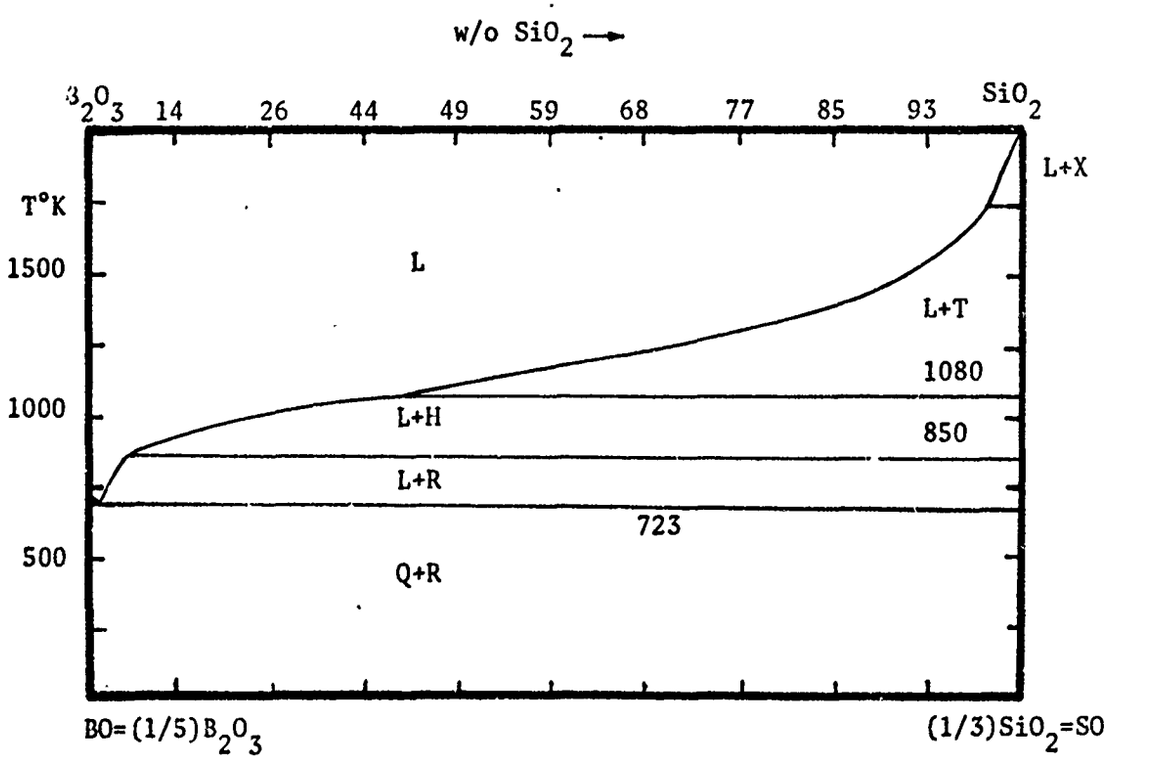

Figure 4. Calculated B_2O_3 - SiO_2 Phase Diagram

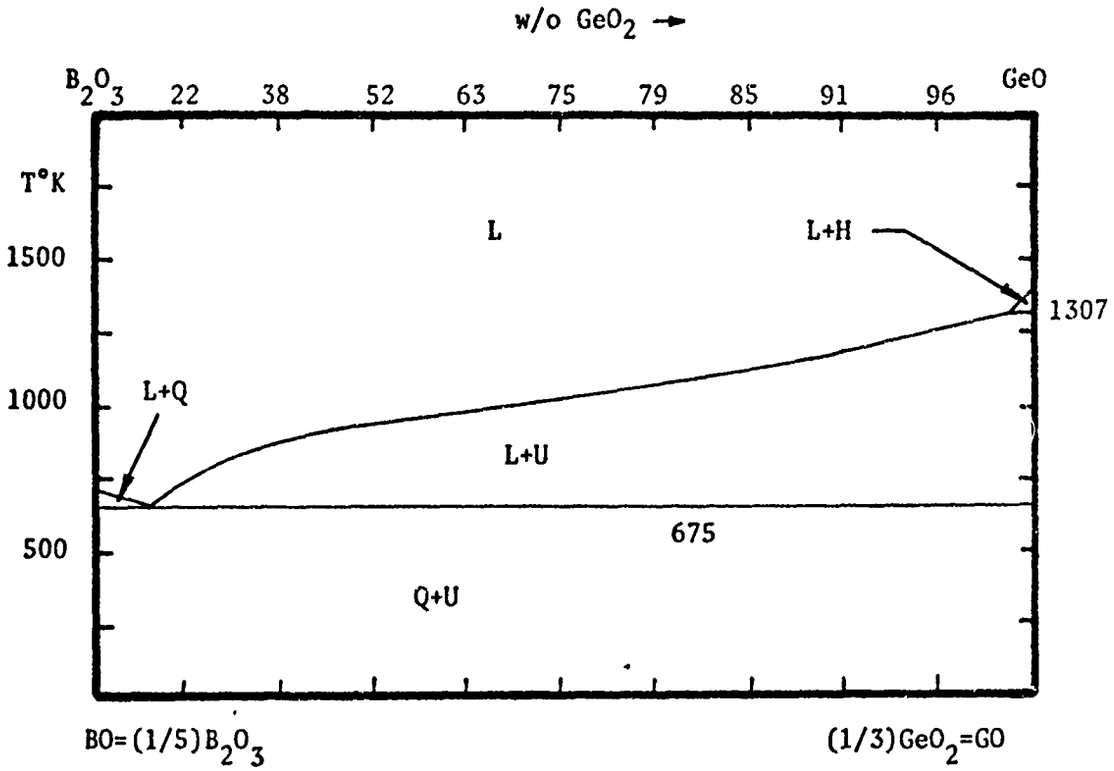

Figure 5. Calculated B_2O_3 - GeO_2 Phase Diagram

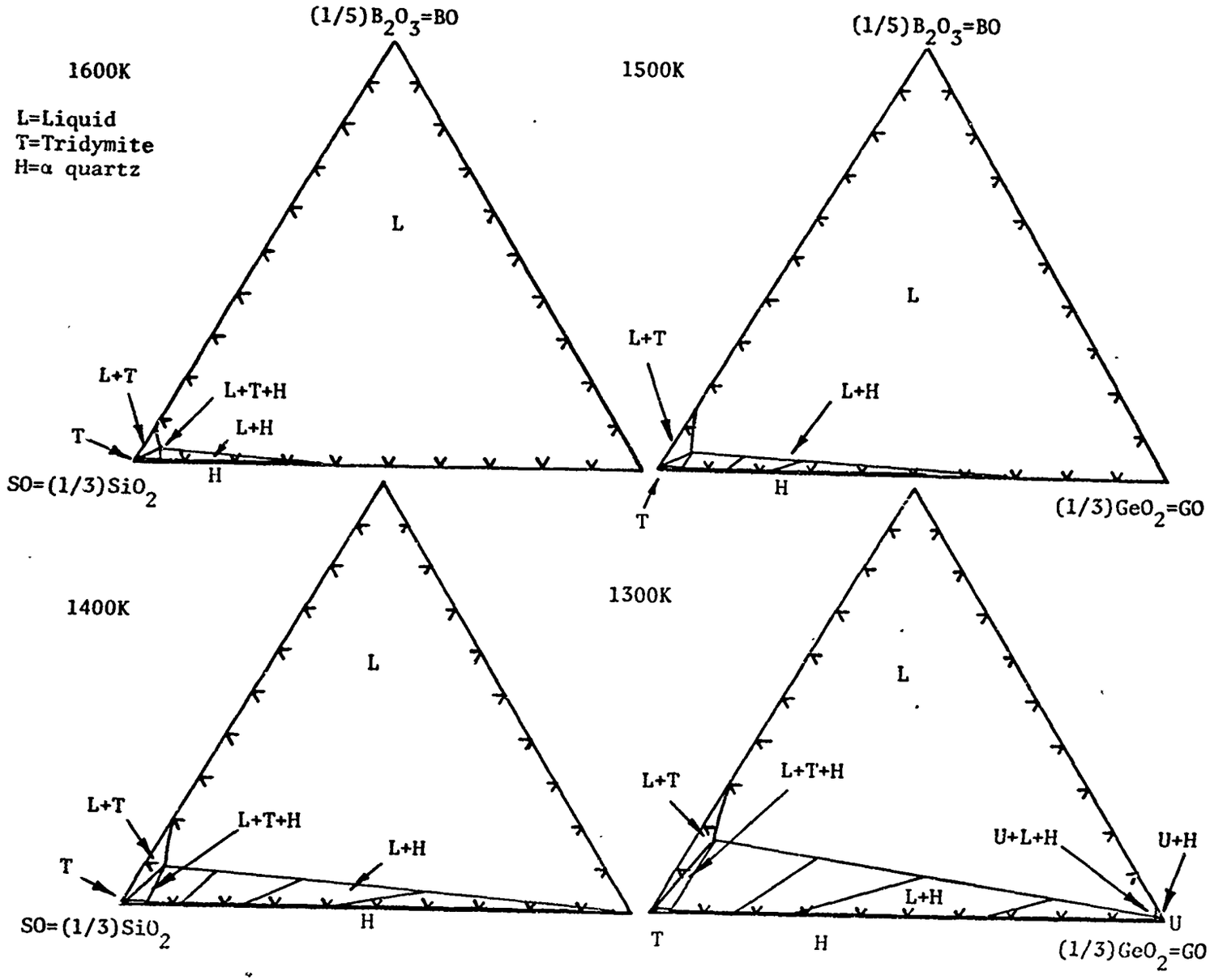

Figure 6. Calculated Isothermal Sections in the B_2O_3-GeO_2-SiO_2 System

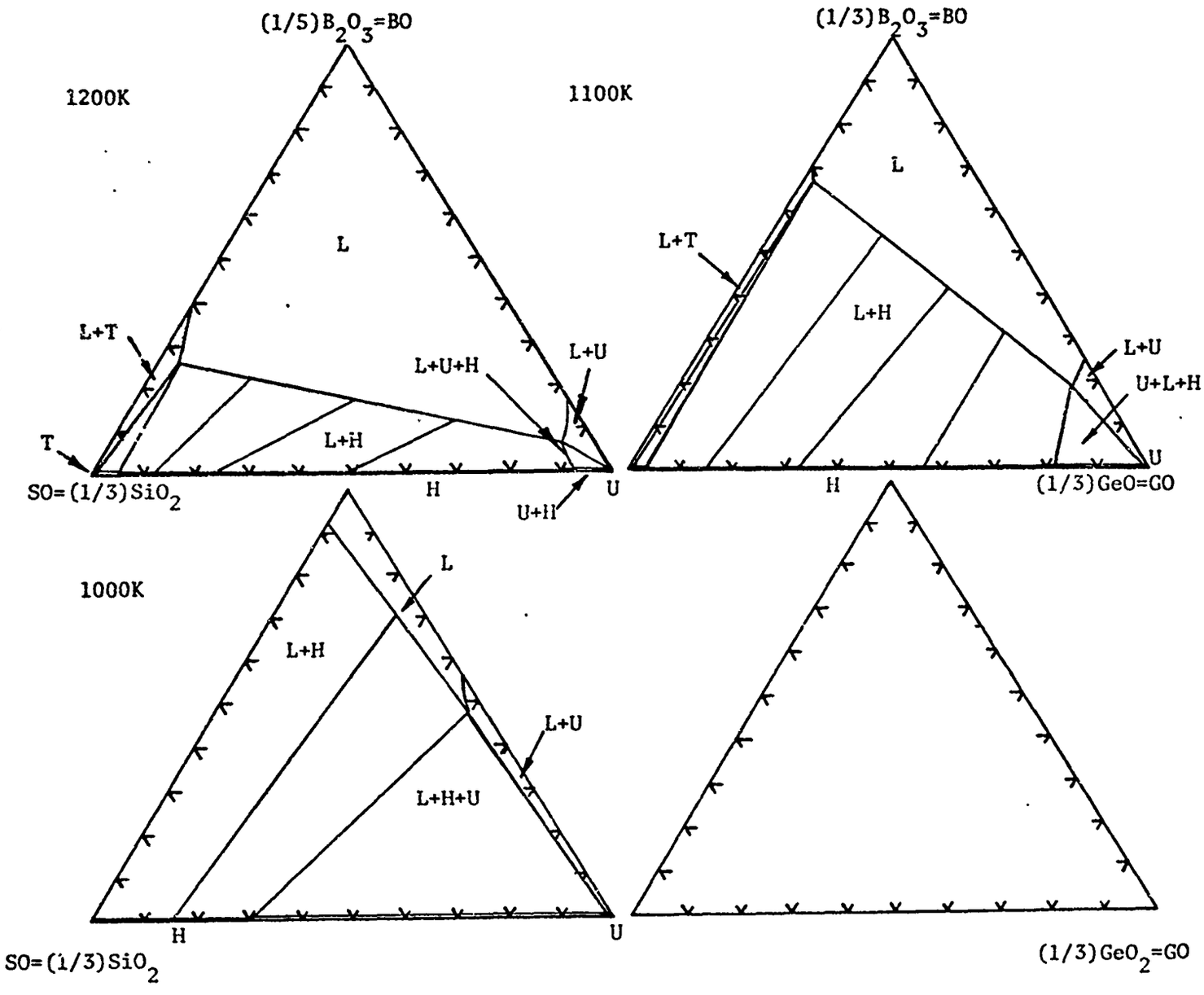

Figure 7. Calculated Isothermal Sections in the B_2O_3 - GeO_2-SiO_2 System